Configuration des systèmes énergétiques hybrides: une approche par l'apprentissage profond

par

Inoussa LEGRENE

THÈSE PAR ARTICLES PRÉSENTÉE À L'ÉCOLE DE TECHNOLOGIE SUPÉRIEURE
COMME EXIGENCE PARTIELLE À L'OBTENTION
DU DOCTORAT EN GÉNIE
Ph.D.

MONTRÉAL, LE 30 JANVIER 2026

ÉCOLE DE TECHNOLOGIE SUPÉRIEURE
UNIVERSITÉ DU QUÉBEC

PRÉSENTATION DU JURY

CETTE THÈSE A ÉTÉ ÉVALUÉE

PAR UN JURY COMPOSÉ DE:

M. Tony Wong, directeur de thèse
Département de génie des systèmes à l'École de technologie supérieure

M. Louis-A. Dessaint, codirecteur
Département de génie électrique à l'École de technologie supérieure

M. Thien-My Dao, président du jury
Département de génie mécanique à l'École de technologie supérieure

M. Julio Montecinos, membre du jury
Département de génie des systèmes à l'École de technologie supérieure

M. Georges Ghazi, membre du jury
Département de génie des systèmes à l'École de technologie supérieure

M. Mathias Adankon, examinateur externe
Directeur | Analyse et intelligence artificielle chez Banque Nationale, Marchés des capitaux

ELLE A FAIT L'OBJET D'UNE SOUTENANCE DEVANT JURY ET PUBLIC

LE 19 JANVIER 2026

À L'ÉCOLE DE TECHNOLOGIE SUPÉRIEURE

AVANT-PROPOS

La présente thèse s'inscrit dans un contexte mondial où la transition énergétique et la décarbonation des systèmes de production électrique sont devenues des enjeux stratégiques majeurs pour répondre aux objectifs de réduction des émissions de gaz à effet de serre. L'intégration croissante des sources renouvelables, comme le solaire photovoltaïque et l'éolien, pose le défi de concevoir des systèmes hybrides (HRES) capables de gérer en temps réel la variabilité des ressources naturelles, tout en assurant la fiabilité et la rentabilité économiques. Les approches traditionnelles basées sur la simulation exhaustive de toutes les combinaisons possibles de configurations énergétiques se heurtent rapidement à des temps de calcul prohibitifs et à une complexité combinatoire importante.

Face à ces limites, ce travail explore successivement trois axes complémentaires : d'abord, la réduction de la complexité de simulation via des méthodes hybrides de sélection de topologies ; ensuite, l'amélioration de la prévision du facteur solaire par des techniques avancées de fouille d'architecture neuronale ; enfin, le développement d'une approche de dimensionnement adaptatif et de gestion multicritère fondée sur l'apprentissage par renforcement profond. Chaque étape s'appuie sur les enseignements tirés de deux communications en conférence : la première met en lumière l'impact des variables de coût et des facteurs contextuels sur la conception de microréseau, tandis que la seconde illustre l'application d'algorithmes génétiques à un modèle de réseaux de neurones à mémoire long et court terme (Long Short-Term Memory, LSTM) pour la prévision solaire. Ce cheminement a ensuite conduit à la rédaction de quatre articles scientifiques.

La progression méthodologique décrite dans cette thèse reflète une volonté de passer d'un prototypage initial reposant sur des simulateurs complexes à des solutions autonomes capables de s'adapter dynamiquement aux conditions environnementales et aux objectifs économiques. En perspective, les méthodes développées ouvrent la voie à l'intégration de nouvelles sources d'énergie (stockage thermique, hydrogène), à la prise en compte des véhicules électriques comme composants énergétiques actifs, et à la validation expérimentale sur des micro-grids pilotes et des réseaux intelligents en conditions réelles. Cette démarche vise à fournir des outils robustes

et évolutifs pour le déploiement de réseaux intelligents durables, alliant efficience, résilience et respect de l’environnement.

REMERCIEMENTS

Faire un doctorat n'a pas été qu'une succession de bonnes notes : c'est avant tout une aventure collective, nourrie par l'expertise de celles et ceux qui m'ont précédé·e et par la richesse des échanges au sein de notre communauté scientifique.

Mon parcours doctoral, motivé par ma passion pour les énergies renouvelables et la conviction de leur rôle essentiel dans l'amélioration des conditions de vie, s'est révélé être bien plus qu'un simple projet personnel. Grâce à la possibilité d'entrer directement en doctorat sous condition, j'ai pu rejoindre ce programme, et j'ai eu la chance de le mener à terme avec enthousiasme et engagement.

Je tiens à exprimer ma profonde gratitude :

- Au Professeur Tony Wong, directeur de thèse, pour sa vision scientifique éclairée, ses conseils avisés et son soutien indéfectible tout au long de ces années.
- Au Professeur Louis-A. Dessaint, codirecteur, pour ses remarques pointues et son aide précieuse lors de la rédaction des articles.
- À Nicolas Mary, pour nos échanges stimulants et ses commentaires constructives.

Je remercie également mes collègues et toute l'équipe du laboratoire pour leur entraide quotidienne et leur bonne humeur, ainsi que l'École de technologie supérieure de m'avoir offert un environnement de recherche stimulant et des infrastructures de pointe.

À ma famille, j'adresse ma reconnaissance la plus profonde :

- À ma mère, pour son amour constant et sa confiance inébranlable dans mes ambitions.
- À mon père (paix à son âme), dont le rêve de me voir médecin m'a toujours encouragé à viser l'excellence, même en suivant un autre chemin.
- À mes frères et sœurs, pour leur présence réconfortante et leurs encouragements sans faille.

Merci enfin à mes ami·e·s proches, pour leur soutien moral dans les moments de doute et leur capacité à me motiver jusqu'à l'aboutissement de ce travail.

À toutes et à tous, merci pour votre confiance et votre appui : sans vous, cette réalisation n'aurait pas été possible.

Configuration des systèmes énergétiques hybrides: une approche par l'apprentissage profond

Inoussa LEGRENE

RÉSUMÉ

Cette thèse se structure en trois étapes majeures, appuyées par deux communications préliminaires en conférence et quatre articles scientifiques, afin d'aborder le dimensionnement et la gestion des systèmes hybrides d'énergie renouvelable (HRES) sous les angles de la réduction de la complexité, de l'optimisation de la prévision climatique et de l'intelligence décisionnelle adaptative.

Dans la première communication, l'analyse portait sur l'influence des paramètres économiques (coût du capital, d'installation et d'exploitation) et des facteurs contextuels (profil de charge, ressources renouvelables locales, tarifs d'achat) sur la conception de micro-grids, révélant le compromis essentiel entre rentabilité et fiabilité. Sur ces fondations, une méthode hybride combinant l'algorithme Branch & Bound et le k-Nearest Neighbors pour élaguer l'arbre des configurations PV+WT+BESS+DG sous Simulink a été proposée. À partir d'un jeu de données météorologiques synthétiques et de profils de charge, 5 390 configurations ont été générées, caractérisées par des vecteurs de temps de charge, de production prédictive et de taux de pénétration, puis filtrées par Branch & Bound pour sélectionner un sous-ensemble initial. Un algorithme kNN a ensuite classifié les configurations restantes selon leur similarité, éliminant les branches non prometteuses. Cette démarche a conduit à une réduction de 45 % à 95 % du temps de simulation, tout en maintenant plus de 83 % de précision dans l'identification de la topologie optimale.

La seconde communication présentait un prototype simplifié couplant un algorithme génétique avec un modèle LSTM pour la prévision de l'irradiance solaire (GHI), démontrant la faisabilité de l'association de la modélisation statistique et du calcul évolutif. De ce constat, les travaux se sont concentrées sur la prévision du GHI via une fouille d'architecture neuronale (NAS) améliorée par le transfert d'apprentissage (TL), l'adaptation dynamique de l'espace de recherche (DSS) et extrapolation de courbe d'apprentissage. Plus d'une centaine d'architectures candidates, chacune définie par plusieurs hyperparamètres (nombre de couches, taille de noyau, taux d'apprentissage, etc.), ont été explorées. Le DSS ajuste dynamiquement l'espace de fouille en fonction de la distribution des erreurs observées, permettant un abandon anticipé des architectures coûteuses. Pendant ce temps, l'extrapolation de courbe d'apprentissage stoppe précocement les réseaux à faible convergence. Comparée à des approches classiques (GA, PSO, DE, ABC), cette stratégie a réduit jusqu'à 89 % la durée du NAS et amélioré la précision des prévisions de GHI de 33 % à 99 % en RMSE sur des horizons de 6 à 72 heures.

La dernière partie de ces travaux introduit un cadre complet de dimensionnement adaptatif et de pilotage multicritère basé sur l'apprentissage par renforcement profond (DRL). L'espace d'état intègre le niveau de charge de batterie, l'irradiance et la vitesse du vent prédites, ainsi que les niveaux de production en cours, tandis que l'espace d'action couvre la régulation des puissances

attribuées aux panneaux photovoltaïques, aux éoliennes, à la batterie et au générateur diesel ou au réseau. L'algorithme Twin Delayed Deep Deterministic (TD3) assure stabilité et exploration efficace. La fonction de récompense cumulative combine le coût actualisé de l'énergie (LCOE), la fraction d'énergie renouvelable (REF) et la probabilité de perte d'alimentation électrique (LPSP), en intégrant une pénalisation de l'usage des sources fossiles. Appliquée à des profils de consommation réels du NREL, cette approche réduit le LCOE de 21 % à +30 %, accroît la part d'énergie renouvelable de +86 % et diminue la probabilité de perte de charge de 8,9 %, avec des performances maximales de 19,7 % de LCOE, +86 % de REF et 8,9 % de LPSP, surpassant NSGA-II et MOPSO sur la plupart des indicateurs. Ensemble, ces contributions illustrent la valeur d'une démarche progressive allant de la réduction de la complexité de simulation à l'intelligence décisionnelle adaptative. L'objectif étant de définir un cadre de conception des micro réseaux et intelligents de nouvelle génération, résilients, performants et respectueux de l'environnement.

Mots-clés: apprentissage profond, apprentissage automatique, énergie renouvelable, fouille heuristique, incertitudes, optimisation multi-objectifs, prédiction

Configuration of Hybrid Energy Systems : A Deep Learning Approach

Inoussa LEGRENE

ABSTRACT

This thesis is organized into three major stages, supported by two preliminary conference communications and four scientific articles, to address the sizing and management of hybrid renewable energy systems (HRES) from the perspective of complexity reduction, improvement of weather forecasting, and adaptive decision intelligence.

In the first communication, we analyzed the influence of economic parameters (capital, installation, and operating costs) and contextual factors (load profiles, local renewable-resource availability, feed-in tariffs) on microgrid design, revealing the essential trade-off between profitability and reliability. Building on this foundation, we proposed a hybrid method combining the Branch Bound algorithm with k-Nearest Neighbors to prune the configuration tree of PV+WT+BESS+DG systems within Simulink. From a synthetic meteorological dataset and load profiles, we generated 5,390 configurations—each characterized by vectors of load duration, predicted production, and penetration rate—and filtered them using Branch Bound to select an initial subset. A kNN algorithm then classified the remaining configurations by similarity, eliminating unpromising branches. This approach reduced simulation time by 45 %–95 % while maintaining over 83 % accuracy in identifying the optimal topology.

The second communication introduced a simplified prototype coupling a genetic algorithm with an LSTM model for global horizontal irradiance (GHI) forecasting, demonstrating the feasibility of combining statistical modeling with evolutionary computation. From this insight, we focused on GHI prediction via neural architecture search (NAS) enhanced by transfer learning (TL), dynamic search-space adaptation (DSS), and learning-curve extrapolation. Over one hundred candidate architectures—each defined by multiple hyperparameters (number of layers, kernel size, learning rate, etc.)—were explored. DSS dynamically refines the search space according to observed error distributions, enabling early abandonment of costly architectures, while learning-curve extrapolation halts networks with poor convergence. Compared to classical methods (GA, PSO, DE, ABC), this strategy reduced NAS runtime by up to 89 % and improved GHI-forecast accuracy by 33 %–99 % in RMSE over horizons of 6 to 72 hours.

The final stage introduces a comprehensive adaptive sizing and multi-objective control framework based on deep reinforcement learning (DRL). The state space incorporates battery-state-of-charge, forecasted irradiance and wind speed, and current generation levels, while the action space covers power dispatch among PV panels, wind turbines, battery, diesel generator, and grid. The Twin Delayed Deep Deterministic (TD3) algorithm ensures stability and efficient exploration. The cumulative reward combines the levelized cost of energy (LCOE), renewable-energy fraction (REF), and loss-of-power-supply probability (LPSP), with a penalty on fossil-fuel usage. Applied to real NREL load profiles, this approach reduced LCOE by 21 % to 30 %, increased renewable-energy share by 86 %, and decreased LPSP by 8.9 %, with peak performance of –19.7 % LCOE, +86 % REF, and –8.9 % LPSP—outperforming NSGA-II and MOPSO on

most indicators. Together, these contributions illustrate the value of a progressive methodology spanning complexity reduction through simulation pruning and adaptive decision intelligence. The ultimate goal is to establish a design framework for next-generation smart microgrids that are resilient, high-performance, and environmentally friendly.

Keywords: deep learning, heuristic search, machine learning, multi-objective optimization, prediction, renewable energy, uncertainties

TABLE DES MATIÈRES

Page

INTRODUCTION 1
0.1 Énoncés des problèmes 4
0.2 Modélisation du problème 6
0.2.1 Coût actualisé de l'énergie 7
0.2.2 Probabilité de perte de puissance 8
0.2.3 Fraction d'énergie renouvelable 9
0.3 Défis liés aux problèmes 10
0.4 Objectif général de la recherche 10
0.5 Objectif spécifiques 10
0.6 Organisation de la thèse et contributions originales 11
0.7 Limites de la recherche 17

CHAPITRE 1 REVUE DE LITTÉRATURE 19
1.1 Introduction 19
1.2 Dimensionnement d'un système hybride d'énergie renouvelable 20
1.2.1 Catégorisation des outils de décision 20
1.2.2 Étapes clés du dimensionnement 21
1.2.3 Réduction du temps de simulation 23
1.2.4 Approches classiques de réduction d'ordre 23
1.2.5 Approches par apprentissage profond 24
1.2.6 Substitution par des modèles prédictifs (ML global) 24
1.2.7 Limites et perspectives 25
1.3 Prédiction de l'irradiance solaire et recherche d'architectures neuronales 26
1.3.1 Formulation du GHI 26
1.3.2 Sources de données historiques et enjeux 27
1.3.3 Techniques l'apprentissage profond pour la prévision du GHI 27
1.3.4 Fouille d'architecture neuronale 28
1.3.5 Méthodologie hybride adaptative 30
1.4 Conception et dimensionnement des HRES 30
1.4.1 Diversité des composants et topologies 30
1.4.2 Outils de simulation utilisés 32
1.4.3 Algorithmes métaheuristiques pour l'optimisation multiobjectifs 32
1.4.4 Critères de sélection et contraintes spécifiques 33
1.5 Analyse de sensibilité des HRES 34
1.5.1 Objectifs et méthodes d'analyse de sensibilité 34
1.5.2 Paramètres sensibles et impacts observés 35
1.5.3 Aspects peu couverts et perspectives 37
1.5.4 Approches par apprentissage par renforcement profond (DRL) 38
1.5.5 Du métaheuristique au DRL 38
1.5.6 Intégration des contraintes DG/GRID 39

1.5.7 Exemples d'implémentations DRL pour les HRES 40
1.5.8 Limites actuelles et perspectives de recherche 40
1.6 Conclusion 43

CHAPITRE 2 REDUCTION IN MICROGRID TOPOLOGY SELECTION TIME VIA HYBRID BRANCH AND BOUND AND K-NEAREST NEIGHBORS TECHNIQUES 45
2.1 Abstract 45
2.2 Introduction 46
2.3 Solution Approach 52
2.3.1 Stepwise 52
2.3.2 Methodology 55
2.3.2.1 Branch and Bound Algorithm 58
2.3.2.2 k-Nearest Neighbors 59
2.4 Results and Discussion 59
2.4.1 Type of System Evaluated 60
2.4.2 Parameter Definition 62
2.4.3 Simulation Results and Discussion 65
2.4.3.1 Proposed BB and kNN Results 65
2.4.3.2 Comparing the Proposed BB and kNN Approach with the Traditional Process 68
2.5 Conclusions 70

CHAPITRE 3 ENHANCING NEURAL ARCHITECTURE SEARCH USING TRANSFER LEARNING AND DYNAMIC SEARCH SPACES FOR GHI PREDICTION 71
3.1 Abstract 71
3.2 Introduction 72
3.3 Neural Architecture Search – NAS 74
3.3.1 Architecture Search Space 74
3.3.2 Search strategy 75
3.3.3 Performance estimation strategy 76
3.4 Proposed Approach of NAS Application 78
3.4.1 LSTM Model 79
3.4.2 Metaheuristic algorithms 80
3.4.2.1 Artificial Bee Colony - ABC 80
3.4.2.2 Genetic Algorithm-GA 81
3.4.2.3 Differential Evolution Algorithm - DE 82
3.4.2.4 Particle Swarm Optimization-PSO 83
3.4.2.5 Hyperparameter Encoding and Tuning 84
3.4.3 Solution Approach 85
3.4.3.1 Dynamic Search Space-DSS 87
3.4.4 Application and Evaluation 88
3.5 Results and discussion 89

3.5.1 Data acquisition and modeling 89
3.5.1.1 Data acquisition 89
3.5.1.2 Data modeling 90
3.5.2 General architecture definition parameters 91
3.5.3 Detailed results of four approaches 94
3.5.3.1 Grid Search results 94
3.5.3.2 Metaheuristics Results Without TL and DSS 95
3.5.3.3 Metaheuristics results with TL and DSS 96
3.5.3.4 Comparison of the results 98
3.5.4 Comparison with other research 104
3.6 Conclusion 107

CHAPITRE 4 DEEP REINFORCEMENT LEARNING APPROACH FOR HYBRID RENEWABLE ENERGY SYSTEMS OPTIMIZATION 109
4.1 Abstract 109
4.2 Introduction 110
4.3 Related reviews 112
4.4 System and Problem Formulation 115
4.4.1 System Modeling 116
4.4.1.1 Solar panel model 116
4.4.1.2 Wind turbine model 118
4.4.1.3 Battery energy storage system 120
4.4.1.4 Diesel generators 122
4.4.1.5 Hybrid converter 123
4.4.2 Energy management strategies 124
4.4.3 System analysis factors 126
4.4.3.1 Levelized cost of energy 127
4.4.3.2 Loss of power supply probability - LPSP 129
4.4.3.3 Renewable energy fraction 129
4.4.3.4 Constraints 130
4.4.4 Problem formulation 130
4.4.5 Research approach 131
4.4.5.1 Deep reinforcement learning 131
4.4.5.2 Approach 132
4.4.5.3 Particle swarm optimization 137
4.4.5.4 Multi-objective Particle Swarm Optimization 139
4.4.5.5 Non-dominated Sorting Genetic Algorithm II 141
4.5 Results and discussions 143
4.5.1 Study data 143
4.5.2 Study systems 148
4.5.2.1 Comparison between Deep Reinforcement Learning and Benchmarks 157
4.5.2.2 Comparison of the proposed DRL approach with other works 162

4.6 Conclusion 164

CONCLUSION ET RECOMMANDATIONS 167

BIBLIOGRAPHIE 173

LISTE DES TABLEAUX

Page

Tableau 1.1 Analyse des paramètres et impacts observés dans diverses études 36

Tableau 1.2 Comparaison synthétique des principales familles d'approches pour le dimensionnement des HRES. 42

Tableau 2.1 Summary of methodologies and applications 50

Tableau 2.2 Parameters to be defined in the proposed methodology 56

Tableau 2.3 Example parameter value definitions 62

Tableau 2.4 Parameter initialization 63

Tableau 2.5 Case study projects and their numbers of configurations 64

Tableau 2.6 Parameters considered in this study 65

Tableau 2.7 Simulation time results 66

Tableau 2.8 Percentage time reduction using the proposed BB and kNN method ... 69

Tableau 3.1 Architecture Training Parameters 92

Tableau 3.2 Search parameters 92

Tableau 3.3 Search parameter boundaries 93

Tableau 3.4 Grid Search Best models details 94

Tableau 3.5 Grid Search results for different forecasting windows 95

Tableau 3.6 Results without TL and DSS 96

Tableau 3.7 Results with TL and DSS 97

Tableau 3.8 Comparisons between GS and NAS approaches 99

Tableau 3.9 Direct comparison between our approaches and a non-enhanced approach 99

Tableau 3.10 Comparison between the proposed approach and other related research (1/2) 105

Tableau 3.11 Comparison between the proposed approach and other related research (2/2) 106

Tableau 4.1 PV specifications 118

Tableau 4.2 WT Specifications (Faria, Marques, Pombo, Mariano, and Calado, 2023) 119

Tableau 4.3 BESS Specifications 121

Tableau 4.4 Generator Specifications 123

Tableau 4.5 12 kW ELIOS Hybrid Converter Specifications 124

Tableau 4.6 DRL train and decision parameters 137

Tableau 4.7 PSO Parameter specifications 138

Tableau 4.8 MOPSO Parameter specifications 141

Tableau 4.9 NSGA-II Parameter specifications 143

Tableau 4.10 Descriptive analysis of time series data 146

Tableau 4.11 DRL vs. PSO, MOPSO and NSGA-II comparison table, P1 151

Tableau 4.12 DRL vs. PSO, MOPSO and NSGA-II comparison table, P2 152

Tableau 4.13 DRL vs. PSO, MOPSO and NSGA-II comparison table, P3 153

Tableau 4.14 DRL Simulation results 155

Tableau 4.15 Comparison with other research 164

LISTE DES FIGURES

Page

Figure 0.1 Système hybride d'énergie renouvelable 3

Figure 2.1 Key steps of proposed hybrid renewable energy system (HRES) methodology 53

Figure 2.2 Energy management process 53

Figure 2.3 Process of the proposed methodology 55

Figure 2.4 Schematic of considered hybrid renewable energy system 61

Figure 2.5 Simulation times for different numbers of configurations 63

Figure 2.6 Simulations time by method and number of configurations 67

Figure 2.7 kNN processing time depending on the number of configurations 68

Figure 3.1 (S) Search space and (a) a possible candidate architecture 75

Figure 3.2 Methodology : Presents the steps involved in the metaheuristic algorithms, from defining the initial population to determining the best architecture. These steps demonstrate the dynamic adaptation of the search space and the transfer of learning from parent architectures to new child architectures 86

Figure 3.3 NAS approach WITHOUT TL and DSS : Shows the number of candidate architectures evaluated per method and the order of magnitude of the RMSE errors obtained 100

Figure 3.4 NAS approach WITH TL and DSS : Shows the number of candidate architectures evaluated per method and the order of magnitude of the RMSE errors obtained 101

Figure 3.5 Proposed ABC candidate solutions' evolution : Shows the number of candidate architectures and the order of magnitude of RMSE errors for the candidate architectures with and without TL-DSS 102

Figure 3.6 Proposed DE candidate solutions' evolution : Shows the number of candidate architectures and the order of magnitude of RMSE errors for the candidate architectures with and without TL-DSS 102

Figure 3.7 Proposed GA candidate solutions' evolution : Shows the number of candidate architectures and the order of magnitude of RMSE errors for the candidate architectures with and without TL-DSS 103

Figure 3.8 Proposed PSO candidate solutions' evolution : Shows the number of candidate architectures and the order of magnitude of RMSE errors for the candidate architectures with and without TL-DSS 103

Figure 4.1 Hybrid Renewable Energy System (HRES) (Legrene, Wong, Mary, and Dessaint, 2025) 116

Figure 4.2 Energy management process 125

Figure 4.3 Proposal approach steps 134

Figure 4.4 MOPSO approach steps 140

Figure 4.5 NSGA-II approach steps 142

Figure 4.6 Average monthly energy consumption 144

Figure 4.7 Profiles comparative boxplots 145

Figure 4.8 Time Series Data 147

Figure 4.9 Correlation matrix of time series data 147

Figure 4.10 LCOE vs. Profile for Different Systems 149

Figure 4.11 Heatmap of LCOE 154

Figure 4.12 Heatmap of LCOE average by profile and method 158

Figure 4.13 Comparison of systems by profile and method (DRL vs. PSO vs. MOPSO vs. NSGA-II) 158

Figure 4.14 Heatmap of LPSP average by profile and method 160

Figure 4.15 Heatmap of REF average by profile and method 161

LISTE DES ABRÉVIATIONS, SIGLES ET ACRONYMES

ABC	Artificial Bee Colony
ACO	Ant Colony Optimization
AFSO	Artificial Fish Swarm Optimization
AGA	Adaptative Genetic Algorithm
ANN	Artificial Neural Network
AnS	Apprentissage non Supervisé
ARMA	Auto-Regressive Moving Average
AS	Apprentissage Supervisé
CA	Courant Alternatif
CC	Courant Continu
CCNUCC	Convention Cadre des Nations Unies sur les Changements Climatiques
CNN	Convolution Neural Network
CO^2	Dioxyde de Carbone
COA	Cuckoo Optimization Algorithm
COP21	Conférence de Paris, 21e Conférence des Parties
CPU	Central Processing Unit
CRF	Recovery Factor
DC	Direct Current
DE	Differential Evolution
DG	Diesel Generator
DoD	Depth of Discharge
DL	Deep Learning
DNN	Deep Neural Network
DSS	Dynamic Search Spaces
DRL	Deep Reinforcement Learning

EFCS	Electrolyzer Fuel Cell Energy Storage System
GA	Genetic Algorithm
GEN	Generator
GES	Gaz à effet de serre
GHI	Global Horizontal Irradiance
GRG	Generalized Reduced Gradient
GS	Grid Search
GU-DHOA	Grey Update Deer Hunting Optimization Algorithm
GWO	Grey Wolf Optimization
HOGA	Hybrid Optimization by Genetic Algorithms
HOMER	Hybrid Optimization Model for Energy Renewable
HRES	Hybrid Renewable Energy System
HS	Heuristic Search
ICSA	Improved Crow Search Algorithm
IGWO	Improved Grey Wolf Optimization
IEEE	Institute of Electrical and Electronical Engineers
LBNS	Low Burden Narrow Search
LSTM	Long Short-Term Memory
LSSVM	Least Square Support Vector Machine
MAE	Mean Absolute Error
MARL	Multi Agents Reinforcement Learning
MCAR	Missing Completely At Random
MERRA-2	Modern Era Retrospective Analysis for Research and Applications, Version 2
ML	Machine Learning
MLP	MultiLayer Perceptron
MLP-NN	MultiLayer Perceptron Neural Network
MOPSO	Multi Objectives Particule Swarm Optimization

MSE	Mean Squared Error
MSTL	Multi-seasonal Trend decomposition of Time Series
NAS	Neural Architecture Search
NREL	National Renewable Energy Laboratory
NSGA-II	Non-Dominated Sorted Genetic Algorithm II
NSRDB	National Solar Radiation Database
OSSO	Opposition based Social Spider Optimization
PMM	Predictive Mean Matching
PSO	Particle Swarm Optimization
RNN	Recurrent Neural Network
RL	Reinforcement Learning
RBM	Restricted Boltzmann Machine
RMSE	Root Mean Squared Error
SADE	Self-Adaptive Differential Evolution
SARIMAX	Seasonal Auto-Regressive Integrated Moving Average with eXogenous factor
SDG	Stochastic Gradient Descent
SVM	Support Vector Machine
SSA	Salp Swarm Algorithm
SSO	Social Spider Optimization
TL	Transfer Learning
WT	Wind Turbine

LISTE DES SYMBOLES ET UNITÉS DE MESURE

$Mtep$	Mégatonne équivalent pétrole
kW	Kilowatt
MW	Mégawatt
kWh	Kilowatt-heure
kg	Kilogramme
kg/kW	Kilogramme par kilowatt
kg/L	Kilogramme par litre
m^2	Mètre au carré
m/s ou $m \cdot s^{-1}$	Mètre par seconde
C	Degré Celsius
$\%/C$	Pourcentage par degré Celsius
W/m^2	Watt par mètre carré
$\$/kWh$	Dollar par kilowatt-heure
$\$/kW$	Dollar par kilowatt
$\$/L$	Dollar par litre
E_a	Energy bought from grid
E_v	Energy sold on the grid
E_{ch}	Load energy
E_{dis}	Energy available in the BESS
h_{rf}	Reference height
$I(t)$	Solar irradiance at time t
I_{nom}	Solar irradiance at standard operating conditions
N_{PV}	Number of PV panels
N_{WT}	Number of wind turbines
P_{DG}	Power generation by generator

$P_{\mathrm{DG}}^{\mathrm{rated}}$	Diesel generator rated power
P_{GRID}	Power from connected grid
P_L	Load demand
P_{PV}	Power generation by PV
$P_{\mathrm{PV}}^{\mathrm{rated}}$	PV panel rated power
P_{WT}	Power generation by wind turbine
$P_{\mathrm{WT}}^{\mathrm{rated}}$	Wind turbine rated power
S_{PV}	PV installation area
T_a	Ambient temperature
$T_c(t)$	PV panel temperature at time t
T_{nom}	Temperature at standard operating conditions
$v(t)$	Wind turbine hub speed at time t
$v_{\mathrm{rf}}(t)$	Wind speed at the reference height at time t
η_{cab}	Efficiency of the wiring
η_{ch}	BESS charge efficiency
η_{dis}	BESS discharge efficiency
$\eta_{\mathrm{PV}}^{\mathrm{conv}}$	Inverter efficiency on PV side
$\eta_{\mathrm{BESS}}^{\mathrm{conv}}$	Inverter efficiency on BESS side
η_{PV}	PV efficiency
η_r	PV effectiveness
k_p	Maximum power coefficient of temperature
τ_a	Rate of purchase energy from grid
τ_v	Rate of sale of energy on the grid
α	Coefficient of friction
γ	Rate of energy permissible via the grid
τ	Rate for energy permissible by the generator
a	Architecture candidate $a = (L, NL, H)$

S	Espace de recherche
L	Ensemble des couches neuronales
NL	Nombre de couches neuronales
H	Ensemble des hyperparamètres
$f(a, H)$	Fonction objectif (p. ex. RMSE)
h^*	Vecteur optimal d'hyperparamètres
$\tilde{\mathrm{w}}$	Poids du meilleur modèle courant
$\Delta \mathrm{w}$	Variation de poids pour un nouveau modèle
x	Vecteur d'entrée
z	Vecteur de sortie
W	Matrice des poids
b	Vecteur des biais
$P(a, t)$	Perte d'apprentissage à l'instant t
Δt	Durée maximale autorisée
Y_t	Série observée au temps t
$\hat{T}_t$	Composante tendance
$\hat{S}_t^{(i)}$	Composante saisonnière i-ème
$\hat{R}_t$	Composante résiduelle
x_{scaled}	Valeur normalisée (min-max)
$x_{\min}, x_{\max}$	Valeurs minimale et maximale pour l'échelle

INTRODUCTION

La demande croissante d'énergie, conjuguée aux préoccupations concernant la pollution environnementale et la production de gaz à effet de serre, favorise l'adoption de sources d'énergie renouvelable. Parmi ces sources d'énergie figurent le solaire et l'éolien qui connaissent la croissance la plus rapide au Canada (naturelle Canada, 2024). Au Québec, l'énergie éolienne produit environ 4000 MW d'électricité sur 44 sites en activité et on prévoit l'ajout de 10000 MW d'ici 2035 (Hydro-Québec, 2024). En dépit de l'augmentation des coûts, la filière éolienne demeure l'une des moins coûteuses parmi les sources d'énergie renouvelable. D'après les données publiées dans (Hydro-Québec, 2025), le coût de l'éolien varie de 7 à 10 ¢/kWh ce qui est supérieur à l'hydroélectricité que nous estimons à moins de 4 ¢/kWh à partir de l'entente intervenue entre Québec, Terre-Neuve-et-Labrador (Whitmore, 2025). Cependant, Hydro-Québec prévoit adopter une stratégie misant sur des projets publics de 1000 à 1500 MW et sur des projets d'autoproduction de 300 à 350 MW pour atteindre l'objectif fixé pour l'an 2035 (Hydro-Québec, 2025).

Du côté de la filiale solaire, on vise la production de 3000 MW d'énergie solaire d'ici 2035 par le biais de programmes incitatifs et subventions qui prendront effet en 2026. D'ailleurs, un appel d'offres pour acquérir 300 MW a été lancé en mai 2025 (Radio-Canada, 2025). Selon Hydro-Québec, les territoires québécois bénéficient d'un taux d'ensoleillement annuel de 2190 heures, soit 20 % supérieur à des pays comme l'Allemagne, qui produit déjà plus de 80000 MW en énergie solaire (Hydro-Québec, 2025). L'engouement pour le solaire s'explique aussi par la baisse des prix de production. Présentement, le coût du solaire au Québec se situe entre 8 à 11 ¢/kWh. Ce coût de production d'électricité est supérieur à des pays comme la France et l'Allemagne, mais il est inférieur à d'autres sources d'énergie tels le gaz, le charbon et le nucléaire (Hydro-Québec, 2025). De plus, les études de Casey (2025) montrent que la baisse du coût de production solaire devra s'accélérer pour atteindre la moyenne mondiale de 25 $ US/MWh en 2035.

Malgré cette projection optimiste sur les coûts de production, les sources éoliennes et solaires utilisables dans une région donnée peuvent ne pas répondre aux besoins énergétiques prévus. Plus important encore, la disponibilité de ces sources d'énergie est souvent intermittente (Scher and Messori, 2018). Par conséquent, pour garantir la continuité de la disponibilité énergétique, les sources d'énergie renouvelable sont souvent associées à des générateurs et à des systèmes de stockage pour compenser le manque de production. Ces combinaisons sont appelées systèmes hybrides d'énergie renouvelable (HRES). En effet, l'adoption des HRES est l'une des options intéressantes pour réduire les gaz à effet de serre car elle peut remplacer directement l'électricité produite à partir de combustibles fossiles, tels que le charbon, le pétrole et le gaz naturel. La combustion de ces combustibles fossiles est une source majeure d'émissions de dioxyde de carbone (CO_2) et d'autres gaz à effet de serre.

Les objectifs de décarbonisations encouragent les villes, les industries et régions éloignées à privilégier l'adoption de solutions énergétiques à l'échelle de la communauté. Cette approche communautaire n'est pas nouvelle. Déjà en 2009, le gouvernement fédéral avait publié un plan d'action visant la gestion et l'amélioration du rendement énergétique au sein des collectivités canadiennes (des ministres de l'Énergie, 2009). Avec l'engouement pour le solaire et la possibilité de l'autoproduction éolienne, ces sources d'énergie renouvelable feront désormais partie du plan de l'autosuffisance et l'amélioration du rendement énergétique au Québec et au Canada (de l'énergie renouvelable, 2024). Aujourd'hui, les HRES combinant solaire, éolien, stockage et générateurs d'appoint sont disponibles sur le marché commercial. Leur intégration dans un microréseau électrique permet de gérer, d'une façon locale, la production et la distribution de l'énergie électrique. La décarbonisation à l'échelle de la communauté est désormais réalisable et même abordable. La Figure 0.1 est une illustration montrant les principaux composants d'un HRES. Ce système considère deux sources renouvelables de production d'énergies (le solaire et l'éolien). Ces sources sont associées à un générateur et au réseau public comme sources de secours. Quant aux batteries, elles servent de moyens de sauvegarde du surplus de production.

Les convertisseurs jouent un rôle crucial de conversion de l'énergie. Du courant continu (DC) en courant alternatif (AC) directement exploitable par les charges. Où applique le processus inverse afin d'assurer une sauvegarde dans les batteries.

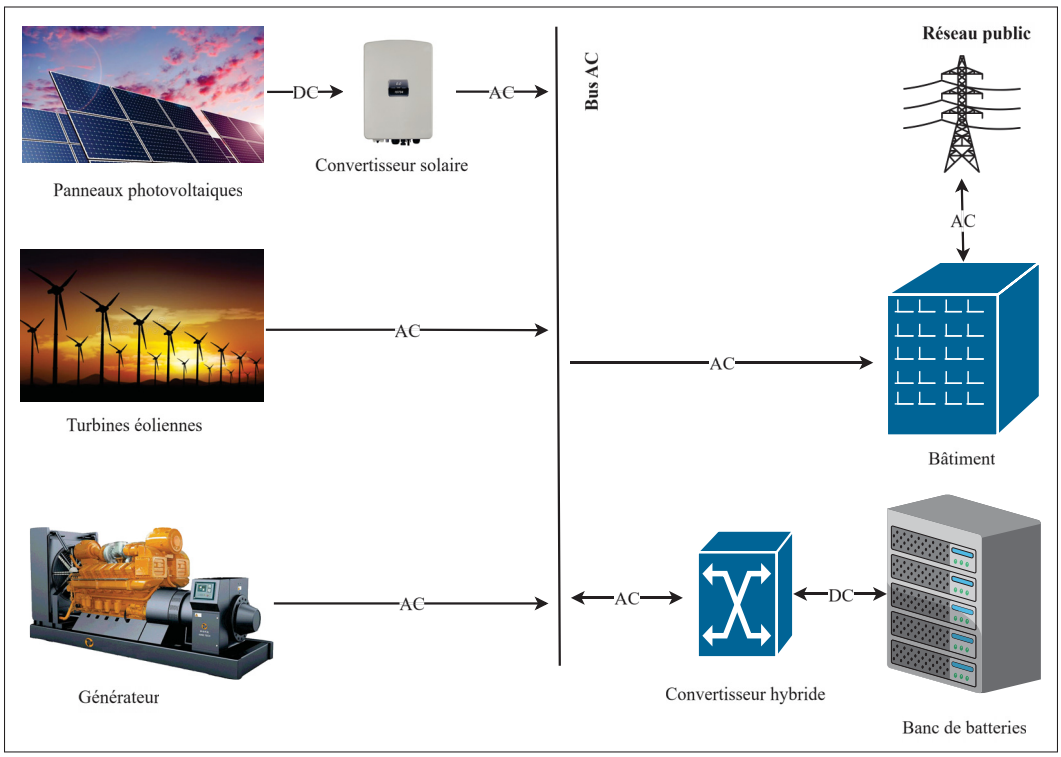

Figure 0.1 Système hybride d'énergie renouvelable

Dans un HRES, chaque composant possède des paramètres à ajuster afin de satisfaire des critères d'opération et de performance. Parmi ces critères, le coût de production influence directement la rentabilité du système.

Toutefois, réduire le coût en s'appuyant davantage sur l'injection depuis le réseau peut rendre marginale la contribution de l'éolien et du solaire. Or, pour des raisons environnementales, il est souhaitable de maximiser la part d'énergie renouvelable.

Enfin, un coût faible et une forte pénétration renouvelable ne garantissent pas, à eux seuls, une fourniture satisfaisante d'électricité. Il faut aussi minimiser l'écart entre l'énergie produite et la demande. Ces critères, de natures et d'unités différentes, rendent le réglage d'un HRES complexe et expliquent pourquoi la sélection d'une configuration est souvent un casse-tête pour les opérateurs.

0.1 Énoncés des problèmes

Charge de calcul : Un projet HRES typique génère 1000 à plus de 10000 configurations possibles si l'on tient compte des paramètres, tels que la puissance des panneaux photovoltaïques (PV), l'inclinaison de ceux-ci, le type de turbine éolienne (WT), la capacité de stockage des batteries, la puissance des générateurs et le choix des onduleurs.

Sélectionner manuellement une configuration convenable n'est tout simplement pas envisageable. La modélisation et la simulation du HRES peuvent automatiser la procédure de sélection. Or, simuler seulement quelques milliers de ces configurations sur une année météorologique type (8760 heures) peut exiger plusieurs heures de calcul (Bahgaat, 2023; Lu, Wang, Zhang, and Cheng, 2017). Cette charge de calcul élevée est causée en partie par la présence de non-linéarités dans le modèle. En effet, le vieillissement des batteries, les pénalités associées au démarrage des générateurs et la limite de consommation du combustible fossile nous imposent des pas de calcul qui sont très petits par rapport à l'horizon temporel de simulation (Legrene, Wong, and Dessaint, 2024a; Mostafa, Abdel Aleem, Ali, Ali, and Abdelaziz, 2020).

Choix multicritère : La sélection d'une configuration HRES est normalement basée sur un ensemble de critères. De plus, les critères de sélection sont souvent antagonistes. Par exemple, accroître l'apport de l'énergie renouvelable dans un HRES fait augmenter le coût de production et peut même aggraver l'état de sous-production. Les procédures de sélection par agrégation (somme pondérée ou autres opérations similaires) sont difficilement applicables, puisqu'elles

exigent des critères comparables (homogènes), normalisables et non antagonistes (Taherdoost and Madanchian, 2023). Ce qui n'est pas le cas des HRES. Il existe des approches par décomposition qui ne requièrent pas de fonction d'agrégation dans la sélection multicritère. Pour ces approches, les critères comparables sont placés dans le même niveau hiérarchique jusqu'à ce que tous les critères soient hiérarchisés. Les choix sont comparés entre eux en utilisant les critères hiérarchisés du plus prioritaire aux moins prioritaires (Taherdoost and Madanchian, 2023). Ces approches supposent qu'il existe une hiérarchisation des critères et qu'un choix reste valable même s'il satisfait à peine les critères les moins prioritaires. Dans le choix d'une configuration HRES, il est difficile d'établir une priorisation des critères. En effet, le coût de production, l'apport de l'énergie renouvelable et la sous-production d'énergie sont intimement reliés et on ne peut pas les classer selon un ordre hiérarchique.

Optimisation multi-objectif : Si les critères de sélection sont antagonistes et de priorité égale, on peut alors les considérer comme des objectifs et de traiter le problème résultant comme un problème d'optimisation multi-objectif (Sharma and Kumar, 2022). Ainsi, on réalise à la fois le réglage des paramètres du HRES et le choix d'une configuration. De plus, bien des techniques de solution multi-objectives n'exigent pas l'agrégation ou la priorisation des critères de sélection. Le résultat de l'optimisation est un ensemble de configurations qui sont non dominées par d'autres configurations. Les configurations non dominées sont celles qui ont les meilleures valeurs pour au moins un objectif mais pas nécessairement pour tous les objectifs. La cardinalité de l'ensemble non dominé est généralement beaucoup plus petite que l'ensemble des configurations possibles d'un HRES. Ainsi, on peut sélectionner facilement une configuration non dominée parmi l'ensemble. Pour la suite de cette thèse, on écrira le « dimensionnement » du HRES pour désigner le problème d'optimisation multi-objectif et les techniques de solution associées.

0.2 Modélisation du problème

La configuration d'un HRES peut être représentée par un vecteur de décision discret x. De plus, une configuration x est acceptable si elle atteint simultanément les objectifs du problème. Nous avons identifié trois (3) qui sont couramment rencontrées dans la littérature (Memon, Upadhyay, and Patel, 2021; Mansouri Kouhestani, Byrne, Johnson, Spencer, Brown, Hazendonk, and Scott, 2020; Baidas, Almusailem, Kamel, and Alanzi, 2022) et ils sont :

- coût actualisé de l'énergie à minimiser, $\min \mathrm{LCOE}(\mathrm{x})$;
- fraction d'énergie renouvelable à maximiser, $\max \mathrm{REF}(\mathrm{x})$;
- probabilité de perte de puissance à minimiser, $\min \mathrm{LPSP}(\mathrm{x})$.

Ainsi, le problème du dimensionnement peut être représenté par le modèle suivant :

$$\begin{aligned} & \min_{\mathrm{x}\in\mathrm{X}} \mathrm{LCOE}(\mathrm{x}), \\ & \min_{\mathrm{x}\in\mathrm{X}} \mathrm{LPSP}(\mathrm{x}), \\ & \max_{\mathrm{x}\in\mathrm{X}} 1 - \mathrm{REF}(\mathrm{x}), \\ \text{sujet à} \quad & x_i^{(L)} \leq x_i \leq x_i^{(U)}, \quad i = 1, 2, \ldots, n. \end{aligned} \tag{0.1}$$

où $\mathrm{x} = (x_1, x_2, \ldots, x_n)$ est une configuration, $x_i^{(L)}, x_i^{(U)}$ sont les bornes inférieures et supérieures de la variable de décision x_i. Dans cette thèse, les variables décisions sont le nombre de panneaux photovoltaïques (N_{PV}), le nombre de turbines éoliennes (N_{WT}), la capacité du banc de batteries (C_{BESS}), et éventuellement la puissance installée du générateur d'appoint P_{DG}. Enfin, X est l'ensemble des configurations possibles. À noter que X est déterminé par des contraintes physiques, techniques et économiques du projet.

0.2.1 Coût actualisé de l'énergie

Le coût actualisé de l'énergie LCOE, en $\$/kWh$, est le coût moyen de l'énergie produite par le système. Une configuration HRES doit avoir un LCOE plus petit que le coût de l'énergie achetée sur le réseau ou à un coût acceptable pour les HRES sans raccordement au réseau public d'Hydro-Québec. Le coût actualisé du HRES est défini comme étant le rapport du coût total du système $\mathbb{C}_{\text{Total}}$ (en \$) sur la somme de la demande de charge à tout instant t ($P_L(t)$ en kWh). Dans cette thèse, nous considérons les données horaires sur une année de 365 jours, équivalent à 8760 données horaires. Ainsi, nous pouvons écrire :

$$\text{LCOE(x)} = \frac{\mathbb{C}_{\text{Total}}\,(\text{x})}{\sum_{t=1}^{8760} P_L(t)} \tag{0.2}$$

Le coût total du système implique le coût du capital $\mathbb{C}_{\text{Capital}}$, les coûts de remplacement $\mathbb{C}_{\text{Remp}}$ et les coûts d'opération et de maintenance $\mathbb{C}_{\text{Op\&Maint}}$. Le coût total s'écrit donc par :

$$\mathbb{C}_{\text{Total}} = \mathbb{C}_{\text{Capital}} + \mathbb{C}_{\text{Remp}} + \mathbb{C}_{\text{Op\&Maint}} \tag{0.3}$$

Le coût en capital est la somme du produit du coût initial $\mathbb{C}^{j}_{\text{initial}}$ de chaque équipement j par son facteur de recouvrement $\text{CRF}\left(r, m_j\right)$. Le facteur de recouvrement d'un composant j traduit l'investissement initial de chaque équipement j en une charge annuelle équivalente, en fonction du taux de rendement interne r et de sa durée de vie m_j, ce qui permet de comparer et d'agréger les coûts dans l'analyse économique globale du système.

$$\mathbb{C}_{\text{Capital}} = \sum_{j} \mathbb{C}^{j}_{\text{initial}} \times \text{CRF}\left(r, m_j\right), \tag{0.4}$$

où $\mathrm{CRF}\left(r, m_j\right) = \frac{r(1+r)^m}{(1+r)^{m_{j-1}}}$ et $\mathbb{C}^j_{\text{initial}} = \mathrm{Cap}_j \times \mathbb{C}^j_{\text{unit}}$. Les termes Cap_j et $\mathbb{C}^j_{\text{unit}}$ sont respectivement la capacité énergétique et le coût unitaire des composants. Le coût de remplacement $\mathbb{C}_{Remp}$ de l'équation (0.3) est ajouté pour compenser le dysfonctionnement d'un composant. Généralement pris en compte lorsque la durée de vie du système m_s est plus grande que la durée de vie du composant m_j . Ce coût de remplacement est :

$$\mathbb{C}_{\text{Remp}} = \sum_j \mathbb{C}^j_{\text{initial}} \times \frac{\left(m_s - m_j\right)}{m_j}, \quad m_s > m_j. \tag{0.5}$$

Quant au coût d'opération et de maintenance $\mathbb{C}_{\text{Op\&Maint}}$, il est le principal coût pour le fonctionnement du HRES (Mahmoud et al., 2022). Il renferme le coût d'opération (ou de maintenance) à l'heure de chaque composant $\mathbb{C}^j_{\text{Op\&Maint}}$ et la durée de l'opération et la maintenance $t^j_{\text{Op\&Maint}}$. La relation reliant ces deux quantités est donnée par :

$$\mathbb{C}_{\text{Op\&Maint}} = \sum_j \mathbb{C}^j_{\text{Op\&Maint}} \times t^j_{\text{Op\&Maint}}. \tag{0.6}$$

0.2.2 Probabilité de perte de puissance

La probabilité de perte de puissance LPSP (en %) est généralement utilisée pour mesurer la fiabilité du HRES. Elle exprime la quantité de sous-production d'énergie produite par le système en comparaison à la demande de charge. C'est la somme totale de toute la perte d'énergie observée durant une année météorologique type qui compte 8760 heures. Elle s'exprime par :

$$\mathrm{LPSP(x)} = \frac{\sum_{t=1}^{8760} \mathrm{LPS}(t)}{\sum_{t=1}^{8760} P_L(t)} \times 100 = \frac{\sum_{t=1}^{8760} (P_L(t) - P_{\text{Total}}(t))}{\sum_{t=1}^{8760} P_L(t)} \times 100 \tag{0.7}$$

où $P_L(t)$ et $\mathrm{LPS}(t) = P_L(t) - P_{\text{Total}}(t)$ sont respectivement la demande de charge et la perte d'énergie à l'instant t. Lors du fonctionnement du HRES, lorsque l'énergie fournie par le système

PV/WT est incapable de satisfaire la demande de charge, alors l'énergie disponible dans la batterie est utilisée pour alimenter les charges. En cas d'insuffisance malgré les batteries, le générateur diesel est utilisé pour alimenter les charges avec la contrainte de carburant définie. Lorsque toute cette énergie disponible $P_{\text{Total}}\,(t)$ ne satisfait pas la demande de charge, alors nous avons une perte de puissance LPS. Le seuil acceptable pour la fiabilité d'un système hybride d'énergie renouvelable est habituellement réglé à 5 % (Mansouri Kouhestani et al., 2020).

0.2.3 Fraction d'énergie renouvelable

La fraction d'énergie renouvelable (REF), exprimée en pourcentage (%), est un indicateur permettant de mesurer la part d'énergie produite à partir de sources renouvelables dans chaque système énergétique. La REF contribue à quantifier les progrès vers des objectifs énergétiques plus durables (Al-Quraan and Al-Mhairat, 2024). La combinaison de la REF avec l'analyse de l'efficacité totale du système permet de déterminer dans quelle mesure l'ajout de capacités renouvelables réduit la consommation de combustibles fossiles. La fraction d'énergie renouvelable est définie comme le rapport de l'énergie produite par les sources renouvelables à la consommation totale d'énergie :

$$\text{REF(x)} = \frac{\sum_{t=1}^{8760} P_{\text{renewable}}\,(t)}{\sum_{t=1}^{8760} P_{\text{Total}}\,(t)} \times 100 = \frac{\sum_{t=1}^{8760} (P_{\text{WT}}(t) + \eta_{\text{PV}} \times P_{\text{PV}}(t))}{\sum_{t=1}^{8760} (P_{\text{WT}}(t) + \eta_{\text{PV}} \times P_{\text{PV}}(t) + P_{\text{GRID}}(t) + P_{\text{DG}}(t))} \times 100 \tag{0.8}$$

$P_{\text{WT}}(t)$ et $\eta_{\text{PV}} \times P_{\text{PV}}(t)$ représentent respectivement la quantité de production des éoliennes et des panneaux photovoltaïques à l'intant t. η_{PV} est le rendement des panneaux photovoltaïques. $P_{\text{GRID}}(t)$ et $P_{\text{DG}}(t)$ représentent la quantité d'électricité produite par le réseau et le générateur diesel au temps t.

0.3 Défis liés aux problèmes

Le domaine des systèmes hybrides d'énergie renouvelables est confronté à plusieurs défis techniques et technologiques :

- **un goulot d'étranglement calculatoire (dimensionnement exigeant en simulation)** : chaque évaluation d'une configuration typique nécessite une simulation annuelle détaillée qui est couteuse en temps de calcul ;
- **une incertitude épistémique (précision des ressources renouvelables)** : la variabilité et l'imprécision des ressources renouvelables (irradiance et vent) affectent significativement la qualité des solutions obtenues ;
- **un problème de contrôle dynamique à objectifs multiples (optimisation multicritères)** : les arbitrages en temps réel entre coût, fraction renouvelable et fiabilité ne peuvent pas être capturés efficacement par les méthodes d'optimisation classiques.

0.4 Objectif général de la recherche

La détermination de la configuration adéquate sujette à des contraintes pour HRES se présente comme un défi majeur à l'utilisation des énergies renouvelables. De ce fait, il nous faut concevoir une méthode qui est rapide et précise pour le dimensionnement optimal des systèmes hybrides d'énergies renouvelables.

0.5 Objectif spécifiques

Afin d'atteindre l'objectif général de cette recherche, nous proposons les objectifs spécifiques ci-dessous.

- **Objectif I** : proposer une nouvelle approche disruptive permettant de surmonter le verrou technico-computationnel des simulations des HRES ;
- **Objectif II** : proposer une méthode de réduction des incertitudes liées à la variabilité des ressources renouvelables ;
- **Objectif III** : concevoir une nouvelle approche de dimensionnement multicritère, évolutive, capable de s'adapter aux conditions météorologiques changeantes, ainsi qu'aux contextes variants de chaque pro sommateurs.

En combinant, optimisation multicritère, évolutivité et adaptation, cette thèse vise à rendre le dimensionnement et l'exploitation des systèmes hybrides d'énergie renouvelable scalables, robustes et réellement adaptatifs, conditions préalables à un futur électrique décarboné et pourtant fiable.

0.6 Organisation de la thèse et contributions originales

Cette thèse est une thèse par articles organisés comme suit :

Partie I – Fondations

Introduction

La présente introduction établit le cadre conceptuel de la thèse. Elle clarifie les objectifs poursuivis, les innovations proposées et la manière dont les articles articulés répondent, pas à pas aux verrous techniques identifiés.

Chapitre 1 : Revue de la littérature

Ce chapitre présente une vue d'ensemble de la littérature mettant en évidence les approches classiques (modèles réduits, exécution parallèle, métaheuristiques) comme les avancées récentes

(apprentissage automatique, recherche d'architectures neuronales, apprentissage par renforcement profond), tout en soulignant leurs limites et les défis encore ouverts auxquels répondent les contributions de cette thèse.

Partie II – Travaux de recherche et développements méthodologiques

Cette partie constitue le noyau central de cette thèse. Elle regroupe l'ensemble des étapes qui exposent, de manière progressive et structurée, les problématiques abordées, les méthodologies proposées ainsi que les résultats obtenus. Chaque section illustre une ou plusieurs contributions scientifiques spécifiques et met en évidence la valeur ajoutée des approches développées au regard des objectifs de recherche initiaux. L'enchaînement de ces étapes reflète une logique évolutive, allant de la réduction du coût computationnel lié aux simulations, vers la réduction de l'incertitude inhérente aux données d'entrée par la prévision de l'irradiance solaire, pour finalement déboucher sur une optimisation dynamique et multicritères par apprentissage par renforcement profond.

Étape 1 : proposer une nouvelle approche disruptive permettant de surmonter le verrou technico-computationnel des simulations des HRES.

Problématique : le dimensionnement des systèmes hybrides d'énergies renouvelables repose traditionnellement sur des outils de simulation détaillés, tels que HOMER ou Simulink. Ces approches permettent d'évaluer les performances techniques et économiques de milliers de configurations possibles, mais elles présentent un inconvénient majeur : des temps de calcul extrêmement élevés. En effet, l'exploration exhaustive de l'espace des solutions devient rapidement impraticable dès que le nombre de sources, de profils de consommation ou de contraintes augmente. Cette lourdeur computationnelle constitue un véritable goulot d'étranglement qui ralentit la sélection des topologies adéquates et limite l'applicabilité pratique des méthodes classiques de dimensionnement.

Contributions apportées : répondre à la problématique de cette étape a nécessiter le développement d'une méthode hybride combinant la recherche arborescente déterministe (Branch and Bound) et la classification par plus proches voisins (k-Nearest Neighbors). L'objectif est de réduire le temps nécessaire à l'évaluation exhaustive des configurations de systèmes hybrides d'énergies renouvelables. L'approche exploite les capacités de Branch and Bound pour explorer efficacement l'espace de recherche tout en utilisant KNN pour élaguer des groupes de configurations jugées non prometteuses.

Les résultats expérimentaux, obtenus sur plusieurs ensembles de configurations (330 à 5390 configurations), démontrent des gains significatifs : une réduction du temps de simulation allant de 45,85 % à 94,68 % et une précision comprise entre 83,36 % et 97,25 %. Ces résultats montrent que l'approche permet d'accélérer le processus décisionnel sans compromettre la fiabilité des choix.

Ce travail répond ainsi à l'**objectif I** de la thèse, en atténuant le goulot d'étranglement computationnel lié aux méthodes classiques de dimensionnement basées sur la simulation.

Publications associées :

- **Journal** : Reduction in microgrid topology selection time via hybrid Branch and Bound and k-Nearest Neighbors techniques, publié dans la revue avec comité de lecture Mathematics, 2025 (**Chapitre 2**).
- **Conférence avec comité de lecture** : Practical Cost-Effectiveness Analysis for Solar Energy Systems, présenté à la conférence avec comité de lecture IEEE CPE-POWERENG, 2024.

Étape 2 : proposer une méthode de réduction des incertitudes liées à la variabilité des ressources renouvelables.

Problématique : bien que l'approche hybride présentée à l'étape précédente ait permis de réduire significativement le temps de sélection des topologies HRES, elle demeure fortement dépendante

de la qualité des données d'entrée utilisées dans les simulations. Or, l'un des paramètres les plus critiques pour la performance des systèmes photovoltaïques est l'irradiance solaire globale horizontale. La variabilité temporelle et spatiale de cette ressource entraîne une forte incertitude dans les évaluations énergétiques et économiques. Une mauvaise estimation du GHI conduit à des erreurs de dimensionnement, à des surcoûts d'investissement ou à une fiabilité insuffisante du système. Les méthodes de prédiction existantes, qu'elles soient statistiques ou basées sur des modèles neuronaux, présentent deux limites majeures :

1. Une rigidité des architectures, qui ne s'adaptent pas aux changements des conditions opérationnelles ;
2. Une exigence computationnelle élevée, notamment dans les approches NAS classiques, qui ralentit la recherche d'architectures performantes.

Contributions apportées : dans la continuité de l'étape 1 de cette recherche, cette étape traite de la prévision de l'irradiance solaire globale horizontale. L'approche proposée repose sur une combinaison innovante dea trois techniques ci-dessous.

1. *Neural Architecture Search (NAS)* pour explorer automatiquement des modèles neuronaux adaptés,
2. *Transfer Learning (TL)* pour réutiliser l'expérience de modèles préalablement entraînés et réduire les coûts d'apprentissage,
3. *Dynamic Search Space (DSS)* pour restreindre progressivement l'espace de recherche autour des solutions prometteuses.

Cette méthodologie permet de concevoir des modèles LSTM prédictifs tout en diminuant considérablement la charge computationnelle. Les résultats montrent une réduction du temps

de recherche allant jusqu'à 89,09 % selon les algorithmes évolutifs employés, ainsi qu'une amélioration de précision de l'ordre de 99 % par rapport aux approches NAS classiques.

Ce travail répond à l'**objectif II** de la thèse en apportant une solution robuste et efficace pour la réduction des incertitudes, clé de voûte du dimensionnement et de la gestion opérationnelle des systèmes photovoltaïques.

Publications associées :

- **Journal** : Enhancing Neural Architecture Search Using Transfer Learning and Dynamic Search Spaces for Global Horizontal Irradiance Prediction, publié dans la revue avec comité de lecture Forecasting, 2025 (**Chapitre 3**).
- **Conférence avec comité de lecture** : Horizontal Global Solar Irradiance Prediction Using Genetic Algorithm and LSTM, présenté à la conférence avec comité de lecture IEEE ICIEA, 2024.

Étape 3 : concevoir une nouvelle approche de dimensionnement multicritères, évolutive, capable de s'adapter aux conditions météorologiques changeantes, ainsi qu'aux contextes variants de chaque pro sommateurs.

Problématique : les méthodes développées aux étapes précédentes ont permis, d'une part, d'accélérer le processus de sélection des topologies optimales (étape 1), et d'autre part, de fiabiliser les données d'entrée grâce à la prédiction du rayonnement solaire (étape 2). Cependant, ces approches restent fondamentalement statiques, car elles aboutissent à un dimensionnement fixé à partir d'un jeu de données ou de scénarios donnés. Or, dans un contexte réel, les systèmes hybrides d'énergies renouvelables sont soumis à une variabilité permanente :

- fluctuations des profils de consommation,
- changements rapides des conditions météorologiques,
- variations des coûts énergétiques et des politiques tarifaires,

- contraintes opérationnelles et technico-économiques liées au stockage et aux générateurs externes.

Les approches classiques d'optimisation (simulation exhaustive, métaheuristiques comme PSO ou GA, ou encore méthodes déterministes) peinent à intégrer cette dynamique en temps réel. Elles nécessitent souvent un recalibrage manuel à chaque nouvelle situation, ce qui limite leur efficacité et leur applicabilité pratique. Ainsi, il devient nécessaire de développer une méthodologie adaptative et évolutive, capable de gérer simultanément plusieurs critères contradictoires et de s'ajuster automatiquement aux changements de l'environnement.

Contributions apportées : après avoir réduit les temps de simulation (étape 1) et amélioré la qualité des données d'entrée via la prédiction du GHI (étape 2), l'étape 3 s'attaque à la problématique de la gestion globale, adaptative et en temps réel des HRES. L'approche repose sur un agent d'apprentissage par renforcement profond (DRL) interagissant avec l'environnement énergétique et optimisant une fonction de récompense multicritères intégrant :

- le coût actualisé de l'énergie (LCOE),
- la fraction d'énergie renouvelable (REF),
- la fiabilité du système (LPSP).

Cette méthodologie permet à l'agent d'apprendre de façon autonome et continue, sans nécessiter de recalibrage manuel, et de s'adapter aux variations de consommation, aux incertitudes météorologiques et aux contraintes technico-économiques. Les résultats expérimentaux montrent une réduction du coût énergétique de 21,33 % à 30,09 % selon les profils de consommation, tout en augmentant la part d'énergie renouvelable et en renforçant la stabilité du système.

Ainsi, ce chapitre atteint l'**objectif III** de la thèse en proposant une approche flexible, évolutive et résiliente adaptée aux conditions opérationnelles réelles des HRES.

Publications associées :

- **Journal** : Deep Reinforcement Learning Approach for Hybrid Renewable Energy Systems Optimization, publié dans la revue avec comité de lecture Engineering Applications of Artificial Intelligence, 2025 (**Chapitre 4**).
- **Journal** : Parameter Sensitivity Analysis of Generators and Grid-connected Constraints in Hybrid Microgrids Using Deep Reinforcement Learning, soumis à la revue avec comité de lecture Applied Sciences, 2025.

Partie III – Conclusion et perspectives

Cette thèse se conclut par un récapitulatif sur la portée des trois contributions : i) la réduction drastique du temps de sélection des topologies HRES par l'hybride BB-kNN ; ii) l'amélioration de la prévision des ressources via un NAS enrichi par TL et DSS et iii) le dimensionnement dynamique multicritère grâce au DRL.

Au-delà des gains démontrés en coût énergétique, en part renouvelable et en fiabilité, plusieurs pistes se dégagent : généraliser les modèles à d'autres contextes climatiques, intégrer des marchés de flexibilité (tarifs dynamiques, stockage thermique ou hydrogène) et coupler l'agent DRL à des jumeaux numériques en ligne pour un recalibrage continu. Ces perspectives ouvrent la voie à des microréseaux véritablement autonomes, sobres en carbone et robustes face aux incertitudes futures.

0.7 Limites de la recherche

Cette recherche se concentre sur un périmètre clairement défini afin de développer, tester et valider des méthodologies novatrices d'optimisation des systèmes hybrides d'énergies renouvelables. Les limites retenues dans ce travail sont les énumérées ci-dessous.

- **Technologies considérées** : les systèmes étudiés intègrent exclusivement des panneaux photovoltaïques (PV), des éoliennes (WT), des batteries (BESS) comme solution de stockage, et comme source de secours, un générateur diesel (GD) et le réseau public. D'autres sources renouvelables ou options de stockage ne sont pas incluses dans le cadre de cette recherche.
- **Objectifs de performance** : les contributions se concentrent principalement sur trois dimensions clés :
  1. la réduction du temps de simulation pour la sélection des topologies,
  2. la prédiction fiable du rayonnement solaire global horizontal,
  3. l'optimisation dynamique et multicritères (LCOE, REF, LPSP) par apprentissage par renforcement profond.

  Les autres aspects de performance, tels que l'impact environnemental détaillé, la résilience aux défaillances matérielles ou la planification à long terme des infrastructures, ne sont pas abordés.
- **Données et contexte étudiés** : les validations sont effectuées à partir de données représentatives issues de profils de consommation et de bases de données climatiques (irradiance solaire, vent) disponibles. La recherche ne prétend pas couvrir l'ensemble des contextes géographiques ou des environnements réglementaires.
- **Niveau d'analyse** : les travaux portent sur la phase de conception et d'optimisation des HRES. Les aspects liés à la mise en œuvre pratique, à l'exploitation en conditions industrielles réelles ou à l'intégration dans des réseaux de grande échelle dépassent le champ de cette recherche.

CHAPITRE 1

REVUE DE LITTÉRATURE

1.1 Introduction

La transition énergétique mondiale s'appuie de plus en plus sur les énergies renouvelables (solaire, éolien, biomasse, hydraulique, géothermie), tant pour réduire la dépendance aux combustibles fossiles que pour atténuer les émissions de gaz à effet de serre. Cependant, en dépit de leur caractère propre, ces sources demeurent caractérisées par une production intermittente et variable selon la météo et les saisons, ce qui rend nécessaire la mise en place de solutions assurant une fourniture continue d'électricité (Kavadias and Triantafyllou, 2021). C'est dans ce contexte qu'apparaissent les systèmes hybrides d'énergie renouvelable (HRES), qui combinent une ou plusieurs sources renouvelables à des unités de stockage (batteries, volants d'inertie), à des générateurs d'appoint (diesel, gaz naturel) et au réseau principal. Cette complémentarité vise à assurer la fiabilité du réseau tout en minimisant l'empreinte carbone (Alluraiah and Vijayapriya, 2023).

Le dimensionnement de ces HRES représente un défi majeur : d'une part, il s'agit de déterminer la taille optimale de chaque composant afin de répondre à la demande énergétique prévue, et d'autre part, il faut ajouter des marges de sécurité pour pallier les aléas (Baghaee, Mirsalim, Gharehpetian, and Talebi, 2016; Tounsi, 2022). Dans la pratique, on inclut souvent un générateur thermique pour desservir les charges critiques (hôpitaux, stations de pompage), tout en limitant sa puissance afin de réduire la consommation de combustibles fossiles et les émissions de CO_2 (Kavadias and Triantafyllou, 2021).

Ce chapitre synthétise les approches de la littérature en suivant une logique de décision allant du dimensionnement statique vers des stratégies plus adaptatives. Il est structuré comme suit :

- la chaîne de dimensionnement et les familles d'outils de décision (Section 1.2) ;
- les leviers d'accélération et d'automatisation (modèles rapides, apprentissage automatique) (Secton 1.3) ;

- la conception/optimisation des HRES et les critères de sélection (Section 1.4) ;
- l'analyse de sensibilité et les paramètres dominants (Section 1.5).

1.2 Dimensionnement d'un système hybride d'énergie renouvelable

Le dimensionnement d'un HRES se découpe classiquement en trois étapes successives, chacune reposant sur des outils et des méthodologies spécifiques. Ces étapes se fondent sur une catégorisation des outils de décision et visent à construire une chaîne de calcul cohérente, de la création des scénarios à la sélection finale de la configuration optimale.

1.2.1 Catégorisation des outils de décision

Dans un premier temps, il importe de choisir les outils adaptés à chaque étape du processus de décision. La littérature identifie quatre grandes familles.

- **Outils d'analyse de préfaisabilité** : ces logiciels fournissent une évaluation rapide des grandes lignes d'un HRES, en s'appuyant sur des règles empiriques et des données météorologiques de base. Ils permettent notamment de vérifier si la ressource solaire ou éolienne est suffisante pour justifier l'investissement initial (Kavadias and Triantafyllou, 2021).
- **Outils de dimensionnement** : leur objectif est de déterminer les dimensions exactes des composantes (nombre de panneaux PV, nombre de turbines éoliennes, puissance du générateur diesel, capacité de stockage), en optimisant une ou plusieurs fonctions objectifs (coût total, parts renouvelables, émissions de CO_2). On y retrouve notamment des approches métaheuristiques (algorithmes génétiques, optimisation par essaims particulaires, algorithmes génétiques à tri non dominé au sens de Pareto) qui parcourent l'espace des paramètres pour identi¬fier les configurations candidate (Mansouri Kouhestani et al., 2020; Mohamed, Eltamaly, and Alolah, 2016).
- **Outils de simulation** : ce sont généralement des logiciels propriétaires (HOMER Pro, PVsyst, PVGIS) qui prennent en entrée une structure exacte du système (composants, géolocalisation, profil de charge) et calculent, du pas de temps horaire au pas de temps journalier, la production,

les flux d'énergie entre générateur et stockage, et le bilan financier (Bahgaat, 2023; Lu et al., 2017). Ils offrent un niveau de détail élevé, mais au prix d'un temps de calcul souvent prohibitif (Banihashemi, Weber, and Lang, 2022).

- **Outils à architecture ouverte** : destinés à la recherche et au développement, ces cadres d'applications (MATLAB/Simulink, Python avec Pyomo, OpenModelica) permettent de personnaliser entièrement la structure du modèle : définir de nouvelles contraintes, ajouter des flux de matière ou simuler des stratégies de contrôle avancées (Aranguren, 2023). Ils sont particulièrement prisés pour évaluer des solutions innovantes ou hybrides, non pris en charge par les logiciels commerciaux.

Cette classification guide la sélection de l'environnement de travail le plus approprié, en fonction du degré d'incertitude à traiter, du temps disponible et de la complexité souhaitée dans la modélisation (Kavadias and Triantafyllou, 2021).

1.2.2 Étapes clés du dimensionnement

Une fois les outils choisis, le processus de dimensionnement se décompose classiquement en trois étapes complémentaires et successives.

- **Étape 1 : Génération de scénarios** - pour pouvoir explorer l'espace des solutions, il est nécessaire de créer un ensemble de configurations plausibles. Cela implique :
  - la sélection des sources renouvelables disponibles (photovoltaïque, éolien, biomasse, hydraulique),
  - l'estimation du profil de charge (urbain, rural, industriel),
  - la définition des contraintes locales (coût d'investissement maximal, surface au sol, réglementation environnementale, émissions de CO_2 admissibles).

  Des méthodes telles que les algorithmes génétiques, la simulation de Monte-Carlo ou les graphes probabilistes sont employées pour générer des échantillons de configurations réalistes et couvrir les incertitudes inhérentes aux données météorologiques et aux profils de charge (Alluraiah and Vijayapriya, 2023; Liu, Wang, Cao, Ma, Wang, Li, Liu, and

Zou, 2023a). Par exemple, Al-Ghussain, Samu, Taylan, and Fahrioglu (2020) utilisent une approche de Monte Carlo pour modéliser l'aléa éolien, tandis que Zhang, Qin, Li, Liu, Yao, Wang, Wang, Pei, and Zhou (2020) emploient un algorithme génétique à multiple objectifs afin de produire un jeu de scénarios diversifiés prenant en compte le coût et la fiabilité.

- **Étape 2 : Simulation des configurations** - chaque scénario généré est alors soumis à un simulateur (HOMER Pro, PVGIS, Simulink) pour estimer sa performance énergétique, économique et environnementale (Bahgaat, 2023; Lu et al., 2017). Au sein de cette phase, on intègre souvent un algorithme d'optimisation (PSO, MOPSO, GA, recuit simulé) pour ajuster localement les paramètres (nombre de batteries, puissance du générateur) afin de minimiser le coût total ou maximiser la part d'énergie renouvelable. Ainsi, Mansouri Kouhestani et al. (2020) combinent HOMER Pro avec un PSO multi-objectif pour équilibrer le LCOE et la fiabilité, tandis que Mohamed et al. (2016) associent recuit simulé et modèle Matlab pour affiner la configuration d'un système PV/éolien.
- **Étape 3 : Analyse de faisabilité** - les configurations les plus prometteuses sont ensuite évaluées selon des critères plus larges :
  - technique : disponibilité de la ressource, fiabilité du réseau, taux de défaillance des composants (Awan, Zubair, Sidhu, Bhatti, and Abo-Khalil, 2018).
  - économique : coût actualisé de l'énergie (LCOE), valeur actuelle nette (VAN), indice de profitabilité (PI) (Elkadeem, Kotb, Elmaadawy, Ullah, Elmolla, Liu, Wang, Dán, and Sharshir, 2021).
  - environnemental : émissions de CO_2 évitées, cycle de vie des équipements, empreinte carbone (HassanzadehFard, Tooryan, Dargahi, and Jin, 2021).
  - social : création d'emplois, acceptabilité locale, impact sur la qualité de vie (Awan et al., 2018). Cette étape permet de confronter les systèmes retenus aux contraintes réelles (subventions, politiques tarifaires, volatilité des prix), et de sélectionner la solution optimale selon un compromis entre ces différents indicateurs.

Ainsi, la combinaison de ces trois phases permet une exploration exhaustive des configurations potentiellement viables, garantissant ainsi une évaluation complète des différentes alternatives. Toutefois, cette exhaustivité présente plusieurs inconvénients majeurs. Elle engendre d'abord un temps de calcul très élevé, lié au grand nombre de scénarios à simuler, auquel s'ajoute une forte consommation de ressources informatiques qui peut devenir prohibitive pour des systèmes complexes. La précision des résultats reste par ailleurs tributaire de la qualité et de la disponibilité des données d'entrée, introduisant une incertitude difficile à maîtriser. Enfin, cette approche offre une faible adaptabilité aux conditions dynamiques, car les résultats obtenus demeurent figés dans le cadre des hypothèses de simulation. Ainsi, malgré ses avantages en termes de couverture de l'espace des solutions, elle reste limitée par des contraintes computationnelles, opérationnelles et pratiques qui freinent son applicabilité à grande échelle (Javed, Ma, Jurasz, and Mikulik, 2021; Rtemi, El-Osta, and Attaiep, 2023).

1.2.3 Réduction du temps de simulation

Lorsque l'on doit simuler des dizaines, voire des centaines de milliers de configurations, le temps de calcul devient rapidement rédhibitoire. Plusieurs travaux se sont alors intéressés à l'accélération des simulations, en recourant tantôt à des méthodes de réduction d'ordre, tantôt à des approches basées sur l'apprentissage automatique (ML).

1.2.4 Approches classiques de réduction d'ordre

Les méthodes de réduction d'ordre visent à simplifier les modèles physiques ou numériques, tout en conservant un niveau de précision acceptable pour évaluer la performance globale d'un HRES (Martínez-Turégano, Añó-Villalba, Bernal-Perez, and Blasco-Gimenez, 2019). Par exemple :

- modèle d'admittance : destiné initialement aux parcs éoliens en mer, il permet de réduire la complexité mathématique des équations différentielles en se concentrant sur les variables essentielles (courant, tension). Toutefois, cette approche engendre une perte de précision par négligence de certains phénomènes dynamiques fins liés aux générateurs et aux convertisseurs

(Martínez-Turégano et al., 2019). Cette faiblesse limite la représentativité des résultats en dehors de son contexte d'application initial et peine à modéliser correctement les phénomènes transitoires rapides ou les comportements fortement non linéaires.

- sous-modèles Simulink : Tounsi (2022) propose de remplacer des blocs dynamiques complexes (pales d'éolienne, convertisseur) par des versions linéarisées ou identifiées par régression, ce qui diminue significativement la durée de simulation dans Simulink. Toutefois, cette méthode demeure spécifique à chaque cas d'étude et exige une revalidation pour chaque nouvelle configuration.

1.2.5 Approches par apprentissage profond

Les approches par apprentissage profond (DL) tel que les auto-encoder apprennent à comprimer un jeu de données tout en préservant sa structure de variabilité. Dans le contexte énergétique, Banihashemi et al. (2022) utilisent un auto-encoder pour extraire les principales composantes d'un modèle de bâtiment (consommation, production PV, charge dynamique). Les sorties condensées de l'auto-encoder servent ensuite d'entrée à un simulateur léger, réduisant ainsi le temps de calcul de façon notable. Cependant, la reussite de cette approche est sujette à la condition de disposer d'un volume de données historiques représentatives et de qualité suffisante. Tenant compte du contexte spécifique de chaque pro sommateur, la collecte de données historiques universellement représentatives reste un défi majeur à relever.

1.2.6 Substitution par des modèles prédictifs (ML global)

Certaines approches vont plus loin en remplaçant entièrement la boucle de simulation par un modèle prédictif supervisé (Mange and Skowronska, 2023). Dans cette démarche, il est nécessaire de collecter préalablement un grand nombre de simulations détaillées (carte PV, profils de charge, scénario météorologique) pour entraîner un réseau de neurones ou une forêt aléatoire. Une fois entraîné, ce modèle est capable de prédire directement le résultat (LCOE, GHI, fiabilité) en quelques millisecondes, sans recourir à une simulation pas à pas. Cependant,

cette approche exige une phase d'entraînement lourde et suppose que la variabilité du jeu de données couvre l'ensemble des cas réels envisagés.

1.2.7 Limites et perspectives

Malgré l'efficacité des méthodes de réduction d'ordre, plusieurs limites subsistent :

- la dépendance à des données historiques fiables et suffisamment diversifiées pour entraîner les auto-encodeurs ou les réseaux neuronaux (Banihashemi et al., 2022; Dou, Qian, Li, Lin, Wang, Cheng, and Xu, 2021).
- le caractère spécifique de chaque étude de cas, qui nécessite de réajuster les sous-modèles ou de réentraîner les réseaux pour chaque nouvelle localisation ou configuration (Tounsi, 2022).
- l'impossibilité, dans certains cas, d'intégrer directement certains logiciels propriétaires de simulation et de dimensionnement (tels que HOMER ou PVGIS) dans la phase d'optimisation, ce qui limite la portée pratique de l'approche (Martínez-Turégano et al., 2019).

Face à ces limitations, la littérature récente propose des méthodologies hybrides combinant recherche heuristique et approches d'apprentissage automatique, sans nécessiter une construction complète du simulateur initial (Sampat, Baranwal, and Ramachandran, 2020; Zhaoqian and Edahiro, 2019). Ces stratégies consistent à :

- utiliser un échantillon réduit pour lancer des simulations complètes,
- entraîner un modèle ML sur ces résultats afin de prédire rapidement la performance de nouvelles configurations,
- affiner l'optimisation par une boucle heuristique légère (PSO, GA) qui exploite les prédictions du modèle ML pour explorer plus efficacement l'espace de recherche.

Cette combinaison permet de trouver un compromis entre précision et vitesse de calcul, tout en restant compatible avec les simulateurs commerciaux existants. Toutefois, elle présente certaines limites : la dépendance à la qualité des données issues de l'échantillon initial, le risque de perte

de précision lorsque le modèle ML est généralisé à des configurations éloignées de l'espace appris, ainsi que la nécessité d'un réglage soigneux des heuristiques (PSO, GA), dont l'efficacité reste sensible aux paramètres choisis.

1.3 Prédiction de l'irradiance solaire et recherche d'architectures neuronales

Un élément crucial du dimensionnement des HRES est l'estimation fine du rayonnement solaire, souvent exprimé par le Global Horizontal Irradiance (GHI). Une prévision précise du GHI permet d'anticiper la production PV, d'ajuster la stratégie de stockage, et d'améliorer la fiabilité de l'ensemble du système. En effet, une estimation imprécise du GHI peut conduire soit à un surdimensionnement coûteux des équipements, soit à un sous-dimensionnement compromettant la continuité d'alimentation. De plus, comme le GHI est fortement influencé par la variabilité météorologique (nuages, saisons, conditions locales), sa prédiction constitue un facteur déterminant pour réduire l'incertitude dans la planification et assurer une gestion énergétique optimale (Legrene et al., 2024a).

1.3.1 Formulation du GHI

Le GHI se calcule habituellement à partir des composantes suivantes (equation 1.1) :

$$\mathrm{GHI} = \mathrm{DNI} \times \cos(\varphi) + \mathrm{DHI} + \kappa \times \mathrm{GHR} \tag{1.1}$$

où :

- DNI (Direct Normal Irradiance) est le rayonnement solaire direct reçu perpendiculairement aux rayons du soleil,
- DHI (Diffuse Horizontal Irradiance) est le rayonnement diffus réfléchi par l'atmosphère,
- GHR (Ground-Reflected Irradiance) exprime la fraction du rayonnement solaire réfléchie par le sol (albédo),

- φ est l'angle zénithal du soleil (l'angle entre la verticale et la direction du soleil) (Chinnavornrungsee, Kittisontirak, Chollacoop, Songtrai, Sriprapha, Uthong, Yoshino, and Kobayashi, 2023).
- κ est un coefficient sans dimension (facteur de pondération, souvent assimilé à un albédo effectif) qui ajuste la contribution de la composante réfléchie par le sol (GHR) dans le calcul du GHI ($0 \leq \kappa \leq 1$),

1.3.2 Sources de données historiques et enjeux

Les bases de données comme la National Solar Radiation Database (NSRDB) ou MERRA-2 (NASA) offrent des séries horaires ou journalières de GHI, mais leur résolution spatiale et temporelle peut parfois s'avérer insuffisante, surtout dans les zones présentant une forte variabilité locale (OpenWeather, 2021). Par conséquent, de nombreux auteurs se tournent vers des techniques d'apprentissage profond pour combler ces manques, en intégrant des variables météorologiques auxiliaires (température, humidité, couverture nuageuse) et des images satellitaires (Haider, Sajid, Sajid, Uddin, and Ayaz, 2022; Shawki, Nunez, Obeid, and Picone, 2021).

1.3.3 Techniques l'apprentissage profond pour la prévision du GHI

Plusieurs approches de réseaux de neurones sont mises en œuvre pour prédire le GHI :

- réseaux convolutionnels (CNN) : adaptés au traitement d'images satellitaires, ils extraient efficacement des caractéristiques spatiales et temporelles (Chen, Huang, Cai, Shen, and Lu, 2020). Leur principal avantage réside dans leur capacité à capter automatiquement des motifs complexes à différentes échelles, ce qui améliore la précision des prévisions même dans des environnements hétérogènes. Toutefois, ces modèles requièrent généralement de larges volumes de données annotées et une puissance de calcul élevée, et ils peuvent souffrir d'un manque de généralisabilité lorsqu'ils sont appliqués à des régions ou à des conditions climatiques différentes de celles utilisées pour l'entraînement.
- réseaux récurrents (LSTM, GRU) : ils modélisent les séries temporelles en traitant les dépendances à long terme entre les pas de temps (Haider et al., 2022). Leur structure

permet de mieux capturer la dynamique séquentielle du GHI et d'intégrer des corrélations sur plusieurs horizons temporels, ce qui améliore la qualité des prévisions. Toutefois, l'entraînement de ces réseaux reste coûteux en temps de calcul et sensible au problème du gradient évanescent ou explosif, et leurs performances peuvent se dégrader face à des séries très bruitées ou présentant des variations abruptes.

- modèles hybrides CNN–LSTM : combinent l'extraction spatiale des caractéristiques par CNN et la modélisation temporelle des dépendances par LSTM, ce qui permet d'obtenir des prévisions horaires plus robustes et précises (Chinnavornrungsee et al., 2023). Cette approche exploite à la fois la richesse des données satellitaires et la dynamique séquentielle du GHI, renforçant ainsi la capacité de généralisation. Néanmoins, l'intégration de deux architectures profondes accroît la complexité du modèle, requiert des ressources computationnelles importantes, et peut exposer l'entraînement au risque de surapprentissage lorsque la quantité de données disponibles est limitée.

De plus, la performance de ces modèles reste fortement tributaire de la structure du réseau et de l'ajustement de ses hyperparamètres, ce qui implique une phase d'expérimentation longue et laborieuse (Shawki et al., 2021).

1.3.4 Fouille d'architecture neuronale

La performance d'un réseau de neurones dépend fortement de sa structure (nombre de couches, type d'opérations, hyperparamètres). Déterminer manuellement cette structure reste un processus complexe, chronophage et hautement dépendant de l'expertise humaine. De plus, la meilleure architecture varie selon la nature des données, l'horizon de prédiction et les contraintes de calcul. Pour pallier ces limites, la fouille d'architecture neuronale (Neural Architecture Search – NAS) a émergé comme une solution permettant d'explorer automatiquement et de manière algorithmique l'espace des architectures possibles. Les approches principales incluent :

- algorithmes évolutifs : par exemple, Liu, Simonyan, Vinyals, Fernando, and Kavukcuoglu (2017) propose un algorithme hiérarchique qui optimise séquentiellement la profondeur et la

largeur des couches, tandis que Niu, Li, Zhang, and Kang (2019) introduisent PNAS basé sur le *particle swarm optimization* (PSO) pour la classification CIFAR-10. Ces méthodes se distinguent par leur capacité d'exploration massive et leur robustesse face à des espaces de recherche complexes. Toutefois, elles nécessitent un grand nombre d'évaluations de modèles, ce qui entraîne des temps de calcul très élevés et limite leur applicabilité pratique.

- approches bayésiennes : PC-DARTS (Xu, Xie, Zhang, Chen, Qi, Tian, and Xiong, 2019) illustre cette catégorie en utilisant une approximation continue de l'espace d'architecture, permettant une exploration plus rapide qu'une recherche exhaustive. Ces méthodes offrent une convergence plus efficace et intègrent naturellement la gestion de l'incertitude. En revanche, elles restent sensibles au choix des fonctions de vraisemblance et peuvent explorer de manière incomplète des espaces de grande dimension.
- méthodes basées sur l'apprentissage par renforcement : Ding, Chen, Li, Zhao, Sun, and Chen (2022) développe BNAS, qui emploie un agent RL pour sélectionner dynamiquement les opérations de convolution et de pooling. Ces approches présentent l'intérêt d'adapter progressivement les choix architecturaux en fonction d'une récompense, améliorant la qualité des architectures découvertes. Cependant, leur principal inconvénient réside dans leur coût computationnel très élevé, car l'agent doit évaluer un grand nombre de candidats avant d'atteindre une politique stable.

En résumé, ces stratégies visent à équilibrer l'exploration (tester un large éventail d'architectures) et l'exploitation (affiner les architectures prometteuses), tout en réduisant le nombre d'itérations coûteuses (Chitty-Venkata, Emani, Vishwanath, and Somani, 2022; Elsken, Metzen, and Hutter, 2019). Néanmoins, les approches NAS classiques demeurent limitées par une consommation excessive de ressources de calcul, une dépendance à de vastes ensembles de données d'entraînement et une difficulté à s'adapter dynamiquement à des conditions changeantes. Ces lacunes justifient le développement de méthodologies hybrides et adaptatives visant à rendre la recherche d'architecture plus rapide, plus précise et plus robuste.

1.3.5 Méthodologie hybride adaptative

Récemment, plusieurs études proposent des méthodes hybrides alliant transfert d'apprentissage et extrapolation des courbes d'entraînement afin d'éliminer précocement les architectures sous-optimales (Duan, Zuo, Bai, Chang, Chen, Wang, Ma, and Chen, 2023; Gallo, Castangia, Macii, Macii, Patti, and Aliberti, 2022; Niccolai, Orooji, Matteri, Ogliari, and Leva, 2022). Le principe est le suivant :

- phase d'exploration initiale : un sous-ensemble réduit d'architectures est entraîné durant quelques époques pour obtenir des courbes de pertes partielles.
- extrapolation des performances : à partir des premières valeurs de la courbe d'apprentissage, on prédit la performance finale théorique de l'architecture (Duan et al., 2023).
- transfert d'apprentissage : les poids des couches communes entre architectures parentes et nouvelles architectures sont transférés, réduisant le temps d'entraînement (Gallo et al., 2022).
- élagage progressif : les architectures dont l'extrapolation indique une performance médiocre sont éliminées, et seules les plus prometteuses poursuivent l'entraînement.

Appliqué à la prévision du GHI, ce cadre permet d'obtenir des modèles précis en un temps significativement réduit par rapport à une recherche exhaustive (Niccolai et al., 2022).

1.4 Conception et dimensionnement des HRES

Après avoir précisé les méthodes de simulation rapide et les techniques de prédiction du GHI, il convient d'examiner la littérature concernant la conception proprement dite des HRES, c'est-à-dire la sélection des composants, des topologies et des algorithmes d'optimisation.

1.4.1 Diversité des composants et topologies

Les études révèlent une grande hétérogénéité dans le choix des composants.

- Sources renouvelables : photovoltaïque (PV), éolien terrestre (WT), éolien offshore, biomasse, petites centrales hydro (Faria et al., 2023; Samy, Sarhan, Barakat, and Al-Ghamdi, 2018).
- Systèmes de stockage : batteries lithium-ion, batteries vanadium-redox, volants d'inertie, stockage par air comprimé (Medghalchi and Taylan, 2023; Mokhtara, Negrou, Settou, Settou, and Samy, 2021).
- Générateurs d'appoint : groupes diesel (DG) pour l'hybridation hors réseau, raccordement au réseau principal (GRID), générateurs à biomasse (BG) (Bouafia, El Fathi, El-Hammouchi, and El Akchioui, 2023; Kushwaha and Bhattacharjee, 2024).
- Systèmes complémentaires : pompes hydrauliques, stations de compression, échangeurs thermiques pour valorisation thermique (Samy, Mosaad, El-Naggar, and Barakat, 2021).

Les combinaisons courantes incluent :

- PV–WT–BESS–DG pour l'électrification rurale (Mokhtara et al., 2021).
- PV–WT–BESS–BG pour limiter les émissions dans les zones forestières (Bouafia et al., 2023).
- PV–WT–BESS–GRID pour les sites périurbains équipés d'un réseau faiblement stable (Samy et al., 2021).
- PV–BESS–DG dans des régions isolées à ressource éolienne faible (Kushwaha and Bhattacharjee, 2024).

Légende : PV = Photovoltaïque, WT = Éolien terrestre, BESS = Système de stockage par batteries, DG = Générateur diesel, BG = Générateur biomasse, GRID = Réseau principal.

Malgré cette diversité, la littérature souligne l'absence de consensus sur la topologie « universelle », chaque cas d'étude (climat, coût du carburant, politique tarifaire) exigeant une adaptation spécifique (Faria et al., 2023; Kushwaha and Bhattacharjee, 2024).

1.4.2 Outils de simulation utilisés

Les simulateurs commerciaux jouent un rôle prépondérant dans la comparaison des topologies :

- HOMER Pro (Lilienthal, 2005) est utilisé pour évaluer la rentabilité et la fiabilité d'un grand nombre de combinaisons prédéfinies. Par exemple, Baidas et al. (2022) ont comparé différentes configurations pour un site nord-africain, concluant que l'association éolien–batterie minimise le coût net actualisé (NPC).
- PVGIS (Lemaire, Castro, and Montemor, 2024) fournit des données satellitaires pour la ressource photovoltaïque, utilisées en complément de HOMER pour valider les prévisions de production PV (Bahgaat, 2023; Lu et al., 2017).

Ces simulateurs sont généralement couplés à des algorithmes d'optimisation externes (PSO, GA, recuit simulé), créant ainsi une boucle itérative indispensable au dimensionnement précis (Javed et al., 2021; Rtemi et al., 2023).

1.4.3 Algorithmes métaheuristiques pour l'optimisation multiobjectifs

La majorité des travaux s'appuie sur des métaheuristiques pour gérer la complexité multiobjective du problème (coût, fiabilité, émissions) :

- Particle Swarm Optimization - (PSO) et variantes multi-objectif (MOPSO) : Mansouri Kouhestani et al. (2020) démontrent que le MOPSO parvient à identifier un front de Pareto équilibrant LCOE et fiabilité, avec une convergence généralement rapide et une mise en œuvre simple. Toutefois, il reste sensible au choix des paramètres (nombre de particules, coefficients d'inertie) et peut facilement se piéger dans des optima locaux.
- Genetic Algorithm (GA) : utilisés par Medghalchi and Taylan (2023) pour explorer la combinatoire PV–WT–BESS, ces méthodes offrent une grande capacité d'exploration grâce aux mécanismes de croisement et mutation, favorisant la diversité des solutions. En revanche,

elles nécessitent souvent un temps de calcul important et une calibration fine pour éviter la convergence prématurée.

- Non-Dominated Sorting Genetic Algorithm II (NSGA-II) : Samy and Barakat (2019) montrent que ce GA multiobjectif assure une bonne diversification du front de Pareto et maintient un équilibre entre convergence et diversité. Cependant, son efficacité diminue pour des problèmes de très grande dimension et son temps de calcul croît fortement avec la taille de la population.
- Grey Wolf Optimizer (GWO), Improved Grey Wolf Optimizer (IGWO), Salp Swarm Algorithm (SSA) : Mahmoud, Diab, Ali, El-Sayed, Alquthami, Ahmed, and Ramadan (2022) comparent SSA, GWO et IGWO pour un système PV/WT/BESS/DG, et concluent que l'IGWO offre une meilleure capacité d'évasion des minima locaux et un coût énergétique inférieur. Néanmoins, ces méthodes sont sensibles aux conditions initiales et leur stabilité peut varier selon la configuration étudiée.
- Marine Predators Algorithm (MPA) : Kushwaha and Bhattacharjee (2024) montrent que le MPA converge rapidement et fournit des solutions économiquement compétitives (0,1799 $\$/kWh$), tout en évitant certains pièges des méthodes classiques. Toutefois, cette approche reste peu étudiée dans le domaine énergétique et son comportement sur des problèmes de grande échelle ou fortement contraints demeure incertain.

En somme, bien que ces algorithmes puissent traiter efficacement des objectifs contradictoires, ils requièrent un réglage minutieux de leurs hyperparamètres (nombre d'itérations, taille de population, coefficients de mutation), ce qui constitue un travail expérimental conséquent (Bouafia et al., 2023; Faria et al., 2023).

1.4.4 Critères de sélection et contraintes spécifiques

La décision finale repose sur la prise en compte :

- des critères de performance : LCOE, fiabilité, taux de pénétration renouvelable, émissions de CO_2 (Kumar, Gopi, Rajarajan, Vaishali, Vasavi, and P, 2024; Nesamalar, Suruthi, Raja, and Tamilarasu, 2021),
- des conditions météorologiques et géographiques : zones soumises à des vents forts ou à un ensoleillement intense influent sur le choix de la topologie (Bakht, Mohd, Shaikh, and Khan, 2024; Hasan, Ahmad, Liaf, Mustayen, Hasan, Ahmed, Howlader, Hassan, and Alam, 2024),
- de la demande énergétique : profil journaliers et saisonniers, charges critiques nécessitant une disponibilité garantie (Serat, Danishmal, and Mohammadi, 2024),
- des contraintes réglementaires et financières : subventions nationales, tarifs de rachat, coûts d'emprunt, incitatifs à la réduction d'émissions (Nallolla and P, 2022).

Il ressort que, bien que les approches métaheuristiques puissent identifier des solutions presque optimales, elles ne garantissent pas une adaptabilité automatique à de nouveaux contextes sans ajustement préalable des données d'entrée et des paramètres de l'algorithme (Mansouri Kouhestani et al., 2020; Medghalchi and Taylan, 2023).

1.5 Analyse de sensibilité des HRES

Au-delà du simple calcul d'un vecteur optimal, il est essentiel de comprendre la robustesse d'un HRES face aux incertitudes et aux variations des paramètres clés (ressources, coûts, politiques). C'est l'objet de l'analyse de sensibilité, qui se découpe en deux principaux volets : identification des facteurs dominants et évaluation de leur impact sur la performance globale.

1.5.1 Objectifs et méthodes d'analyse de sensibilité

L'analyse de sensibilité vise à :

- identifier les paramètres critiques : ceux dont la variation génère les plus fortes fluctuations du LCOE, de la fiabilité ou des émissions (Hasan et al., 2024; Singh and Fernandez, 2018).

- quantifier l'impact de l'incertitude : mesurer la variabilité des indicateurs de performance lorsque les paramètres (irradiance, vitesse du vent, coûts) sont soumis à des marges d'erreur (Nesamalar et al., 2021; Nurunnabi, Roy, Hossain, and Pota, 2019).
- guider la conception : cibler les efforts de collecte de données (ex. : investissements dans la mesure météorologique) sur les facteurs les plus influents pour réduire l'incertitude, et prioriser les composants qui offrent la meilleure robustesse (Sawle, Jain, Babu, Nair, and Khan, 2021).
- établir des marges de sécurité : prévoir des capacités supplémentaires de stockage ou de générateur pour pallier l'incertitude sur le long terme (Singh and Fernandez, 2018).

Parmi les méthodologies employées, on distingue :

- l'analyse de sensibilité locale : un paramètre est varié autour de sa valeur nominale, tandis que les autres restent fixés (Awan et al., 2018).
- l'analyse de sensibilité globale : tous les paramètres sont simultanément soumis à des variations selon une distribution probabiliste (par exemple, Sobol, Morris), afin de capturer les effets d'interaction entre facteurs (Nallolla and P, 2022; Serat et al., 2024).
- l'approches bayésiennes : on associe à chaque paramètre une distribution a priori, on réalise des simulations par échantillonnage (MCMC) pour déterminer les probabilités que la configuration reste viable (Kumar et al., 2024).

1.5.2 Paramètres sensibles et impacts observés

Les principaux paramètres identifiés dans la littérature comme influents sont définis dans le tableau 1.1.

Tableau 1.1 Analyse des paramètres et impacts observés dans diverses études

Paramètre analysé	**Impact observé**	**Références**
Ressources solaires / éoliennes	Coût énergétique, dimensionnement	Hasan et al. (2024); Ji et al. (2021); Kumar et al. (2024); Nesamalar et al. (2021); Singh and Fernandez (2018)
Taux d'actualisation	Rentabilité, configuration optimale	Bakht et al. (2024); Ji et al. (2021); Kumar et al. (2024); Nesamalar et al. (2021); Singh and Fernandez (2018)
Durée de vie des composants	Coût total, fréquence de remplacement	Ji et al. (2021); Kumar et al. (2024); Nurunnabi et al. (2019); Singh and Fernandez (2018)
Prix de l'énergie (connexion au réseau)	Viabilité économique	Ji et al. (2021); Kumar et al. (2024); Nesamalar et al. (2021); Nurunnabi et al. (2019); Serat et al. (2024)
Demande de charge	Dimensionnement, coût opérationnel	Bakht et al. (2024); Hasan et al. (2024); Nallolla and P (2022); Nurunnabi et al. (2019); Serat et al. (2024)
Politiques environnementales	Coût total, choix technologiques	Ji et al. (2021)

Les résultats convergent vers l'idée que la variabilité de l'irradiance solaire et de la vitesse du vent demeure le facteur déterminant pour pouvoir dimensionner adéquatement les composantes

PV et WT (Hasan et al., 2024; Ji et al., 2021). Par ailleurs, le choix du taux d'actualisation influe fortement sur la configuration optimale : un taux plus élevé favorise des systèmes hybrides intégrant davantage de PV et de batteries pour réduire la dépendance aux coûts de carburant, alors qu'un taux faible permet de privilégier des investissements lourds en énergies renouvelables (Bakht et al., 2024; Kumar et al., 2024).

En outre, il ressort que, dans les contextes hors réseau, l'analyse de sensibilité sur la demande des charges critiques (hôpitaux, pompage) est essentielle pour dimensionner la capacité de stockage nécessaire à garantir une autonomie minimale (Hasan et al., 2024; Nallolla and P, 2022). Pour les HRES raccordés au réseau, c'est la structure tarifaire (prix spot, tarifs de rachat) qui détermine le moment opportun pour vendre les surplus, maximisant ainsi la rentabilité globale (Nesamalar et al., 2021; Serat et al., 2024).

1.5.3 Aspects peu couverts et perspectives

Bien que l'analyse de sensibilité soit largement documentée pour les paramètres classiques (ressources, coûts, durée de vie), deux axes demeurent sous-représentés.

1. Sensibilité aux contraintes d'énergie d'appoint (générateurs diesel, réseau) : les systèmes DRL appliqués aux HRES limitent souvent la fraction annuelle d'énergie d'appoint à moins de 5 %, sans toutefois explorer systématiquement l'impact de cette borne sur la performance globale (Xiong, Zhang, Hu, Fang, Liu, and Cheng, 2025). L'idée serait de tester plusieurs niveaux de contraintes DG/GRID pour observer la variation du LCOE et de la fiabilité associée.
2. Dimensionnement dynamique en fonction des signaux prix spot : avec l'émergence de marchés de gros décentralisés, la volatilité des prix de l'électricité entraîne des stratégies d'achat et de revente complexes. Bien que quelques travaux en optimisation stochastique se soient intéressés à ces questions (Ahmadi Jirdehi and Sohrabi Tabar, 2023), peu d'études combinent cette dimension dynamique avec une approche DRL adaptée aux HRES.

Ces deux points représentent des pistes de recherche prometteuses pour renforcer la robustesse des HRES face aux évolutions technologiques (microgrids intelligents, stockage avancé) et aux changements de politiques énergétiques (primes à la flexibilité, pénalités pour les émissions).

1.5.4 Approches par apprentissage par renforcement profond (DRL)

Alors que les métaheuristiques traditionnelles offrent un compromis satisfaisant entre précision et temps de calcul, elles restent statiques : une fois la configuration obtenue, le système ne s'adapte pas aux variations en temps réel (évolution de la demande, coupure temporaire du réseau). Les approches par Deep Reinforcement Learning (DRL) émergent comme une voie pour surmonter cette limitation en apprenant des politiques de contrôle dynamiques.

1.5.5 Du métaheuristique au DRL

Les métaheuristiques (PSO, MOPSO, GA, NSGA-II) se concentrent sur l'optimisation *a priori* du dimensionnement, sans mécanisme intrinsèque de réajustement en cas d'aléas imprévus (temps nuageux prolongé, panne d'un générateur) (Bouafia et al., 2023; Faria et al., 2023). À l'inverse, le DRL apprend une stratégie décisionnelle (policy) qui adapte en continu la répartition des flux d'énergie entre PV, WT, batteries, générateurs et réseau principal en fonction de l'état du système (niveau de charge, disponibilité solaire/vent, prix spot) (Domínguez-Barbero, García-González, Sanz-Bobi, and García-Cerrada, 2024). Cette adaptativité répond à la variabilité opérationnelle mais s'accompagne d'exigences de données et de calcul plus élevées, et d'une ingénierie fine des récompenses et contraintes.

Trois algorithmes de référence se distinguent dans la littérature récente :

- TD3 (Twin Delayed Deep Deterministic Policy Gradient) : deux critiques retardés limitent le biais d'estimation de la valeur et stabilisent l'apprentissage en espace d'actions continu (Domínguez-Barbero et al., 2024). Il convient bien aux politiques fines de charge/décharge et de dispatch continu. En contrepartie, il requiert un réglage soigneux (taux d'apprentissage,

bruit d'exploration, cibles retardées) et peut être sensible au drift de distribution lorsque les régimes météo/prix changent rapidement.

- SAC (Soft Actor-Critic) : l'entropie maximale encourage une exploration robuste, réduisant le risque d'enfermement dans des stratégies myopes ; la mise à jour stochastique confère une bonne stabilité et une convergence fiable dans des environnements bruités (Pei, Yao, Zhao, Ding, and Wang, 2024). Cependant, la température d'entropie et les *targets* exigent une calibration précise ; l'échantillonnage hors politique nécessite des mémoires de rejouent bien équilibrées pour éviter le surapprentissage sur des scénarios rares.
- HDQN (Hierarchical Deep Q-Network) : la décomposition hiérarchique (niveau haut : planification journalière/hebdomadaire ; niveau bas : décisions horaires) facilite l'apprentissage sur de longues séquences et l'incorporation de contraintes opérationnelles (Chen, Liu, Cui, Chen, Wang, and Xiao, 2024). Cette structuration améliore l'échelle temporelle et la lisibilité des décisions, au prix d'une complexité de conception accrue (définition des sous-tâches, signaux de récompense multi-niveaux) et d'un risque de sous-optimisation si la coordination inter-niveaux est imparfaite.

1.5.6 Intégration des contraintes DG/GRID

L'un des défis majeurs dans l'application du DRL aux HRES est l'incorporation explicite des contraintes d'appoint.

- Fraction maximale d'énergie provenant du générateur diesel (DG) : dans de nombreuses études, cette borne est fixée à un pourcentage faible (moins de 5 % de l'énergie annuelle totale), pour limiter les émissions. Le DRL doit apprendre à respecter cette contrainte tout en garantissant la fourniture aux charges critiques (Domínguez-Barbero et al., 2024).
- Limite d'énergie admissible via le réseau principal (GRID) : pour des micro-grids connectés, il s'agit d'optimiser le moment de l'achat/vente d'électricité (Xiong et al., 2025). Cette contrainte varie selon la structure tarifaire (tarif fixe, prix spot), nécessitant une adaptation de la politique d'apprentissage (Pei et al., 2024).

La plupart des travaux se focalisent sur l'allocation optimale en continu entre PV, batterie et générateur, en supposant que la contrainte DG/GRID est statique (fixée *a priori*). Cependant, Blenk and Weindl (2024) et Lambrichts and Paolone (2024) montrent que modéliser ces bornes comme variables d'état, sujettes à des fluctuations (quantité de carburant disponible, signal de prix dynamique), améliore significativement la robustesse du contrôleur DRL.

1.5.7 Exemples d'implémentations DRL pour les HRES

Diverses études attestent de l'efficacité du DRL pour les HRES :

- Domínguez-Barbero et al. (2024) utilisent TD3 pour un système PV–BESS–DG hors réseau. Leur agent apprend à moduler la charge de la batterie et la puissance du générateur en temps réel, minimisant le LCOE tout en respectant une borne de 3 % pour l'énergie diesel annuelle.
- Pei et al. (2024) appliquent SAC à un micro-grid connecteur, où le prix spot de l'électricité varie chaque heure. L'agent SAC apprend non seulement à charger/décharger la batterie, mais aussi à acheter/vendre de l'électricité selon le signal de prix, réduisant ainsi le coût opérationnel de 12 % par rapport à une approche statique.
- Chen et al. (2024) développent un HDQN hiérarchique pour un grand micro-grid urbain intégrant PV, éolien et batterie, avec deux niveaux de décision : un niveau haut détermine la distribution journalière (pourcentage d'énergie à puiser dans chaque source), et un niveau bas ajuste la stratégie horaire en fonction des prévisions météorologiques. Leur approche mène à une réduction de 20 % du LCOE et à une stabilité accrue pendant les périodes de forte demande.

1.5.8 Limites actuelles et perspectives de recherche

Malgré ces avancées, plusieurs défis subsistent nécessitant que l'on s'y intéresse.

1. Généralisation aux nouvelles configurations : la plupart des agents DRL sont entraînés sur des données spécifiques à un site (profil météorologique, tarifaire). Leur transfert vers un

autre site demande une réadaptation (transfer learning), ce qui n'est pas trivial (Blenk and Weindl, 2024).

2. Exploration vs exploitation : la pénalité associée à une coupure de courant (charge critique non alimentée) est très élevée, poussant l'agent à privilégier des actions sûres (utilisation du générateur) plutôt que l'exploration de stratégies potentiellement plus économiques (Xiong et al., 2025).
3. Intégration de l'analyse de sensibilité : très peu d'études combinent analyse de sensibilité globale avec DRL. Pourtant, faire varier simultanément plusieurs paramètres (ressources, tarifs, coûts) pendant l'entraînement permettrait d'obtenir un agent plus robuste face aux incertitudes (Lambrichts and Paolone, 2024).
4. Aspects réglementaires et sociaux : la décision d'utiliser un générateur diesel dépend aussi de facteurs non techniques (politique locale, acceptation sociale), rarement modélisés dans le cadre DRL (Ahmadi Jirdehi and Sohrabi Tabar, 2023).

En somme, bien que le DRL offre une promesse importante pour le contrôle adaptatif en temps réel des HRES, un certain nombre de verrous méthodologiques et pratiques restent à lever avant une adoption industrielle à grande échelle.

Afin de synthétiser les familles d'approches discutées dans ce chapitre, le tableau 1.2 compare leur principe, leurs forces/limites et leur capacité d'adaptation.

Tableau 1.2 Comparaison synthétique des principales familles d'approches pour le dimensionnement des HRES.

Famille	**Principe**	**Forces / limites typiques**	**Adaptation**
Simulation exhaustive	Évalue un grand nombre de configurations via des simulateurs détaillés.	+ Fidélité élevée. – Temps de calcul prohibitif lorsque l'espace de recherche croît.	Faible
Métaheuristiques (GA/PSO/NSGA-II, etc.)	Recherche de solutions quasi-optimales par itérations (population, exploration/exploitation).	+ Flexible et multiobjectif. – Réglage d'hyperparamètres, recalibrage fréquent, dépendance aux scénarios.	Faible–moyenne
Accélération / modèles rapides	Réduction de modèle, parallélisation et approximations pour réduire le coût de calcul.	+ Réduction du temps d'évaluation. – Biais possible si approximation insuffisante ; généralisation limitée.	Moyenne
ML / NAS (ex. GHI)	Améliore la qualité des données (prévision) et automatise la conception des modèles.	+ Réduit l'incertitude et automatise. – Coût d'entraînement et dépendance aux données (si recherche large).	Moyenne

1.6 Conclusion

La littérature existante sur les systèmes hybrides d'énergie renouvelable (HRES) présente un panorama riche d'approches visant un objectif commun : fournir de l'électricité de manière fiable, économique et respectueuse de l'environnement. Les points saillants de cette revue, en cohérence avec la synthèse du Tableau 1.2, peuvent être résumés comme suit :

(1) chaîne de dimensionnement : l'enchaînement *génération de scénarios* → *simulation* → *analyse de faisabilité* constitue le socle commun à la plupart des méthodologies (Alluraiah and Vijayapriya, 2023).

(2) accélération des simulations : la réduction d'ordre, l'apprentissage profond ou le remplacement partiel de la boucle de simulation par des modèles ML réduisent le temps de calcul. Ces gains restent toutefois conditionnés par la qualité et la représentativité des données d'entraînement (Banihashemi et al., 2022).

(3) optimisation métaheuristique (multiobjectif) : PSO, GA, NSGA-II, SSA, GWO, MPA, IGWO et autres offrent une boîte à outils robuste pour le dimensionnement multiobjectif, à condition de calibrer soigneusement les hyperparamètres et d'assurer la stabilité des résultats selon les scénarios (Kushwaha and Bhattacharjee, 2024; Mahmoud et al., 2022).

(4) analyse de sensibilité : elle demeure fondamentale pour quantifier l'impact des incertitudes (ressources, prix, taux d'actualisation), guider la collecte de données, et définir des marges de sécurité adaptées (Hasan et al., 2024; Serat et al., 2024).

(5) apprentissage par renforcement profond (DRL) : le DRL ouvre la voie à une gestion adaptative, intégrant des signaux dynamiques (prix, état de charge, météo) et des contraintes complexes (DG/GRID). Néanmoins, son adoption est freinée par la généralisation limitée à d'autres environnements et par l'intégration encore partielle de l'analyse de sensibilité globale (Domínguez-Barbero et al., 2024; Lambrichts and Paolone, 2024).

En synthèse, le Tableau 1.2 met en évidence une tension structurante : les approches fondées sur la simulation et l'optimisation multiobjectif sont efficaces mais coûteuses en calcul et sensibles aux hypothèses, tandis que les approches d'apprentissage (ML/NAS, DRL) améliorent l'automatisation et l'adaptation, au prix d'exigences fortes en données et de défis de généralisation/validation. Ces constats motivent la nécessité d'une démarche combinant accélération du processus de sélection, réduction d'incertitude sur les entrées critiques et optimisation adaptative sous contraintes réalistes d'exploitation des HRES.

CHAPITRE 2

REDUCTION IN MICROGRID TOPOLOGY SELECTION TIME VIA HYBRID BRANCH AND BOUND AND K-NEAREST NEIGHBORS TECHNIQUES

Inoussa Legrene[1] , Tony Wong[1] , Nicolas Mary[2] , Louis-A. Dessaint[2]

[1] Département de Génie des Systèmes,
[2] Département de Génie Électrique,
École de Technologie Supérieure,
1100 Notre-Dame Ouest, Montréal, Québec, Canada H3C 1K3

Article publié dans la revue « Mathematics », janvier 2025
DOI : https://doi.org/10.3390/math13030360

2.1 Abstract

The global adoption of hybrid renewable energy systems (HRESs) is accelerating as a strategic response to escalating energy demands and the imperative to mitigate greenhouse gas emissions. Despite the development of various technological tools, such as pre-feasibility analysis, sizing, and simulation tools, challenges persist due to their limited flexibility in modifying system architectures and their typically long computation times, which hinder their practical efficiency. This study introduces a novel hybrid method that integrates the Branch and Bound (BB) heuristic search algorithm with the k-Nearest Neighbors (kNN) algorithm to drastically reduce the simulation time of microgrid models in Simulink. Validation considering four distinct case studies reveals that our method can decrease the simulation time by up to 94.68% while maintaining an acceptable accuracy. Specifically, simulation times in certain cases were reduced from approximately 21,780 and 118,580 s to 1442.7969 and 6306.0625 s, respectively. This significant reduction facilitates the rapid evaluation and selection of optimal HRES configurations, enhancing the efficiency of both editable and non-editable systems. Through streamlining the simulation process, this approach not only accelerates the design and analysis phases but also supports the broader adoption and deployment of HRESs, which is critical for achieving a sustainable future. This advancement offers a robust and efficient methodology for optimizing

simulation times, thereby addressing a key bottleneck in the development and implementation of hybrid renewable energy solutions.

2.2 Introduction

The growing demand for energy, combined with the growing concern about environmental pollution and greenhouse gas production, is contributing to the increased use of renewable energy sources, including solar, wind, biomass, hydraulic, and geothermal sources. Although these sources are diverse, each has a unique energy supply issue. This uniqueness is mainly due to the energy source, the load demand to be met, and the implementation conditions. Moreover, the renewable sources that can be used in an area may not meet the projected energy demands and/or are subject to significant fluctuations. Therefore, renewable sources are often combined with generators for compensatory energy production and storage systems for energy storage to ensure the continuity of energy availability. These combinations are deemed hybrid renewable energy systems (HRESs).

Several technologies and approaches have been proposed to ease the problematic decision-making process related to choosing the right system. These are grouped into four subcategories (Kavadias and Triantafyllou, 2021) with complementary objectives. Pre-feasibility analysis tools help engineers in their initial analysis of the suitability of a renewable energy system. Sizing tools help to find the best values for various parameters, such as the number of solar photovoltaic panels to be used to meet energy demand. These tools consider energy demand as an objective and deal with the problem by searching for values that optimize different objective functions. There are also simulation and open architecture tools. Simulation tools, as the name suggests, are based on user-provided specifications, such as the size of the system to implement. The simulation tool then provides the user with a detailed analysis of the system's behavior, which is supplied as an input to the simulation model. The last category is open-architecture tools, which are the opposite of the other types (particularly simulation tools, which are primarily black boxes that do not allow for structural modifications). As indicated in their name, such tools offer an open possibility to make modifications thanks to their R&D-oriented components.

The key problem of sizing a hybrid renewable energy system is related to the fact that renewable energy sources cannot consistently produce energy at all times of the day and year, which makes it essential to combine renewables with alternative energy sources. It is also important to find the best size for each source, considering factors such as investment costs and the available installation surface area. Even with a combination of different energy sources, in many cases, it is necessary to add a generator to the system (e.g., to supply energy to medical facilities, which need to be kept powered at all times). Considering when the generator will have to use fossil fuel, depending on the available investment cost, it is important to determine the correct generator size to limit this consumption as much as possible to reduce greenhouse gas emissions. In addition, given the variability of renewable energy production sources, it is necessary to attach external systems.

Adopting a hybrid renewable energy system requires carrying out three essential steps.

Step 1 : Scenario generation—This step consists of defining different potentially feasible configurations of these systems, taking into account various factors such as the renewable energy sources available (solar, wind, biomass), the different energy demand profiles that the system must meet, and, above all, environmental and economic constraints (e.g., the location and total cost of the system must be taken into account) (Alluraiah and Vijayapriya, 2023). The literature abounds with methods, such as genetic algorithms (GA) and probabilistic methods (Monte Carlo), which enable the definition of realistic data sets and scenarios based on temporal correlations and uncertainties (Liu et al., 2023a). Considering that renewable sources alone do not guarantee system resilience, the generation process can integrate not only storage sources (batteries) but also external production sources (generators) (Al-Ghussain et al., 2020; Zhang et al., 2020).

Step 2 : Simulation of previously generated configurations—Simulation tools and software, such as HOMER/HOMER Pro (version 3.11.6561.20287) (Alluraiah and Vijayapriya, 2023; Kavadias and Triantafyllou, 2021; Thirunavukkarasu, Sawle, and Lala, 2023), are available to evaluate the performance of these configurations (Bahgaat, 2023; Lu et al., 2017). A large

body of research has used optimization algorithms, such as particle swarm optimization (PSO) (Mansouri Kouhestani et al., 2020; Mohamed et al., 2016) and simulated annealing, with the aim of optimizing implementation costs and the proportion of renewable energy (Javed et al., 2021; Rtemi et al., 2023).

Step 3 : Feasibility analysis—This final stage is crucial in determining which of the many final systems will be adopted. It consists of evaluating systems in terms of their technical, economic, environmental, and social aspects. In this stage, energy costs, net present value, CO_2 emissions, job creation rates, and many other factors are evaluated to determine the optimal configuration (Awan et al., 2018; Elkadeem et al., 2021; HassanzadehFard et al., 2021). Implementing these different steps, though necessary, requires significant costs in terms of both time and resources. These processes can take several tens of hours (Baghaee et al., 2016; Tounsi, 2022), depending on the different characteristics considered.

Simulation time is a significant research issue across multiple fields. The problem has attracted the attention of many researchers in various fields, including the energy field (Aranguren, 2023; Banihashemi et al., 2022; Mange and Skowronska, 2023; Martínez-Turégano et al., 2019; Tounsi, 2022) and in the field of image characterization and reconstruction (Dou et al., 2021).

Table 2.1 summarizes the key contributions of previous work on hybrid renewable energy systems. (Martínez-Turégano et al., 2019) have addressed the problem of extended simulation time for wind farms through developing admittance models with the aim of reducing the mathematical complexity and maintaining acceptable accuracy in performance. This approach has proven very useful in the context of large-scale networks, such as offshore wind farms. In light of this work, (Banihashemi et al., 2022) proposed the use of the auto-encoder approach due to its ability to reduce the size of system parameters. In particular, the use of auto-encoders enables the extraction of the essential characteristics of energy systems, considerably reducing simulation times. This approach has many advantages when researchers have sufficient and representative data at their disposal. Regarding the work by Tounsi (2022), the approach consisted of replacing modules which were deemed to be complex in the simulation model. Although this approach

may address the issues of complexity and simulation time, it remains domain-specific. Finally, in a similar vein to the work of Mange and Skowronska (2023); Tounsi (2022); Banihashemi et al. (2022) have proposed the use of machine learning (ML) models. The aim of their research was to replace the entire simulation model with predictive models. This reduces processing time while guaranteeing uncertainty management. In this approach, the ML models need to be trained on high-quality data sets and their reliability assessed based on robust model validation.

Tableau 2.1 Summary of methodologies and applications

Reference	Methodology	Key Points	Applications
Martínez-Turégano et al. (2019)	Using an admittance model	Use of aggregation techniques based on admittance models to reduce simulation time	Offshore wind farms
Banihashemi et al. (2022)	Model order reduction with auto-encoders	Use auto-encoders to extract essential characteristics, reducing the number of parameters simulated	Used in energy models for buildings
Tounsi (2022)	Developing a scale model in Simulink	Replacing complex models with simplified versions in Simulink	Wind energy systems
Mange and Skowronska (2023)	Comprehensive machine learning model	Replace the simulation process with a machine learning model that takes uncertainties and reliability into account	Autonomous and mobile systems

Although these approaches have been effective in their application frameworks, there are a number of limitations. First, reliable data are required to construct machine learning models. In addition, simulations relating to sizing hybrid renewable energy systems remains a problem

relative to each situation. This relativity is an essential problem, as load demands are not the same for two different consumers and energy production sources can differ considerably. When considering the use of a simulation model for hybrid renewable energy systems, such as HOMER (Hybrid Optimization Model for Renewable Energy) (Kavadias and Triantafyllou, 2021; Saxena, Kumar, Manna, Rajput, Agarwal, Diwania, and Gupta, 2025), it is not possible to develop a replacement component for an entity or for the entire model. In many cases, a researcher only has simulation rights for simulating the candidate systems they want to install. Next, the researcher must select an analysis methodology to adopt for the simulation data after running a simulation. The completion of the simulation(s) can be a very long process (Baghaee et al., 2016; Sousa Junior, Montevechi, Miranda, Oliveira, and Campos, 2020).

Various studies have also addressed multi-processor execution techniques (Sampat et al., 2020; Zhaoqian and Edahiro, 2019). A key concern regarding multi-processor execution is that it requires a machine with a multi-core processor and high processing speed (Sampat et al., 2020). Although many methods have been discussed in the literature, these methods can only be applied in well-defined study cases. Their application in our study is limited by (i) the non-availability of historical data to best represent all zones and (ii) the impossibility of having modification access to the model, in order to plan the feature extraction study or the replacement of a part of the model by a new optimized model block. Therefore, this study proposes a new methodology for reducing the simulation waiting time through applying a hybrid method based on machine learning and a heuristic search with no historical data or modification of the initial model. With the aim of simplifying the evaluation process for hybrid energy systems, the proposed hybrid methodology combines the k-Nearest Neighbors and Branch and Bound methods. This approach reduces the waiting time for simulation and feasibility analysis tools.

The main contributions of this work revolve around the following three points :

- **Innovative hybrid kNN and Branch and Bound (BB)**—the integration of kNN with BB optimization establishes a robust framework for the selection process of energy systems ;

- **Targeted exploration optimization**—the application of BB enables a solution to the problem to be found through analyzing nodes and branches. This approach avoids the exploration of unnecessary branches based on the results obtained in the previous steps ;
- **Dynamic definition of sets of hybrid renewable energy systems**—the kNN approach defines sets of feasible systems sharing common characteristics, such as similar neighboring systems. This approach allows for a preliminary classification of systems, which speeds up the search process.

The remainder of this article is structured as follows. Section 2.3 presents the methodology, beginning with our three-phase model, and describes how the two algorithms (kNN and BB) help to achieve the objective of the study. The results and comparison with traditional methods are presented in Section 2.4. The article ends with concluding remarks and recommendations for future work in Section 2.5.

2.3 Solution Approach

This section outlines the study's toolset and comprehensive methodology, describing the approach adopted to address the research objectives.

2.3.1 Stepwise

The tool used in our research is a three-part model, as described in Section 2.3 and illustrated in Figure 2.1. This tool is both a sizing model (Kavadias and Triantafyllou, 2021; Thirunavukkarasu et al., 2023) and a simulation model ; that is, it is a model to predict the behavior of a system extracted from the sizing phase, as well as a feasibility analysis tool (Khan, Ali, Qaisar, Naeem, Chrysostomou, and Iqbal, 2020).

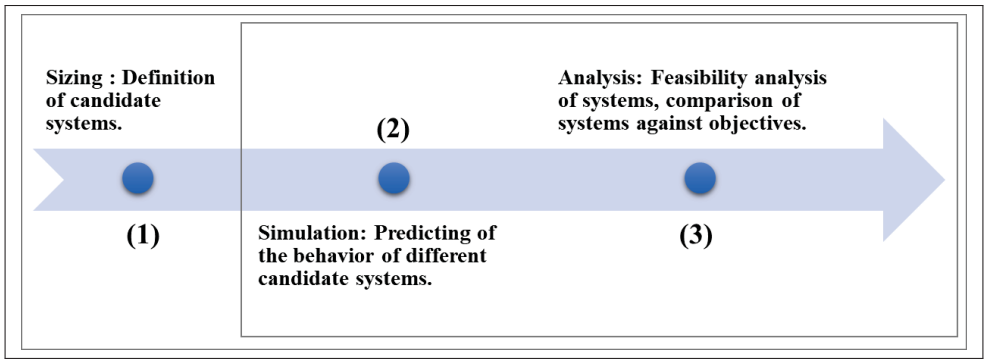

Figure 2.1 Key steps of proposed hybrid renewable energy system (HRES) methodology

A set of feasible systems (phase 1) is proposed based on the defined specifications, including the available installation area, technologies, and existential quantification constraints. These eligible systems are then evaluated one after the other by the tool's core, which consists of a simulation model (phase 2). This simulation model is a multiple-input, multiple-output (MIMO) black-box model, as it does not present any details of its simulation process. When such a model is used in this context, it is important to remember that we will not have any editing rights, only the right to simulate our system.

This simulation model, as shown in Figure 2.2, requires several inputs, which are listed below.

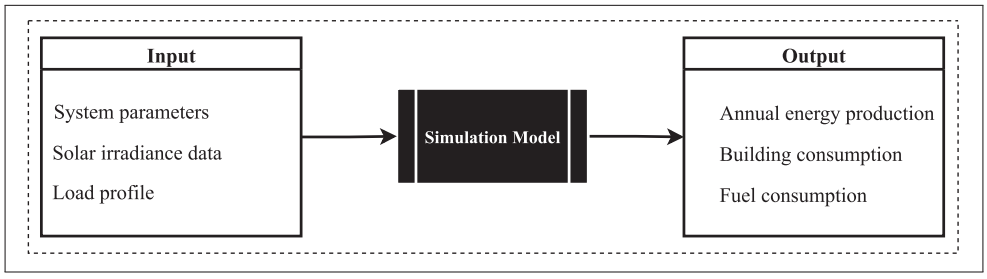

Figure 2.2 Energy management process

- Parameters that define the system to be simulated ;
- An energy demand profile ;
- Energy pricing ;

- Historical solar irradiance data for one year (if evaluating energy production from solar power).

From these inputs, a one-year simulation is run and the outputs listed below are provided.

- Annual energy production ;
- Total annual energy consumption ;
- Fuel consumption.

Once all these simulations of the system have been completed, we move on to phase 3, in which all simulated systems are evaluated using a decision support method to determine the best system to implement based on pre-defined criteria (Al-Ghussain et al., 2020; Mansouri Kouhestani et al., 2020; Tabak, Özkaymak, Güneser, and Erkol, 2017), such as the items listed below.

- Investment costs ;
- System reliability ;
- The capital recovery period ;
- The greenhouse gas emission rate.

The most expensive phases of this modeling tool are phases 2 and 3, comprising the simulation and feasibility analysis (Lu et al., 2017). The search for the best system corresponds to finding y^* as defined by Equation (2.1) :

$$y^* = \{y' \in Y \mid g(y') > g(y), \forall y \in Y\}, \tag{2.1}$$

where g is the fitness function for the feasibility analysis ; Y is the set of simulation results of feasible candidate systems produced by the simulation model, defined by the equation (2.2) ; and y is the simulation result for a feasible candidate system.

$$Y = \{y \mid y = A\mathrm{x}\}, \tag{2.2}$$

where *A* is the simulation model definition matrix and x is the coordinate vector defining the characteristics of the system to be studied.

2.3.2 Methodology

Given the considerable time that such a modeling tool may require, our proposed solution to reduce the waiting time applies to phases 2 and 3 shown in Figure 2.1. The proposed methodology uses a hybrid method based on the Branch and Bound optimization algorithm (BB) and the k-Nearest Neighbors (kNN) machine learning technique to minimize the simulation and analysis time of the candidate systems.

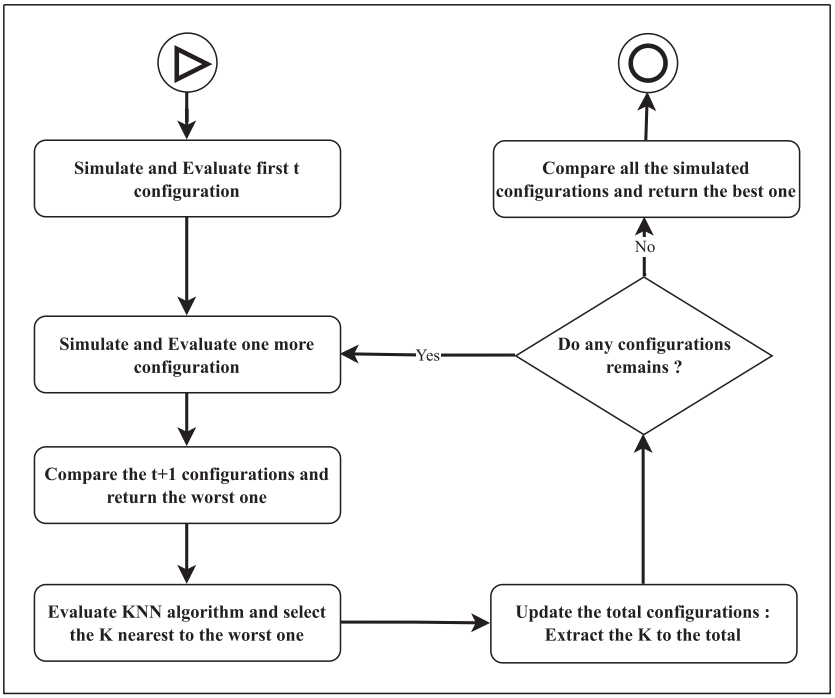

Figure 2.3 Process of the proposed methodology

This hybrid methodology takes advantage of the strengths of each of these methods. Applying the Branch and Bound method, we use the conclusions drawn from an initial evaluation of one of the candidate systems to dispense with the evaluation of other candidate systems and reduce the computation time. This process is called the branch pruning of candidate solutions. Given

the tool we are studying in this research (i.e., a simulation model), we use the kNN algorithm to select candidate systems belonging to a defined set based on the distance criterion. These sets, defined by the kNN algorithm, represent the branches that will be pruned by the Branch and Bound method. The execution of this methodology requires the definition of a few parameters, as shown in Table 2.2. Figure 2.3 presents the sequence of this methodology.

Tableau 2.2 Parameters to be defined in the proposed methodology

Parameter	**Description**
ϱ (seconds)	Minimal time spent searching for the best system
ς (seconds)	Average system simulation time
t	Maximum number of systems to return
σ	Maximum number of systems to simulate
ρ	Minimum number of systems to simulate instead of ϱ, time spent in simulation

The proposed methodology is described in detail in the following paragraphs.

First, we define the amount of time ϱ (in seconds) that we want to spend for the duration of the simulation or the maximum number of systems to be simulated in the search for the best system. Once the duration has been defined, the algorithm defines the number of configurations evaluated, as shown in Equation (2.3) :

$$\rho = \begin{cases} \frac{\varrho}{\varsigma} - t, & \text{if } \rho + t \leq \sigma \\ \sigma - t, & \text{else} \end{cases}, \tag{2.3}$$

where ρ represents the minimum number of systems to be simulated and ς is the average simulation time of a system, considering the characteristics of the used hardware. The total

number of systems to be simulated ($\rho + t$) during parameter initialization must not exceed σ :

$$\rho + t \leq \sigma. \tag{2.4}$$

Next, the process defines several t values for the best-ordered systems to be presented at the end of the process, highlighting the best one to emerge. At the end of this definition, the algorithm evaluates the first t systems utilizing the chosen search strategy. The process utilizes two search strategies : the random search process and the specific subset search process. The random process determines those systems that are simulated randomly, while the subset search process determines those systems with similar traits that are simulated at the same time. For example, systems that use energy storage devices (ESSs) without generators are systems to be analyzed together, and systems with ESSs and with generators will be analyzed together.

Then, once the first t systems have been defined, the algorithm simulates another system. With each simulation, the total number $t + 1$ of simulated systems is compared. The system with the worst result is passed to the filtering program by the kNN, which returns the branch containing the K systems likely to have the same results such that they can be eliminated.

Finally, the algorithm updates the set of candidate systems that have not yet been simulated by eliminating the returned K systems. This process is continuous until no systems are left in the creation stage ; that is, the kNN algorithm will have simulated or eliminated all systems.

Thus, instead of a user defining the time predicted to be spent waiting for the simulation to finish, the number of systems to be evaluated can be defined, that is, σ systems. This number σ must be greater than or equal to ρ and comply with the condition given in Equation (2.5). Thus, the number of neighboring systems K that will be eliminated by applying the kNN algorithm is defined by Equation (2.5).

$$K = \left\lceil \frac{\Gamma - t}{\rho} - 1 \right\rceil, \tag{2.5}$$

where Γ defines the total number of systems for a given project. This means that the number of systems to prune, K, is specific to each project and the best system is to be determined according

to pre-defined constraints. The Branch and Bound method works by defining the branches that do not need to be explored in the search for the best system. Applying the kNN method enables us to eliminate a branch that represents a set of systems with a high probability of encountering the same results as a system which was previously judged to be irrelevant. To verify the results of our methodology, simulation tests with and without the proposed hybrid BB and kNN methodology were carried out for different projects implementing renewable energy hybrid systems.

2.3.2.1 Branch and Bound Algorithm

The Branch and Bound algorithm is an enumeration-based optimization approach (Watanabe, Tamura, Takano, and Miyashiro, 2023). This method subdivides the main problem into smaller sub-problems, each defining easily controllable search areas. The search is performed in a branch-by-branch manner, and those underlying branches that are not likely to provide better results for the cost function evaluation are pruned. In short, the Branch and Bound optimization algorithm reduces the search space for the best solution x_i in the space of possible solutions $X = (x_1, x_2, \ldots, x_n)$ that minimizes (or maximizes) a cost function f, as generally used in combinatorial problems (Equation (2.6)) :

$$\min_{x \in X} f(x). \tag{2.6}$$

This optimization approach defines three essential components : the node, the node branching, and the generation process. The node represents the decision point for dividing a problem (or set) or subproblem (or subset) into subproblems (or search subsets) that are easier to solve. Branching and generating nodes generate all the child nodes that can be derived from a parent node.

The Branch and Bound solution search consists of finding the possible set of solutions X', which is a subset of X corresponding to a limit function f' such that the condition in Equation (2.7) is satisfied :

$$f'(x) \leq f(x) \, \forall x \in X' \subseteq X. \tag{2.7}$$

The major problem faced by this approach is defining the subset X′ and the fitness function f' that best reduces the search space and computation time. Therefore, we apply the kNN machine learning algorithm to define the subset contained in the set of possible solutions.

2.3.2.2 k-Nearest Neighbors

The k-Nearest Neighbors (kNN) algorithm is a basic supervised machine learning method (Zhang, Li, Zong, Zhu, and Wang, 2017), which is mainly used for solving classification problems in various fields (Mladenova and Valova, 2023). The process of the k-Nearest Neighbors (kNN) algorithm involves determining, for a given element or system, k systems with similar features (traits), where k represents an integer value that defines the number of systems with common features that should be considered when applying the algorithm. The kNN algorithm, derived from the Nearest-Neighbor approach (Zhang et al., 2017) for unlabeled data processing problems, is implemented in three steps. First, the algorithm calculates the distances of the input data from the remainder of the available data set. Several distance functions can be applied, including the Euclidean distance (D_e), Manhattan distance (D_m), or the Hamming distance (D_h). Once the various distances have been calculated, the algorithm selects the k systems with the smallest distances to the unlabeled input (the second step). Finally, the majority class among the k selected datasets is assigned to the unlabeled input. The major challenge in applying this algorithm is defining the optimal number of neighbors to be considered (Kumar and Sahu, 2021; Zhang et al., 2017).

For the approach adopted in this study, the kNN algorithm selects the branch of systems to be eliminated, with a maximum of K systems to be eliminated simultaneously.

2.4 Results and Discussion

In this section, we explore the specific system under study by detailing its components and characteristics and defining the parameters used for modeling and evaluation. The simulation results are presented, and an analytical discussion is conducted to interpret the performance

of the proposed methodology. This methodology was implemented using PyCharm, which leverages the Python programming language and its third-party libraries, including Numpy, Pandas, Scikit-Learn, and Scipy. This process facilitated comprehensive system analysis, data manipulation, and algorithm implementation for accurate simulations and robust evaluation.

2.4.1 Type of System Evaluated

The proposed solution approach considers a series-connected hybrid renewable energy system (HRES) (Gourbi, Bousmaha, Brahami, and Tilmatine, 2016; Jacob and Farzaneh, 2022), as illustrated in Figure 2.4. One renewable energy generation source, solar, is used (1). The renewable source is supported by a generator (5) for provision of the energy difference between production and demand. In addition, a battery bank (3) is utilized to back up the surplus energy when the energy produced by the solar system exceeds the energy demand, which is the total amount of energy required to operate the loads (7 and 8). In addition, this study considers that, when the production surplus is very large and impossible to conserve, the consumer can inject it into the public grid (6).

The solar inverter (2) in this system transfers electrical energy from the direct current (DC) produced by the solar panels to an alternating current (AC), which can be used directly by the loads. Meanwhile, the bidirectional converter (4) converts surplus energy from alternating current (AC) to direct current (DC), which is suitable for storage in batteries, to conserve it in battery banks in the event of overproduction or converts the energy stored in batteries from direct current (DC) to alternating current (AC) to supply loads in the event of underproduction.

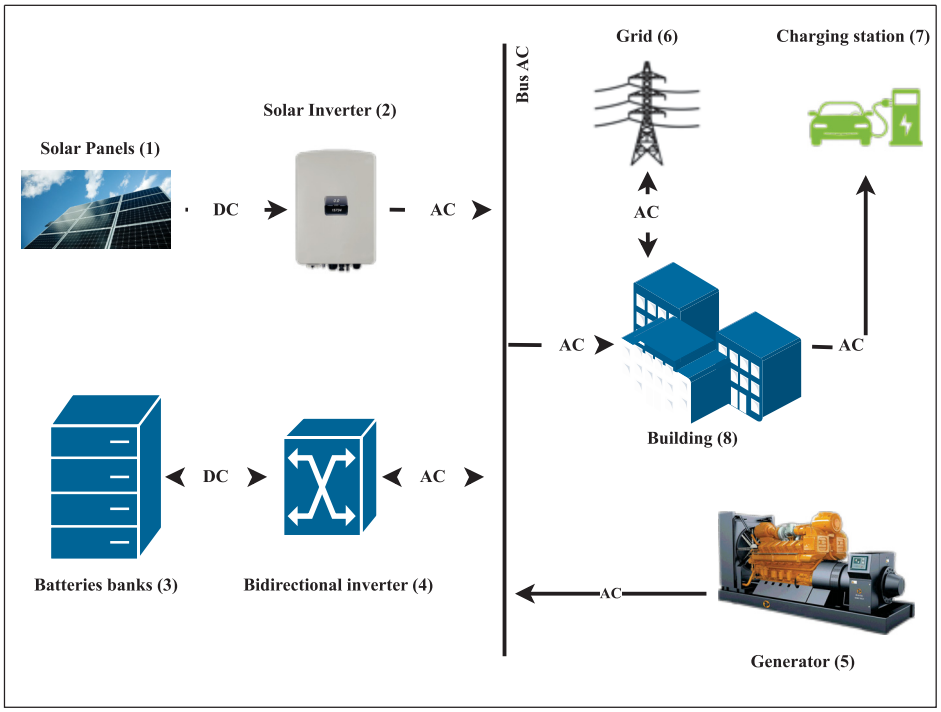

Figure 2.4 Schematic of considered hybrid renewable energy system

Thousands of candidate systems were generated when this HRES was set up. In the following, we refer to these systems as configurations.

A configuration denotes the assignment of specific values to the parameters of the hybrid renewable energy system (Eltamaly and Al-Shamma'a, 2016). These parameters include tilt, azimuth, solar panels, battery storage capacity, generator output, and the number of electric vehicle charging stations installed. Based on the above parameters, we define two configuration examples in Table 2.3 (Mohamed et al., 2016) . To validate our approach, different projects with different numbers of configurations were studied in order to compare the results of this methodology with the traditional approach, which consists of a complete simulation of all configurations before analysis for decision-making.

Tableau 2.3 Example parameter value definitions

Parameter	Configuration i	Configuration j
Number of PV Panels	150	200
Tilt	30	45
Azimuth	South	South-West
Generator Capacity	15 kWh	10 kWh
BESS Capacity	15 kWh	20 kWh
EV Charger	1	3

2.4.2 Parameter Definition

Considering the available computational power—that is, a computer with a 2.8 GHz Intel processor and 16 GB RAM—the first step was to define the average simulation time for a configuration. The time evaluation measure was CPU time. This measure represents the difference between the beginning and the end of the simulation process (i.e., the reception of parameters by the simulation model). For the simulation model considered in this study, the simulation time for 60 configurations was evaluated. The results of this evaluation are shown in Figure 2.5, with minimum and maximum simulation times of 18.17 and 27.64 s, respectively. This gives us an average time of 21.94 s over 60 configurations, which allowed us to consider an average time of 22 s for the remainder of the work. This means that, for a system whose candidate configuration generation generates 1000 configurations, the average simulation time required is 22,000 s (or 6 h, 6 min, and 40 s). Thus, this study considered the basic parameter definitions listed in Table 2.4, including the three simulation waiting times τ of 1 h, 1 h 30 min, and 2 h. The total number of best configurations t that we present at the end of the process is 10.

Tableau 2.4 Parameter initialization

Parameter	Value
ϱ (seconds)	3600, 5400, 7200
ς (seconds)	22
t	10
σ	250
ρ	50

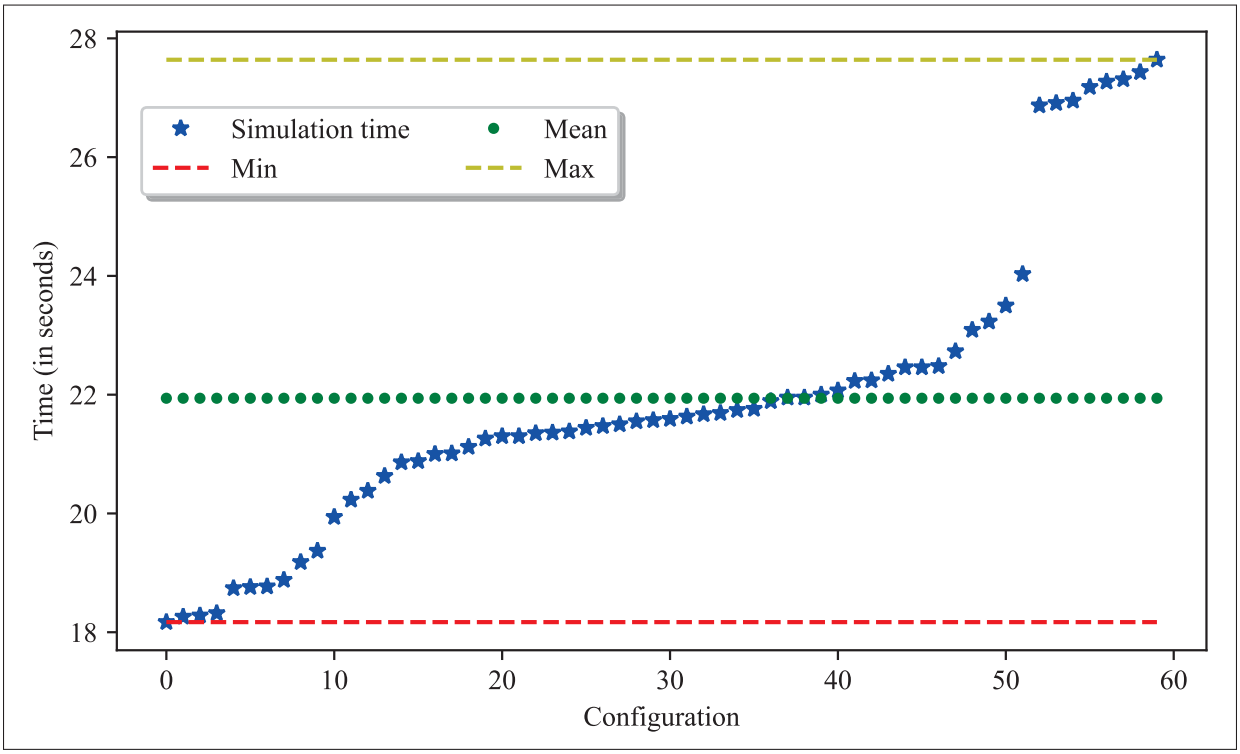

Figure 2.5 Simulation times for different numbers of configurations

Tableau 2.5 Case study projects and their numbers of configurations

Project	Total Number of Configurations
1	330
2	990
3	1540
4	5390

In addition, the maximum number of configurations to be simulated was limited to $\eta = 250$ configurations. This limitation strikes a balance between computational constraints and performance, ensuring efficient simulation without compromising the quality of the results. Instead of defining the time we wish to spend searching for the best configuration, we define the minimum number of configurations to simulate as $\sigma = 50$ configurations. Finally, to validate the approach, different projects with different numbers of configurations to be evaluated, varying between 330 and 5930 (representing small- to large-scale projects), were evaluated to compare the final solution obtained with the proposed approach with that from the traditional approach. The different projects considered and the number of configurations are shown in Table 2.5.

Table 2.5 presents the four test cases and five parameters evaluated. Considering the different variations in the number of configurations (from 330 to 5930) and the simulation waiting time (from 3600 to 7200 s), the number of configurations to be simulated and the number of configurations to be pruned after the simulation of an additional configuration were determined. In the second step, this research provides in Table 2.6 the number of configurations ρ needed to simulate and then calculate the number K of configurations to prune. Notably, the number K is specific to each project.

Tableau 2.6 Parameters considered in this study

	Parameters	**Γ**			
***t* = 10**		**330**	**990**	**1540**	**5390**
Given ϱ, compute rho (ρ) and K	ϱ (seconds)	3600	3600	5400	7200
	ρ	154	154	236	240
	K	1	5	5	21
Given rho (ρ), compute K	ρ	50	50	100	190
	K	4	15	14	27

2.4.3 Simulation Results and Discussion

2.4.3.1 Proposed BB and kNN Results

The results of this methodology are presented in Table 2.7, which shows the simulation time results ; these are also visually represented in Figure 2.6. Both show two projects, each with four different numbers of configurations, defined as ρ and τ. In this case, the results show almost identical simulation times for projects with 330 and 990 configurations when using our proposed BB and kNN approach. It should be noted that the approach implements a machine learning algorithm—the kNN algorithm—which also incurs a computational time cost. From this result, the conclusion was that, even though the proposed approach incorporates an algorithm that requires computations for each pass, the computation time decreases as the simulation process progresses and the final simulation time remained relatively short, compared to the traditional simulation approach. Applying this methodology allows the best configurations to be obtained without running all of the configurations through the simulation process, thereby considerably reducing the time required to select the best configuration.

Tableau 2.7 Simulation time results

Γ	**Method**	**Time to Find the Best Configuration (in Seconds)**	
		Given ϱ	**Given ρ**
330	Traditional process time	7,260	
	Proposed BB and KNN	3931.0156	1214.4219
990	Traditional process time	21,780	
	Proposed BB and KNN	4380.7812	1442.7969
1540	Traditional process time	33,880	
	Proposed BB and KNN	6309.3125	4185.5938
5390	Traditional process time	118,580	
	Proposed BB and KNN	7944.0781	6306.0625

The computation time of the kNN algorithm was evaluated for three types of project—namely, with 330, 990, and 1540 configurations—considering the values $\rho = 50$ and $t = 10$ configurations. Figure 2.7 shows the evolution of the CPU execution time of the kNN algorithm for these three projects. As shown in Figure 2.7, the calculation time decreased over time as each time the algorithm is run, and the number of configurations that must be run is reduced by $K + 1$.

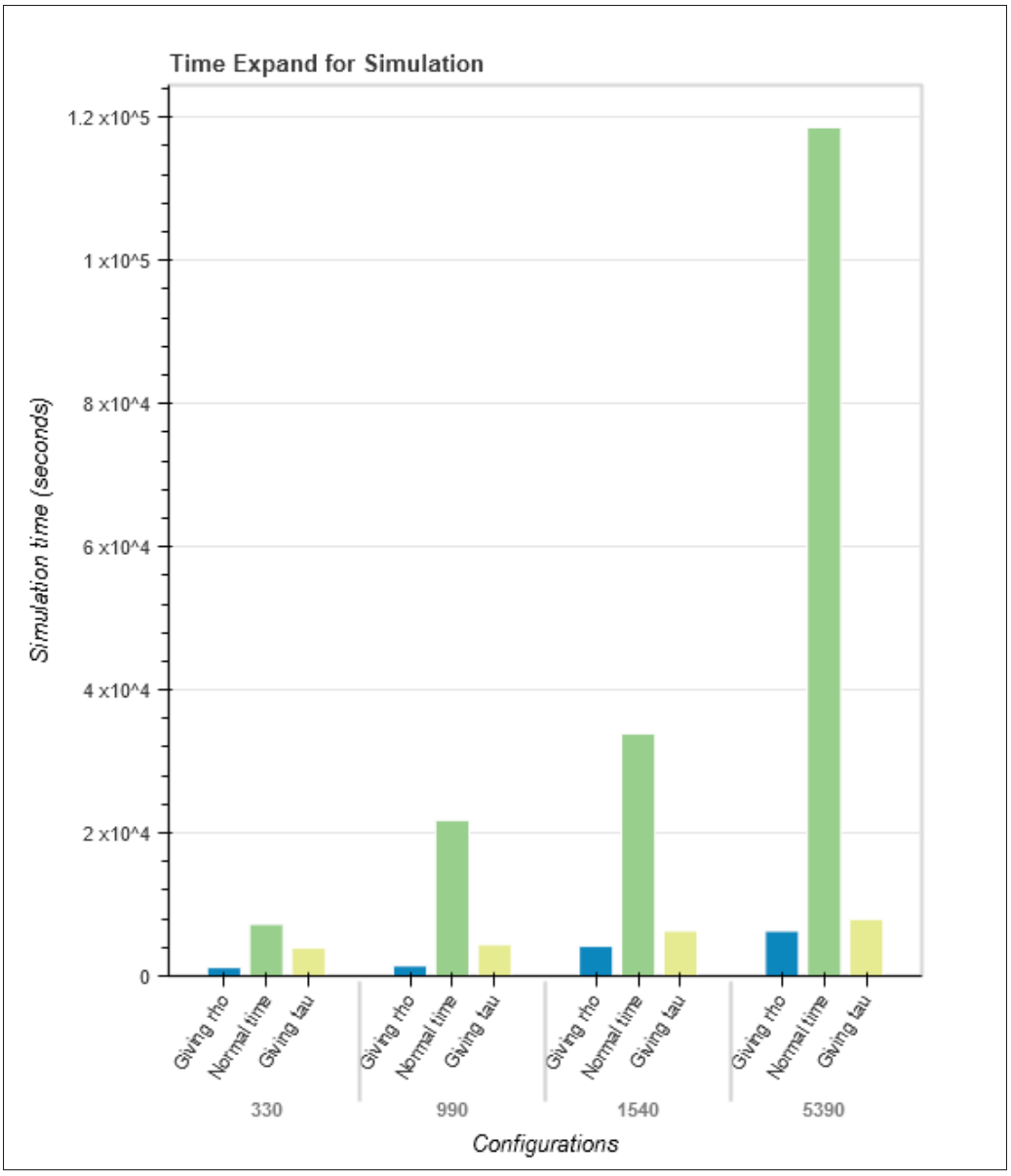

Figure 2.6 Simulations time by method and number of configurations

As can be seen from the results in Table 2.7, considering the two projects with 330 and 990 configurations, which would require 7260 s and 21,780 s, respectively, with the traditional approach and an average simulation time of 22 s, the results showed very similar search times for the best configuration. For a value of $\rho = 50$, the times obtained with the proposed approach were 1214.4219 and 1442.7969 s, respectively, for these two projects. With a value of $\tau = 3600$

s, the simulation obtained times of 3931.0156 and 4380.7812 s, respectively, for the same two projects.

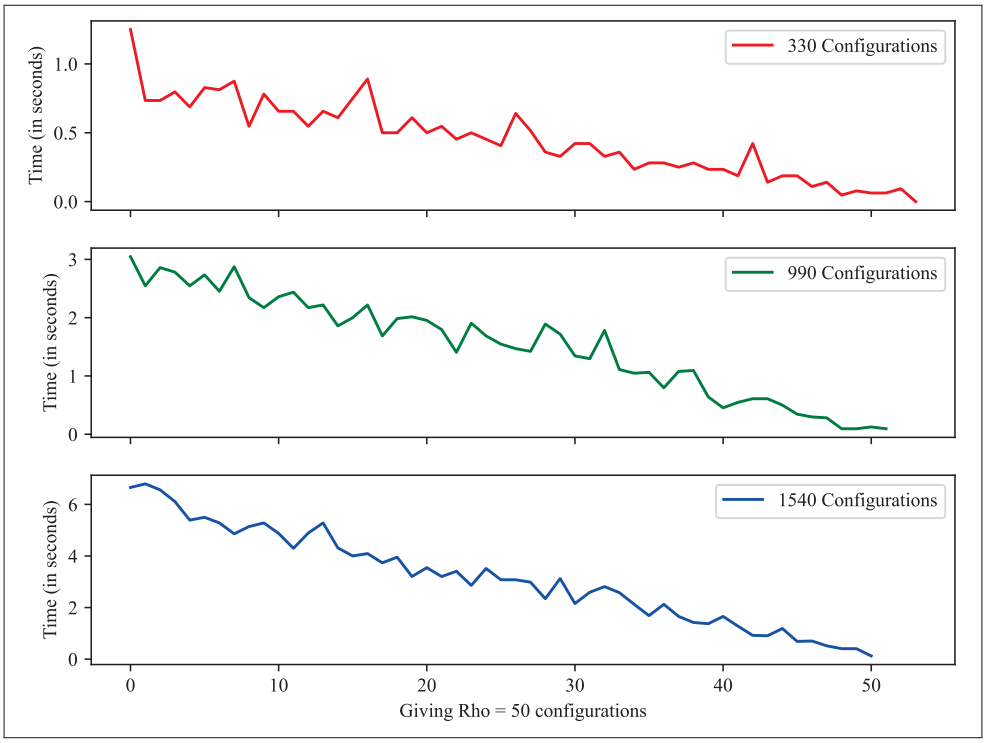

Figure 2.7 kNN processing time depending on the number of configurations

2.4.3.2 Comparing the Proposed BB and kNN Approach with the Traditional Process

Applying the proposed hybrid Branch and Bound and kNN method considerably reduced the time needed to find the best configuration. Depending on the method chosen—that is, the definition of waiting time or the number of minimum configurations to be simulated—the percentage time reduction increases with the size of the project. Table 2.7 shows that the minimum and maximum reduction rates when the waiting time was set to $\tau \in \{3600, 5400, 7200\}$ s were 45.85% and 93.30%, respectively. The minimum and maximum rates were 83.27% and 94.68% for the number of configurations $\tau \in \{50, 100, 190\}$.

The proposed methodology was applied by random selection on the first two projects and by specific area selection on the last two projects. Comparing the best configuration score obtained with the proposed approach with that of the traditional method yielded the score accuracies listed in Table 2.8. The accuracy was measured by comparing the overlap of configurations selected by the proposed and traditional methods. The evaluation shows that the number of simulated configurations impacts the accuracy of the result when compared to the traditional method; namely, the greater the time reduction, the lower the precision. However, it is important to note that the very worst loss obtained was 16.73%, which is very important regarding the research time incurred. When applied to the simulation of hybrid renewable energy system configurations, this approach means that the best configuration can always be achieved while reducing the required time. In addition, the hybrid Branch and Bound and kNN method is versatile and can be adapted to other systems, such as those including fuel cells, with minor modifications to the simulation parameters.

Tableau 2.8 Percentage time reduction using the proposed BB and kNN method

Project Size Γ	**Traditional Process Time (Seconds)**	**Proposed BB and kNN Method**			
		$\rho \in \{50, 100, 190\}$		$\varrho \in \{3600, 5400, 7200\}$	
		Time Reduction (%)	**Accuracy (%)**	**Time Reduction (%)**	**Accuracy (%)**
330	7,260	83.27	83.36	45.85	92.26
990	21,780	93.38	84.21	79.89	95.12
1540	33,880	87.65	95.60	81.38	97.25
5390	118,580	94.68	92.80	93.30	96.27

2.5 Conclusions

The effective deployment of hybrid renewable energy systems hinges on the identification of a well-defined optimal system configuration. This process typically involves extensive and resource-intensive simulations due to the vast number of potential configurations. Our study presented a hybrid methodology that combines the Branch and Bound (BB) heuristic with the k-Nearest Neighbors (KNN) algorithm to significantly reduce the computational time required for selecting the best HRES configuration. Through implementing a continuous pruning process, our approach efficiently narrows down the configuration space, retaining only those sets with similar characteristics.

When applied to four case studies, the proposed method demonstrated a substantial decrease in simulation time—up to 94.68%—while preserving acceptable accuracy. For instance, simulation times were reduced from 21,780 and 118,580 s to 1442.7969 and 6306.0625 s in two projects with differing energy demand profiles. This efficiency gain not only accelerates the selection process but also enhances the feasibility of using simulation tools in real-world scenarios where time and resources are constrained.

In conclusion, the integration of the BB and kNN algorithms provides a robust framework for optimizing simulation times in HRES design, offering a significant improvement over traditional methods. Future research could extend this methodology to other domains requiring rapid simulation and optimization, as well as explore the dynamic adaptation of the kNN algorithm to better handle evolving configuration parameters. This advancement paves the way for more efficient and scalable approaches in the design and deployment of hybrid renewable energy systems, ultimately contributing to a more sustainable energy landscape.

CHAPITRE 3

ENHANCING NEURAL ARCHITECTURE SEARCH USING TRANSFER LEARNING AND DYNAMIC SEARCH SPACES FOR GHI PREDICTION

Inoussa Legrene[1] , Tony Wong[1] , Louis-A. Dessaint[2]

[1] Département de Génie des Systèmes,
[2] Département de Génie Électrique,
École de Technologie Supérieure,
1100 Notre-Dame Ouest, Montréal, Québec, Canada H3C 1K3

Article publié dans la revue « Forecasting », août 2025
DOI : https://doi.org/10.3390/forecast7030043

3.1 Abstract

Neural architecture search is used to automate the engineering of neural network models. Several studies apply this approach, mainly in the field of image processing or natural language processing. Its application generally requires a very long computing time before converging on the optimal architecture. This paper proposes a hybrid approach using transfer learning and dynamic search space adaptation (TL-DSS) to reduce the architecture search time. To validate this approach, Long Short-Term Memory (LSTM) models were designed using different evolutionary algorithms such as artificial bee colony (ABC), genetic algorithm (GA), differential evolution (DE), and particle swarm optimization (PSO) for trend prediction of global horizontal irradiation data. The performance measures of this approach include the performance of the proposed models by RMSE evaluation over a 24-hour prediction window of the solar irradiance data trend on the one hand and the CPU search time on the other. The results show that, in addition to reducing the search time by up to 89.09% depending on the search algorithm, the proposed approach makes it possible to obtain models that are up to 99% more accurate than the non-enhanced approach. This study shows that it is possible to reduce the search time of a neural architecture while guaranteeing models with good performance.

3.2 Introduction

Designing and fine-tuning a suitable deep neural network (DNN) architecture has grown increasingly complex as applications demand ever more sophisticated models Shawki et al. (2021); Sharifi, Zoljodi, and Daneshtalab (2024). The common challenge lies in searching large, high-dimensional design spaces of layer configurations, hyperparameters, and connectivity patterns Elsken et al. (2019); Liang, Zhu, Li, Li, and Gong (2024). Conventional neural architecture search (NAS) methods address this problem by exhaustively or semi-exhaustively exploring candidate models Liang et al. (2024). However, doing so often proves computationally prohibitive Chitty-Venkata, Emani, Vishwanath, and Somani (2023). Studies that adopt NAS frequently fail to address search-space redundancy, inadvertently prolonging search times for candidate architectures that offer only marginal gains Xie, Zheng, Liu, and Lin (2018); Niu et al. (2019). Even more efficient search strategies frequently overlook how to prune unproductive subspaces or how to leverage knowledge gained from previously trained candidates Elsken et al. (2019).

To overcome these limitations, this work proposes a novel hybrid adaptive NAS approach which is specifically designed for global horizontal irradiance (GHI) trend forecasting. GHI is the total amount of solar radiation received per unit area by a horizontal surface on Earth, including both direct sunlight and diffuse sky radiation. GHI measures the solar power available on a flat surface, which is crucial for solar energy production. It influences the dimensioning of renewable energy systems and is used in solar panels and energy storage sizing Mandal, Sen, Goswami, and Chakraborty (2021). Accurate prediction of GHI assists in the design and optimization of solar power systems, ensuring that they are efficient and cost-effective. Historical GHI data are available from the National Solar Radiation Database managed by the National Renewable Energy Laboratory and the Modern Era Retrospective Analysis for Research and Applications, Version 2 (MERRA-2), of NASA. GHI data can also be purchased from non-governmental sources such as the OpenWeather database OpenWeather (2021).

The primary contributions of the proposed method encompass the following :

- Dynamic adaptation of the search spaces (DSS) : In this study, we progressively refine the search space based on interim best models, preventing the exploration of redundant architectures and speeding up convergence ;
- Reduction of exploration time via transfer learning (TL) and extrapolation techniques applied to the learning curve : The knowledge gained by high-performing architectures in initial phases is reused in subsequent generations, thus reducing time and resources, and training for unpromising candidate models is terminated early ;
- The design of high-performance architectures through intelligent adaptive exploration.

Deep learning techniques are currently used in GHI prediction Haider et al. (2022); Chinnavornrungsee et al. (2023). However, the effectiveness of these techniques depends on factors such as the neural network structure and hyperparameter tuning Ranmal, Ranasinghe, Paranayapa, Meedeniya, and Perera (2024). The selection and tuning of a suitable prediction model architecture is essential in deep learning applications Shawki et al. (2021). Combining adaptive exploration, transfer learning, and extrapolation, the proposed NAS drastically reduces the architecture's search time while maintaining high prediction accuracy. Our contributions unify multiple techniques into a single framework that accommodates complex, evolving models with lower computational overhead.

Experiments on historical datasets underscore the advantages of this hybrid approach. The method balances search efficiency by focusing on the most promising candidate architectures and predictive performance, as demonstrated by the RMSE score and significantly reduced NAS runtimes. This study shows that an intelligently curated, adaptive NAS can deliver high-performing and computationally feasible deep learning solutions.

The remainder of this paper is organized as follows. Section 3.3 focuses on definitions of neural architecture search. Section 3.4 presents the proposed approach. Section 3.5 presents the study data, results and discusses them. Section 3.6 summarizes the conclusions and offers proposals for future work.

3.3 Neural Architecture Search – NAS

NAS is a type of search technique for refining a predictive model so that it can best represent the training data. Similar to most search techniques, NAS has three components : (i) a search space containing feasible and unfeasible candidate architectures ; (ii) a search strategy to explore the search space ; and (iii) a performance estimation strategy applied to the candidate architectures to provide feedback to the search strategy (Elsken et al., 2019). The following subsections provide an overview of these components in the context of GHI prediction.

3.3.1 Architecture Search Space

An architecture search space is used to determine which neural architectures are represented. A neural architecture can be defined as a 3-tuple $a = (L, NL, Ha)$, where L is the set of neural layers, NL is the number of neural layers composing the architecture, and H is the set of hyperparameters belonging to neural architecture s. Each architecture can have a different number of neurons, activation functions, dropout rates, learning rate, and batch size. Note that NL is not necessarily equal to the cardinality of set L. From the above description, this study considers a search space S as a collection of neural architectures $S = \{a1, a2, \ldots\}$. Figure 3.1 is the conceptual representation of a search space with NL = 6 neural layers, each having a different number of LSTM cells and hyperparameters. Part (S) of this figure is the initial state where each layer can connect with others. It is a set of possible layers based on the Space parameters. Part (a) shows a possible candidate architecture produced by a sample search strategy.

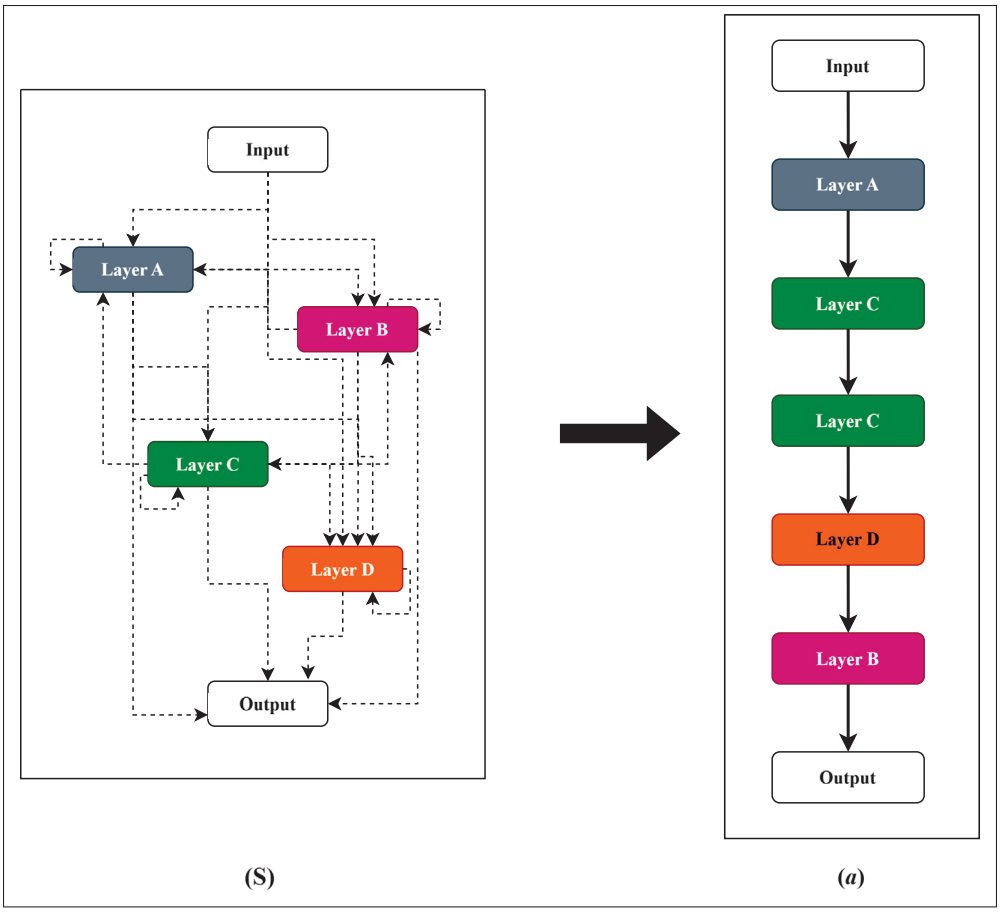

Figure 3.1 (S) Search space and (a) a possible candidate architecture

The definition of a candidate architecture $a \in S$ depends on the value of its parameters, which allow it to define its characteristics.

3.3.2 Search strategy

When building neural architecture, a search strategy is used to explore the search space. It is responsible for ordering and connecting the layers L and selecting the architecture's hyperparameter values. Given a collection of hyperparameters $\mathcal{H} = \{H_1, H_2, \ldots, H_{N_L}\}$, we wish to find an architecture that minimizes an objective function f by selecting the appropriate

hyperparameters $H \in \mathcal{H}$ (equation (3.1)),

$$\arg\min_{a \in S} f(a, H_i), \quad i = 1, 2, \ldots, N_L \tag{3.1}$$

As in most search-oriented approaches, the function f guides the search strategy when exploring the search space. Most NAS strategies design a neural architecture by adding layers sequentially. An effective strategy would both avoid being trapped in local optima and have a fast execution time. Algorithms such as Bayesian optimization, evolutionary optimization, and reinforcement learning are currently used as search strategies (Chitty-Venkata et al., 2022). In this research context, the use of metaheuristic algorithms was proposed. This approach should make it possible to find the ideal compromise between exploring new architectures and exploiting already known architectures. Thus, by defining h^* as the hyperparameters identifying the best architecture being sought, the search strategy is defined by equation (3.2) :

$$h^* = \arg\min_{a \in S} f(a, h^*) \tag{3.2}$$

The objective of the search strategy is to determine the vector of hyperparameters h^* which minimizes the objective function f (representing the Root Mean Square Error in the context of this study).

3.3.3 Performance estimation strategy

Computing the objective function in 3.3.2 represents a significant bottleneck regarding NAS execution time. The full training of neural architecture during the search process is computationally expensive and memory intensive (Elsken et al., 2019). Training using a reduced dataset can shorten the execution time and often involves regularization techniques such as dropouts and weight decay to prevent overfitting, ensuring the model generalizes well to unseen data despite the dataset's limited size. These methods, among others, enable deep learning models to achieve significant performance on small datasets (Baker, Gupta, Raskar, and Naik,

2017; Xie et al., 2018). Based on the above observation, this study proposes using transfer learning and learning curve extrapolation techniques to estimate the objective function value.

Transfer learning is a machine learning concept in which a model previously developed for a specific task is reused as an origin for creating a new model on another task. Initially, this technique is used when the data labeled for the target task is scarce but abundant for another task. The application of transfer learning aims to use the knowledge of the source domain of the basic model to improve learning in a second domain. This knowledge transfer is done by transferring the learned parameters, characteristics, and/or data representations from the original domain to the present research field (Best, Ott, and Linstead, 2020).

Learning curve extrapolation is a technique that aims to predict the future performance of a model based on its past performance. It seeks to optimize the training process by estimating later stages' performance and thereby reducing the training waiting time. This approach allows for learning about the continuation or cessation of the model's training (Viering and Loog, 2023).

Adriaensen, Rakotoarison, Müller, and Hutter (2024) used this approach to perform Bayesian inferences to predict posterior distributions more accurately and quickly than Monte Carlo methods. In the same logic, Chandrashekaran and Lane (2017) used learning curve extrapolation for hyperparameter optimization. In their study, each earlier trajectories are used to predict the next one, thereby ending the process of poorly performing constructions and accelerating the search for hyperparameters.

Let $\tilde{\mathbf{w}}$ be the weights of the current best architecture $\tilde{s}$ found during a search process. We can estimate the weights of a new architecture by

$$\mathbf{w} = \tilde{\mathbf{w}} + \Delta\mathbf{w} \tag{3.3}$$

where $\Delta\mathbf{w}$ represents the total weight of the new layers added to $\tilde{\mathbf{s}}$. The weight refers to the parameters within the network (architecture) that are adjusted during the training process to minimize the error between the predicted output and the observed data. These weights are the

scalar values multiplied by the input features or the output of neurons from the previous layer. By assuming x as the input vector, the output vector z can be expressed by :

$$z = Wx + b \tag{3.4}$$

with W and b representing the matrix of weights and biases for a given layer. Extrapolating the learning curve adds the stopping criterion during the training phase.

$$P(a, t) = P(a, t + \Delta t) \tag{3.5}$$

In equation (3.5) P is the learning loss for candidate architecture $a \in S$ at a given time t, and Δt is the maximum time allowed. If the architecture does not improve, its training process is stopped because extrapolation will lead to an almost identical value at the end of its normal training cycle.

3.4 Proposed Approach of NAS Application

In the proposed approach, the methodology of designing neural architecture by applying NAS was adopted based on its demonstrated high capacity for hyperparameter adjustment (Zhou, Moayedi, Bahiraei, and Lyu, 2020), the model training process for weight adjustment (Chitty-Venkata et al., 2023) and for model design (Telikani, Tahmassebi, Banzhaf, and Gandomi, 2021). Neural architecture design involves the application of different metaheuristics algorithms such as Artificial Bee Colony (ABC), Differential Evolution (DE), Genetic Algorithm (GA), and Particle Swarm Optimization (PSO) due to their unique approaches for solving optimization problems (Karaboga and Basturk, 2008). These methods have proven to be effective in managing high dimensionality in other fields.

Zhou et al. (2020) used ABC and PSO to obtain Multi-Layer Perceptron architectures for predicting heating and cooling loads in residential buildings much more accurately than a natural design.

Civicioglu and Besdok (2013) evaluated ABC, PSO, Cuckoo-search (CK), and DE for their numerical problem-solving and found that DE provides more robust and accurate results than ABC, PSO, and Sossa, Garro, Villegas, Avilés, and Olague (2012) studied ABC, PSO, and DE to design neural network models for classification and pattern recall. Their work showed that these algorithms were more accurate in their architectures than non-heuristic approaches.

These works have shown their value in optimizing architectures to resolve very complex problems. This study combines metaheuristic algorithms with LSTM models, which, unlike RNN networks, are able to save information in their memories, and thus are adapted for the prediction of time series (Li and Yang, 2023). Metaheuristic algorithms are used in this research only to construct the prediction model, i.e., to define the optimal number of layers, of units in each layer, the best learning rate value, and the best dropout rate value. The model's training is the sole responsibility of the backpropagation method (de Campos Souza, 2020). This section starts by presenting the LSTM model architecture, followed by steps that describe the evolutionary algorithms studied in this research and their adoption in our approach. This section ends with the application case and the evaluation strategies utilized to validate the approach

3.4.1 LSTM Model

LSTM (Long Short-Term Memory) models are a type of RNN (Recurrent Neural Network). Originally, RNN models were derived from the Hopfield network for storing and associating models (Grollier, Querlioz, Camsari, Everschor-Sitte, Fukami, and Stiles, 2020). Recurrent neural networks are known for their ability to handle most long-distance prediction problems (Gao, Yin, Zhao, Wang, and Huang, 2022). However, the disappearance of gradients in NNs is one of the main reasons that led to the development of the LSTM model. This model introduces internal trigger processes and memories for long-term information backup.

The core component of an LSTM is the memory cell, which maintains information over long periods. This helps the network to remember important information and forget irrelevant data. LSTMs use three types of gates to control the flow of information : i) Input Gate determines which information from the current input should be added to the memory cell ; ii) Forget Gate decides what information should be discarded from the memory cell ; and iii) Output Gate controls what information from the memory cell should be output at each time step.

The cell state acts as a conveyor belt, carrying relevant information through the sequence. The gates regulate the cell state, ensuring that important information is retained, and irrelevant information is discarded. At each time step, the LSTM processes the input data, updates the cell state, and produces an output. This allows the network to learn and remember patterns over long sequences. Detailed discussion on LSTM can be found in (Legrene et al., 2024a).

3.4.2 Metaheuristic algorithms

This research focuses on four metaheuristic optimization algorithms, ABC, GA, DE and PSO, which are described briefly in the following subsections. ABC performs a local search through cooperative 'bee' behaviors, enabling a focused exploration around promising solutions. DE employs differential mutation, providing robustness and adaptability in high-dimensional search spaces. GA relies on genetic crossover operators to maintain an effective balance between diversity and intensification of the search. Finally, PSO uses particle dynamics to rapidly converge toward the most promising regions of the search space. The choice of these four metaheuristics covers a wide spectrum of exploration and exploitation strategies.

3.4.2.1 Artificial Bee Colony - ABC

The ABC swarm intelligence algorithm is a metaheuristic optimization algorithm inspired by bees' foraging behavior (Dokeroglu, Sevinc, and Cosar, 2019; Yang and Liu, 2023).

Proposed in 2005 by Karaboga, the algorithm consists of three types of bees : employee, following, and scout bees (Dokeroglu et al., 2019). Each group plays a crucial role in the search

process. Employee bees are responsible for the overall exploration of the optimization problem, while follower bees are responsible for developing the best solutions. As for scout bees, their role is to put an end, when necessary, to the process of developing bad solutions. Applying the ABC algorithm to optimize the LSTM neural network architecture for predicting solar irradiance data begins with generating a population of individuals. Each individual or candidate solution $I_i = \{p_{i1}, p_{i2}, \ldots, p_{iD}\}$ is characterized by a set of parameters of dimension D, including as wthe number of neurons on the input layer, the value of the learning rate, as well as several others. Each worker bee is then assigned a candidate solution. At each generation, the bees explore the search space around their current solution by modifying its parameters to discover new potential solutions $p'_{ik} = p_{ik} + \lambda_{ik}(p_{ik} - p_{jk})$ where p'_{ik} is the new parameter value (for example, the learning rate), and λ_{ik} and p_{jk} are the random coefficient used to update the value of the parameter and a randomly chosen value of the same parameter different from p_{ik} (the current value of the parameter), respectively. Next, based on the new candidate solutions provided by the worker bees, the observer or follower bees select the candidate architectures that will be used for the next generation based on their evaluation of the fitness function, in this case, the RMSE criterion. The scout bees' role is to replace candidate architectures that fail to improve after a certain number of generations with new, randomly-generated candidate architectures.

3.4.2.2 Genetic Algorithm-GA

Genetic algorithms (GA) can be used to design LSTM neural network architecture to predict solar irradiance. These algorithms are inspired by the genetic process of biological organisms (Mehboob, Qadir, Ali, and Vasilakos, 2016; Katoch, Chauhan, and Kumar, 2021). At each step, a genetic algorithm selects individuals from the current population to be parents and uses them to produce the children for the next generation. Over successive generations, the population evolves toward a better solution. Each individual $I^k = \left\{g_1^k, g_2^k, \ldots, g_j^k\right\}$ represents the candidate LSTM architecture to be evaluated in predicting the solar irradiance data. Each I^k is composed of genes g_j, and k is the generation number. The genes specify the values of hyperparameters, such as the number of neurons in a particular hidden layer, the type of activation function (ReLU,

Sigmoid, Tanh), the value of the learning rate, and many other factors that define an individual's personality.

A set of individuals $\mathcal{I}^k = \left\{I_i^k, i = 1, \ldots, n\right\}$ is randomly generated at the start of the search. This population of LSTM networks is then improved by applying genetic operators : crossover, mutation and selection. Selection is based on the evaluation results of the previous generation's objective function for candidate architectures. For this research, the objective criterion represents the RMSE function over a 24-hour prediction window. After evaluating the population of a given generation, only the architectures that meet a specific passing condition, in this case, the individuals with a lower RMSE evaluation than the previous best in memory (for $k > 1$), or a certain proportion of the best, will be selected. This process is the selection phase. At the end of the selection phase, the algorithm applies the crossover operation, which merges the previously selected individuals to form a new individual. Finally, the algorithm applies the mutation operation to the children resulting from the crossovers. This may modify the gene values, such as the number of neurons in the first hidden layer or the value of the learning rate. The new candidate architecture population is then formed for the next stage. This process is repeated until the stop condition is met.

3.4.2.3 Differential Evolution Algorithm - DE

The differential evolution algorithm is a stochastic optimization method based on population evolution. Inspired by genetic algorithm operations, including selection, crossover, and mutation, this optimization method keeps the best particles unchanged from one iteration to the next. In contrast, other particles are replaced by new ones thanks to the above-mentioned operations (Singsathid, Puphasuk, and Wetweerapong, 2023).

This algorithm, therefore, implements four phases. An initialization phase, to create a random population of particles, and selection, crossover, and mutation phases, which give rise to the family of new particles to be evaluated. The algorithm begins by generating a family of solution vectors $I_i, i = 1, \ldots, N$ of dimensions D representing the number of parameters to be optimized.

In its general context, a DE algorithm is chiefly inspired by the genetic algorithm and pays particular attention to its mutation and crossover process. In the context of this research, at each generation, the DE algorithm creates a mutant vector $m_i^{(t+1)}$ for each of the individuals $I_i^{(t)}$ in the population. The mutant vector is, therefore, a set of different values for the various parameters used to construct the candidate architecture for solving the problem of predicting solar irradiance data. This vector is created by adding the μ-weighted difference between two or more randomly selected individuals from the population to a final individual, also chosen randomly, thereby introducing diversity into the population. The process of forming the mutant vector from three individuals can be described as $m_i^{(t+1)} = I_a^{(t)} + \mu \times \left(I_b^{(t)} - I_c^{(t)}\right)$.

By defining a combination rate, certain parameters are federated with the parameters of the current individual. This gives rise to a new set of individuals called the trial population. The DE algorithm then selects individuals by comparing the results of the objective function, i.e., the RMSE results of the current individual and its resulting trial. This selection defines the population to be considered for the next iteration. This process is repeated until the stopping condition is reached.

3.4.2.4 Particle Swarm Optimization-PSO

Particle Swarm Optimization (PSO) is a stochastic search algorithm. PSO is a multi-agent parallel search optimization technique first presented in 1995 by Kennedy and Eberhart (1995). This algorithm starts by randomly initializing the particles in the search space. Each potential solution is called a particle, and each particle has a random position, $x_i^{(0)}$, and velocity $v_i^{(0)}$ at the start. As the algorithm unfolds, each particle adjusts its parameters by computing its new velocity (equation (3.6)) and updating its position (equation (3.7)).

$$v_i^{(t+1)} = \omega v_i^{(t)} + c_1 r_1 (\text{pbest}_i - x_i^{(t)}) + c_2 r_2 (\text{gbest}_i - x_i^{(t)}) \tag{3.6}$$

$$x_i^{(t+1)} = x_i^{(t)} + v_i^{(t)} \tag{3.7}$$

As with the previous methods, finding the best LSTM architecture begins with randomly generating a set of individuals called particles. Each particle has a position $x_i^{(t)}$ at each time t representing the generation. The position defines the set of parameters used to build the architecture. In other words, the position includes the number of neurons on the layers and the values of the hyperparameters. The particle also has a velocity $v_i^{(t)}$, which defines the rate of change and the direction when exploring the search space for each particle.

Generation after generation, each particle stores the parameter values for its solution $x_i^{(t)}$ that obtains the best value of the objective function, the RMSE evaluation over a 24-hour prediction window, represented by pbest_i. At each generation, the algorithm updates the best position of the set of particles $\text{gbest}^{(t)}$. Using the coefficients of inertia ω, confidence c_1 and c_2, and random values r_1 and r_2 between 0 and 1, the algorithm defines the adjustments that need to be made to the various parameters, such as the number of neurons in the input layer, the number of neurons in the hidden layers, the learning rate, and many others, generation after generation. Ultimately, the final solution is considered as the best among the different particles' solutions. Just like the methods mentioned above, the objective of the PSO application is to obtain the optimal architecture that makes the best compromise between the complexity of the architecture and its performance.

3.4.2.5 Hyperparameter Encoding and Tuning

In the proposed method framework (ABC, DE, GA, and PSO), each individual in the population is represented by a "gene" vector encoding the neural network architecture hyperparameters.

- Neurons per input, hidden, and output layer (integer value) : Governs model capacity and the bias-variance trade-off ;
- Activation function (categorized as ReLU, Sigmoid, or Tanh) : Affects nonlinearity, convergence speed, and gradient stability ;

- Learning rate (continuous value) : Controls weight update magnitude, balancing convergence speed and oscillations ;
- Number of stacked LSTM units (integer) : Adjusts temporal depth and sequential dependency modeling.

These hyperparameters capture the core dimensions of network complexity (capacity, depth, and nonlinearity) and search strategy (diversification and intensification). Using a uniform encoding across ABC, DE, GA, and PSO ensures fair comparison while leveraging their complementary mechanisms.

3.4.3 Solution Approach

For the proposed approach, the goal is to find a high-performance architecture that best represents the dataset and that can be achieved in a reasonable amount of time. To achieve these dual objectives, this study proposes an approach that dynamically adapts the search space, and then applies transfer learning to reduce the time spent on model design. The methodology of this approach is illustrated in Figure 3.2. The metaheuristic algorithms ABC, DE, GA, and PSO were used to evaluate the impact(s) of the proposed approach.

The architectures are effectively the individuals these algorithms must optimize to obtain the most suitable architecture. In other words, the design process begins with generating a set of architectures. This set constitutes the first generation of the heuristic method.

These candidate architectures are then evaluated by applying the performance estimation strategy of the neural architecture approach. Once this evaluation, which assesses the suitability function of the designated optimization method, is completed, the algorithm selects the architecture(s) with the best value of the suitability function according to its evolution process when the stop condition has not been reached. The search policy defines this stop condition. A new candidate architecture population is generated to produce new individuals from the previous candidate architectures.

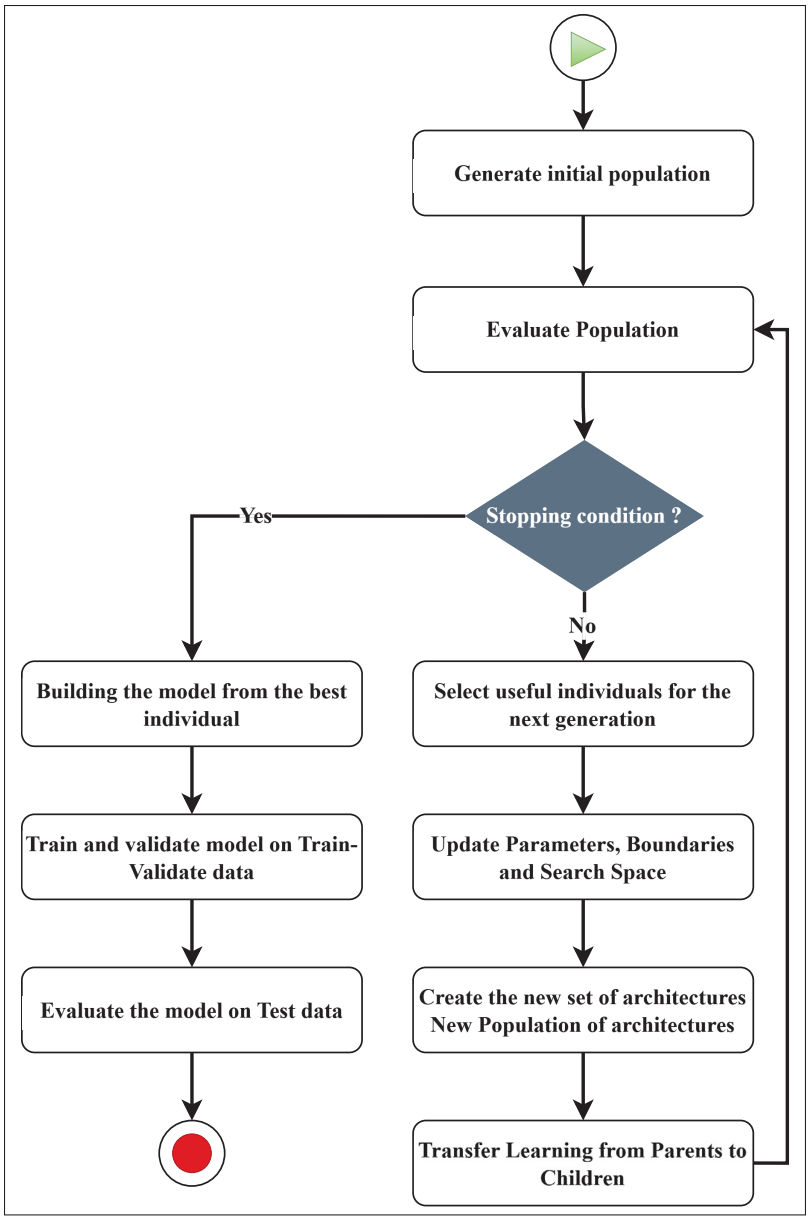

Figure 3.2 Methodology : Presents the steps involved in the metaheuristic algorithms, from defining the initial population to determining the best architecture. These steps demonstrate the dynamic adaptation of the search space and the transfer of learning from parent architectures to new child architectures

The evaluation processes, verification of the stop condition, and evolution of new populations continue until the stop condition is met. When the stop condition is reached, the best individual,

in this case, the best architecture obtained, is used as the most representative model obtained by the metaheuristic optimization method. This process allows these metaheuristic algorithms to be the main decision-makers of the architecture by reducing the researcher's involvement in defining the final size (number of layers, number of cells in each layer) of the prediction model to be designed, as well as the values of some hyperparameters (learning rate and dropout rates). All these processes are presented in Figure 3.2.

The pseudocode presented in Algorithm 3.1, along with Figure 3.2, describes the operating sequence of the proposed approach. This approach ensures an optimal compromise between search efficiency and predictive accuracy.

Algorithme 3.1 Hybrid NAS with Transfer Learning and Dynamic Search Space

Input : Initial population size N, training data D_{train}, validation data D_{val}, test data D_{test}, stopping criteria ε
Initialize : generation counter $g \leftarrow 1$
Generate initial population $\mathcal{P}_0$
Evaluate $\mathcal{P}_0$ using validation loss on D_{val}
while *stopping condition is not met (e.g., best score* $\leq \varepsilon$*)* **do**
    Select useful individuals from $\mathcal{P}_{g-1}$ for next generation
    Update parameters, boundaries, and search space based on best individuals
    Create new population $\mathcal{P}_g$ using evolutionary operations
    Transfer learned weights from parent models to offspring models
    Evaluate $\mathcal{P}_g$ on D_{val}
    $g \leftarrow g + 1$
end while
Let m^* $\leftarrow$ best individual from final population
Train m^* on $D_{\text{train}} \cup D_{\text{val}}$
Evaluate final model m^* on D_{test}
Return final trained model m^*

3.4.3.1 Dynamic Search Space-DSS

The definition of the search space is a crucial aspect in the design of neural architecture using the neural architecture search method (Liu, Sun, Xue, Zhang, Yen, and Tan, 2023b). This approach implements the definition of a dynamic search space (DSS) around the best solution from

one population to another. In this search, the study defines S as the search space from which all possible candidate architectures are derived. Each of the candidate architectures $a \in S$ is defined by a set of parameters π. A fitness function then evaluates each architecture $f(a, \pi)$. The evaluation step then identifies the best architecture a^* defined by its parameters π^*. Next, the proposed approach performs calibration operations around the best π^* parameters to define the new search space. The search space update expression can be represented by $S' = \Psi(S, \pi^*)$ in which Ψ is the adjustment function. This approach makes it possible to adjust the search space continuously around the best architectures of previous populations as the search for the best architecture progresses, allowing the definition of architectures with more and more layers while respecting the exploration stop condition. This process thus allows level-by-level evolution, avoiding the evaluation of highly complex architectures starting from 0, which would probably not lead to the definition of the best overall architecture.

3.4.4 Application and Evaluation

To evaluate and validate this approach, it was applied in the context of trend prediction of global horizontal irradiance data, and the CPU time required by each approach was measured. The training sessions were done on a computer with a 2.8 GHz Intel processor and 16 GB of RAM. The computational performance was measured using the execution time of the program using the process_time() method of the Python standard library, which made it possible to measure only the CPU time consumed by the current process, excluding periods of inactivity. The result returned is the time in seconds of system mode. We eliminate the influence of any irrelevant activity by recording the CPU time just before and just after each algorithm run. The difference between these two times gives the CPU wait time for the program's execution. This measure allows us to show the impact of the proposed solution on search time. However, to ensure that the time reduction that this approach could bring does not have a strong negative effect on the performance of the models, performance measurements were recorded. The performance evaluation of the candidate architectures was carried out using the mean absolute error (MAE)

and root mean squared error (RMSE). Equations (3.8) and (3.9) below express these performance measures.

$$\text{RMSE} = \sqrt{\text{MSE}} = \sqrt{\frac{1}{n}\sum_{i=1}^{n}(y_i - \hat{y}_i)^2} \tag{3.8}$$

$$\text{MAE} = \frac{1}{n}\sum_{i=1}^{n}|y_i - \hat{y}_i| \tag{3.9}$$

Where y_i and $\hat{y}_i$ are the values of the original (observed) and predicted data, respectively. n is the number of time series. Evaluation by MAE or RMSE defines that the best models obtain lower values.

3.5 Results and discussion

This research focused on three areas, one after the other. The first focus was on grid searching, with random searches for a high-performance architecture using the available data. Next, a neural architecture search was conducted, as defined in a non-enhanced approach by the application of evolutionary algorithms. Finally, this study utilized the enhanced version of the neural architecture search, incorporating transfer learning (TL) and adapting dynamic search spaces (DSS). The sub-sections below present the data acquisition, modeling and parameters of the study, followed by the results of the three different approaches. This section concludes with a comparison of the other approaches.

3.5.1 Data acquisition and modeling

3.5.1.1 Data acquisition

For this research, we collected historical global horizontal irradiance (GHI) data using École de technologie supérieure's main campus (Latitude : 45.4948273 and Longitude : -73.5649115) as

a reference point from the OpenWeather database (OpenWeather, 2021). This GHI data was from 2010 to 2020, which were segmented into different parts. The portion from 2010 to 2019 was used to train and validate the model, and the portion from 2019 to 2020 was used for the test phase. These time series data have several components : trend, seasonality, and residues.

3.5.1.2 Data modeling

As an important first step, special attention was invested in data pre-processing. During this pre-processing phase, the data was cleaned, and the distribution of the missing data was carried out. The results of this first step showed that the missing data can qualify as completely random missing data (MCAR).

These missing data were then imputed by the predictive mean matching (PMM) method (Akmam, Siswantining, Soemartojo, and Sarwinda, 2019). Following the imputation of missing values and the analysis of outliers, this study process to model the time series (Bandara, Hyndman, and Bergmeir, 2021). This step made it possible to decompose the data into a trend component, into different seasonal components of 24 hours, 24 hours × seven days, and a residual component. This method of decomposition, called multi-seasonal trend decomposition of time series (MSTL), is defined by equation (3.10) and is inspired by the Loess STL decomposition method.

The modeling method used in this study is the additive method.

$$Y_t = \hat{T}_t + \hat{S}_t^{(1)} + \hat{S}_t^{(2)} + \cdots + \hat{S}_t^{(N)} + \hat{R}_t \tag{3.10}$$

In equation (3.10), Y_t represents the data series at the moment t, $\hat{T}_t$ and $\hat{R}_t$ represent the trend and residuals of the series, respectively, and the seasonal components are represented by $\hat{S}_t^{(0)}$. Applying the MSTL multi-seasonal decomposition to the time-series data allows the components $\hat{T}_t$, $\hat{R}_t$ and $\hat{S}_t^{(i)}$ that compose it to be obtained. The trend makes it possible to represent a long-term evolution of the series, the seasonality of the periodic phenomenon of the identified period (day, week), and finally, through the errors or residues, the random part of the series.

The second phase of data pre-processing consisted of data standardization, a step that brings the data back to the same value scale. Standardization is necessary before data analysis by machine and deep learning models. Equation (3.11) presents the standardization operation by the min-max method.

$$x_{\text{scaled}} = \frac{x - x_{\min}}{x_{\max} - x_{\min}} \times (\max - \min) + \min \tag{3.11}$$

Calculating x_{scaled} ensures that each variable is projected in the same interval of values, preventing certain characteristics, with their higher amplitudes, from dominating the learning phase. More precisely, the minimum value $x_{\min}$ is subtracted from each observation x. The result is then divided by the original range $(x_{\max} - x_{\min})$ to obtain a normalized value between 0 and 1. Finally, multiplication by $(\max - \min)$ and the addition of min rescales the result to the target interval [min, max]. This homogeneous scaling operation facilitates model convergence and improves the robustness of estimates.

3.5.2 General architecture definition parameters

This study considered a 12-hour observation window (Loopback). The candidate architectures were trained to use a batch size of 32, the Adam optimizer, and the Sigmoid activation function, as outlined in Table 3.1 below. These specific parameter values were obtained following a sensitivity analysis involving 6, 12, and 24-hour loop backs, batch sizes of 16, 32, and 64, and two optimizers, Adam and Stochastic Gradient Descent (SGD). This analysis was carried out to design an architecture best suited to a portion of the data by applying the genetic algorithm. This step was conducted in 2 stages, with the first focused on designing an architecture for some of the data. For this procedure, different LSTM layers $L = \{LSTM(u), u \in [32, 512]\}$ and varied loop back values loopback $= \{6, 12, 24\}$ were defined. This stage identified a set of best architectures, which were then evaluated in the second stage by varying the batch size $batchsize = \{16, 32, 64\}$ and the optimizer between Adam and SGD. At the end of these experiments, the values that

provide the best RMSE prediction values for 6, 12, 24, and 48 hours for the rest of the research were retained (Table 3.1).

Tableau 3.1 Architecture Training Parameters

Loopback	Batch size	Optimizer	Activation function
12	32	Adam	Sigmoid

Table 3.2 presents the different numbers of iterations and population sizes used to search for the optimal architecture that minimizes the RMSE (Root Mean Square Error). The studied methods are all metaheuristic searches : Artificial Bee Colony (ABC), Differential Evolution (DE), Genetic Algorithm (GA), and Particle Swarm Optimization (PSO). During the metaheuristic optimization, we performed five full search cycles on the initial population and then reduced this to three cycles for each of the following populations. Each cycle corresponds to one complete application of the algorithm's operators (mutation, crossover, and selection) rather than a training pass through the neural network. For all of the generations, the population size was kept at 10. We adopt these default values to avoid a very long exploration phase. However, for the Grid Search (GS), as the process is highly random, we define a time limit ($\Delta t = 100 Hours$) as a constraint instead of the constraints on iterations and population size.

Tableau 3.2 Search parameters

Method	Iterations	Population size	Search time limit CPU Time (Hours)
Metaheuristics	5 and 3	10	–
Grid Search	–	–	100

Table 3.3 summarizes the different design parameters optimized by the metaheuristic algorithms in this study. The learning rate, a crucial factor in weight adjustment during model training via gradient descent optimization, determines the scale of weight updates.

Tableau 3.3 Search parameter boundaries

Parameters	Boundaries		
	Metaheuristics Without DSS and TL	Metaheuristics With DSS and TL	Grid Search
Number of LSTM layers	1-3	Undefined	1-3
Number of LSTM units	64-128		
Learning rate	0.0001-0.01		
Dropout rate	0.0-0.5		

Simultaneously, the dropout rate, specifying the proportion of randomly-dropped neurons in hidden layers, mitigates overfitting by enhancing the generalization capacity of deep neural networks. Instead of using fixed values as the sensitivity step, the process used them as the hyperparameters that metaheuristics should optimize. Additionally, based on the results of the early phase of the sensitivity analysis, the number of LSTM units in each layer was added as a constraint, between 64 and 128 for the metaheuristic methods and for the grid search approach. The proposed metaheuristic search does not restrict the architecture's depth ; instead, it evolves as a parameter within the metaheuristic method because the search space is updating step by step. However, for NAS without DSS and TL and with the Grid Search approach, the maximum depth of the architecture is set to 3 as defined in Table 3.3.

3.5.3 Detailed results of four approaches

This sub-section presents the results of the various experiments carried out and compares these approaches in order to show how GHI prediction can be affected by the approach adopted.

3.5.3.1 Grid Search results

Grid architecture Search (GS) achieved the best architectures in different simulations, with RMSE values of 0.0005 and 0.0015 for a 24-hour prediction in two test cases with the parameters specified in Table 3.4. GS realized these results after a search time maximum of 100 CPU hours. The results of GS evaluation over different forecast windows ranging from 6 to 72 hours are summarized in Table 3.5.

Although this approach may require a long exploration time, it can provide better architectures with an accuracy of 99% when the search intervals are well-defined. This implies that the researcher has a deep knowledge of the field. Moreover, since this search is entirely random, Table 3.5 shows that there is no guarantee of obtaining the same results from two different runs. The accuracy of two different executions may or may not vary widely due to the randomness of the approach.

Tableau 3.4 Grid Search Best models details

Method	Test Case	Architecture depth	Learning rate	Dropout rate	RMSE-24
GS-LSTM	1	1	0.005	0.0	0.0005
	2	1	0.0042	0.0	0.0015

Tableau 3.5 Grid Search results for different forecasting windows

Test Case	Criteria		Forecasting Windows (hours)			
		6	12	24	48	72
1	RMSE	0.0002	0.0003	0.0005	0.0008	0.0011
	MAE	0.0002	0.0003	0.0004	0.0007	0.0010
2	RMSE	0.0006	0.0009	0.0015	0.0027	0.0039
	MAE	0.0006	0.0009	0.0014	0.0025	0.0035

3.5.3.2 Metaheuristics Results Without TL and DSS

The search time of the Differential Evolution (DE) method is considered the reference time for evaluationg other methods. This approach's time (CPU time) is estimated at 875 hours, 34 minutes, and 57.1 seconds. Table 3.6 presents the results of the architectural search for the four different methods adopted. It is clear that the Genetic Algorithm (GA) method is an optimal architecture, with a comparison to the DE time of 5.66%, i.e., 49 hours, 35 minutes, and 40 seconds. However, the best RMSE rating on a 24-hour prediction was obtained by the DE, rated at 0.0001. The third-ranked method was the ABC-LSTM, with an evaluation of 0.0008 over 24 hours of prediction and a time of 9.12% compared to that of the DE. The PSO-LSTM scores at 0.0010 with an estimated relative time of 23.35% of the DE. Although GA has the shortest search time (5.66% of that of the DE), it remains the method with the lowest estimated evaluation score of 0.0014. In conclusion, it is important to note that based on an assessment of the prediction, neural architecture search guided by the evolutionary algorithm (DE) provides better results but requires a very long search time. So, the choice of algorithms guiding the search is an important aspect that deserves serious attention and awareness of the desired objectives.

Tableau 3.6 Results without TL and DSS

Methods		Evaluation without Transfer Learning and Dynamic Search Space				
	Depth	Learning rate	Dropout rate	RMSE 24H	MAE 24H	Relative CPU Time (%)
ABC-LSTM	3	0.0008	0.02	0.0002	0.0002	9.12
DE-LSTM	3	0.0066	0.3	0.0001	0.0001	100.0
GA-LSTM	2	0.0059	0.36	0.0014	0.0012	5.66
PSO-LSTM	2	0.0049	0.00	0.0010	0.0009	23.35

3.5.3.3 Metaheuristics results with TL and DSS

The Differential Evolution (DE) method was also used as the reference for comparing exploration CPU times when combined with TL and DSS approaches.

Tableau 3.7 Results with TL and DSS

Methods		Evaluation with Transfer Learning and Dynamic Search Space				
	Depth	Learning rate	Dropout rate	RMSE 24H	MAE 24H	Relative CPU Time (%)
ABC-LSTM	2	0.0054	0.07	0.0001	0.0001	37.73
DE-LSTM	1	0.0039	0.00	0.0005	0.0004	100.0
GA-LSTM	2	0.0039	0.30	0.0003	0.0003	25.72
PSO-LSTM	1	0.0033	0.00	0.0001	0.0001	13.42

DE is the method that required the longest search time here, estimated at 166 hours, 16 minutes, and 59 seconds. In this application, DE provides a better depth of a single architecture with an estimated RMSE rating of 0.0005 for a 24-hour prediction window, as shown in Table 3.7. Comparatively, the best evaluation results in terms of search time were obtained by PSO, GA, and ABC, in that order. PSO, with an estimated search time of 13.42% compared to that of DE, had an RMSE rating of 0.0001, while GA hads an RMSE rating of 0.0003 with an estimated search time of 25.72%. ABC scored an RMSE of 0.0001, but with an estimated search time of 37.73% of the DE's time. Thus, the results indicate that applying the proposed approach allows high-performance architectures to be obtained in significantly reduced search times.

3.5.3.4 Comparison of the results

We examine the different applications of the grid search versus searches without and then with the application of transfer learning and the dynamic search space in the GHI trend prediction. The results show that GS scores well without TL and DSS. On a time-based comparison to DE, GS has the third- lowest search time, with 11.94% compared to DE's, as presented in Table 3.8. The fourth position is occupied by the PSO method. While GS can provide a good architecture based on the proposed architecture's performance, being a completely random process, it can often be less efficient. Also, compared to DE, when transfer learning and the dynamic adaptation of the search space are incorporated, the results show that the time set as a method stop condition is far higher than that of the ABC, GA, and PSO methods. In addition, the performances of the models obtained by the ABC, DE, and PSO methods are all improved with the inclusion of TL and DSS. Thus, the results indicate that the application of transfer learning coupled with a dynamic adaptation of the search space helps to reduce search time and provides architecture with better performance.

Table 3.9 compares approaches with and without transfer learning and dynamic search space adaptation for all four methods : ABC, DE, GA, and PSO. It is immediately obvious that without TL and DSS all four methods require the longest computation time. The results show that even for the GA and ABC approaches, which generally require less time, the proposed approach reduces search time by 13.75 and 21.44%, respectively. This time reduction can be significant for the DE and PSO methods at 81.01 and 89.09%, respectively.

Tableau 3.8 Comparisons between GS and NAS approaches

Methods	Comaprison Between GS and DE Without TL and DSS		Comaprison Between GS and DE With TL and DSS	
	Relative CPU Time (%)	RMSE	Relative CPU Time (%)	RMSE
ABC-LSTM	9.12	0.0002	37.73	0.0001
DE-LSTM	100.0	0.0001	100.0	0.0005
GA-LSTM	5.66	0.0014	25.72	0.0003
PSO-LSTM	23.35	0.0010	13.42	0.0001
GS-LSTM	11.94	0.0005	62.85	0.0005
		0.0015		0.0015

Tableau 3.9 Direct comparison between our approaches and a non-enhanced approach

Methods	Comparison Between Approaches without TL and DSS and Approaches with TL and DSS				
	Without		With		CPU Time Reduction (%)
	Relative CPU Time (%)	RMSE	Relative CPU Time (%)	RMSE	
ABC-LSTM	100.0	0.0002	78.56	0.0001	21.44
DE-LSTM	100.0	0.0001	18.99	0.0005	81.01
GA-LSTM	100.0	0.0014	86.25	0.0003	13.75
PSO-LSTM	100.0	0.0010	10.91	0.0001	89.09

In addition, the results show that of all the methods, only the DE-LSTM method achieves an RMSE evaluation result without TL and DSS that is better than when applying TL and DSS, but an almost similar result, as shown in Table 3.9. Not only does this approach reduce search time, but it also allows for the best results on evaluations of the same datasets. Also, as presented in Tables 3.6 and 3.7 above, the depth of architectures obtained without TL and DSS applications is greater than or equal to that of architectures with TL and DSS. However, the complexity of the architecture does not necessarily imply good adaptability to the data. Then, allowing methods to adapt and learn from their parents allows for rapid convergence and fewer complex architectures without losing accuracy.

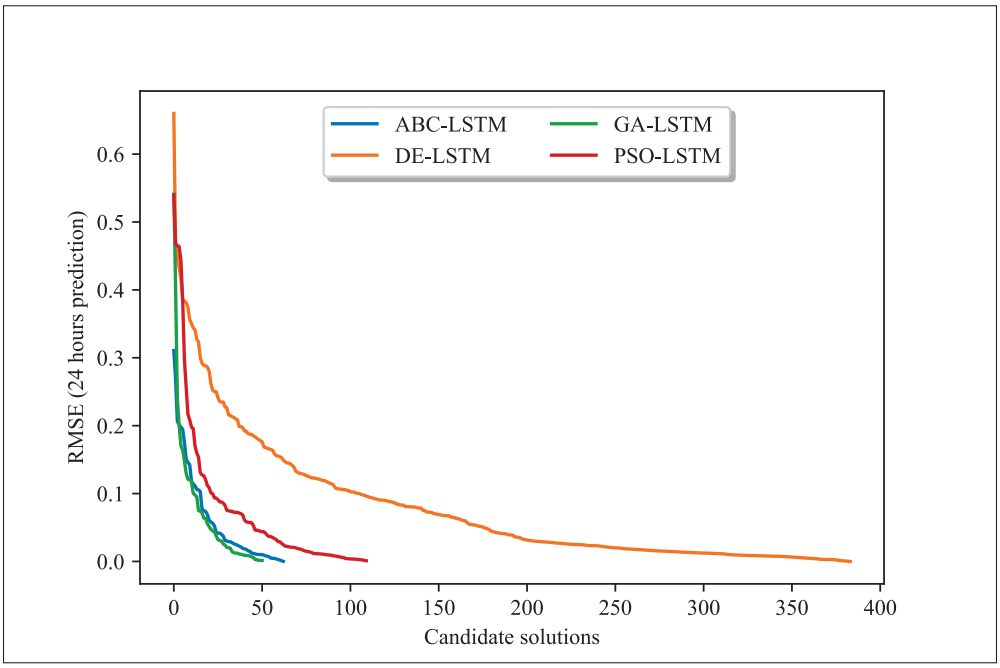

Figure 3.3 NAS approach WITHOUT TL and DSS : Shows the number of candidate architectures evaluated per method and the order of magnitude of the RMSE errors obtained

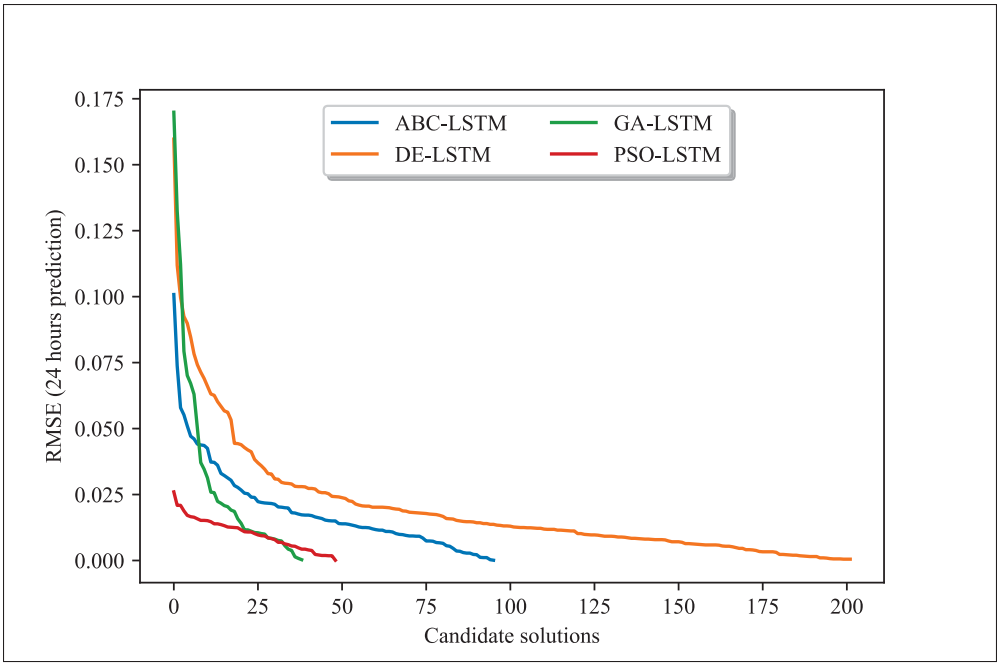

Figure 3.4 NAS approach WITH TL and DSS : Shows the number of candidate architectures evaluated per method and the order of magnitude of the RMSE errors obtained

Figures 3.3 and 3.4 above show, on the x-axis, the number of candidate architectures evaluated by each algorithm according to the methodology adopted, and, on the y-axis, the root mean squared errors (RMSE) obtained. These figures show that by applying the proposed TL and DSS approach, the worst RMSE rating obtained was only 0.175, while with the non-enhanced application of the NAS, the worst RMSE rating was close to 0.660. Also, even though ABC realizes a higher number of evaluations of candidate architectures in the enhanced approach, the overall search time is shorter than with the non-enhanced approach. This shorter search time is achieved because this enhanced approach controls the search space for the design of candidate architectures.

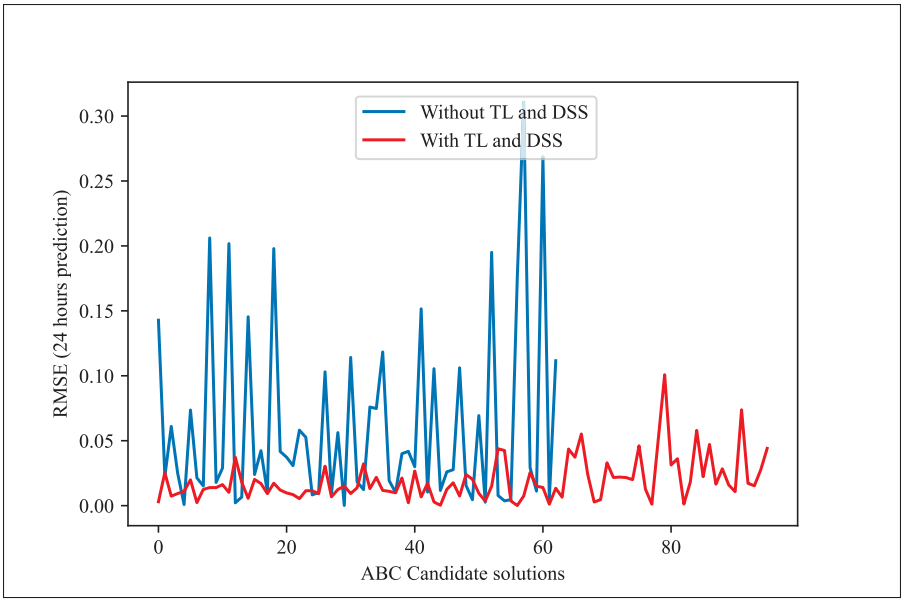

Figure 3.5 Proposed ABC candidate solutions' evolution : Shows the number of candidate architectures and the order of magnitude of RMSE errors for the candidate architectures with and without TL-DSS

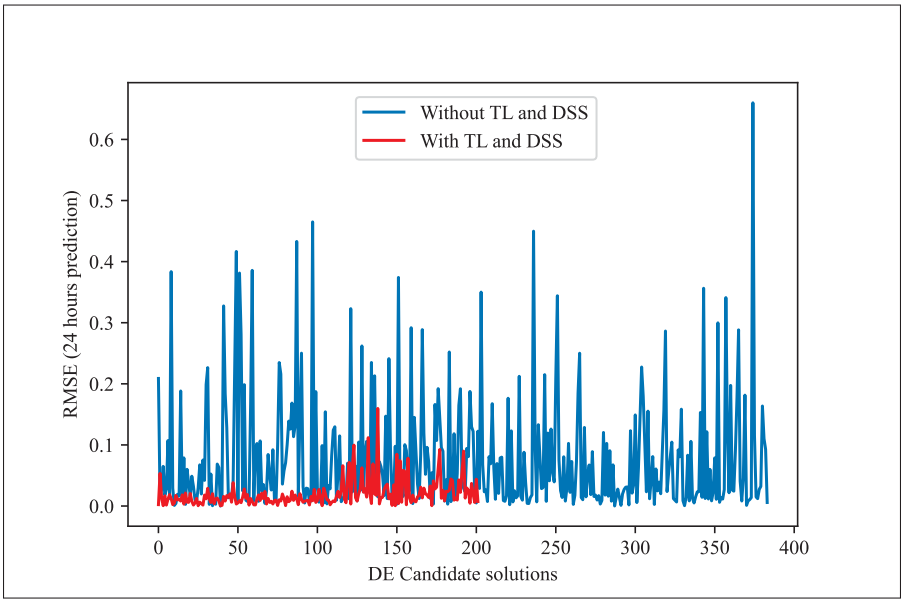

Figure 3.6 Proposed DE candidate solutions' evolution : Shows the number of candidate architectures and the order of magnitude of RMSE errors for the candidate architectures with and without TL-DSS

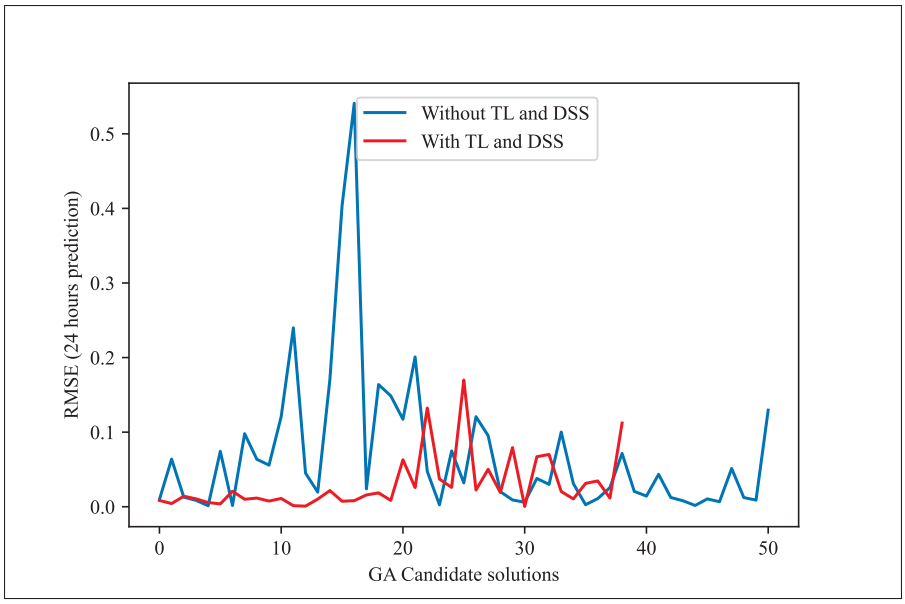

Figure 3.7 Proposed GA candidate solutions' evolution : Shows the number of candidate architectures and the order of magnitude of RMSE errors for the candidate architectures with and without TL-DSS

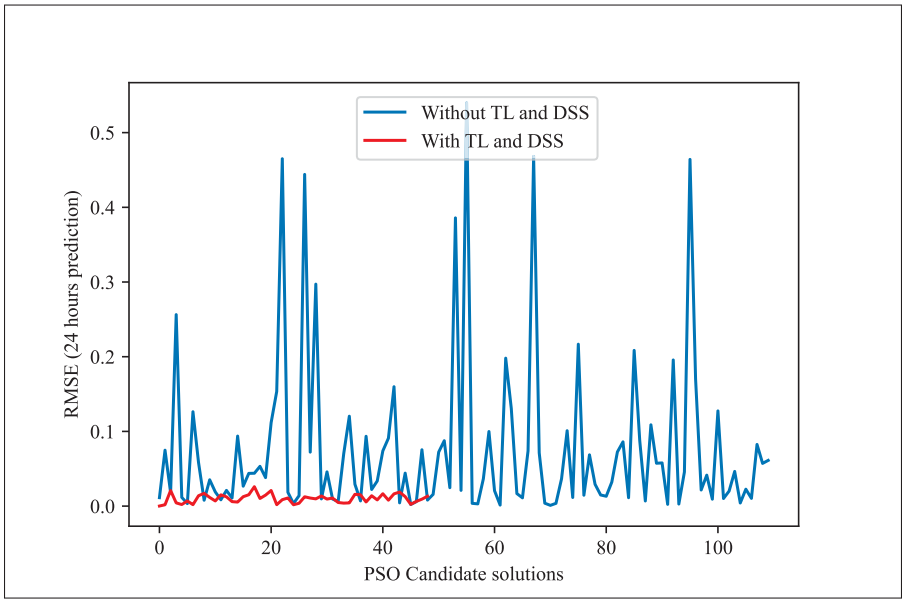

Figure 3.8 Proposed PSO candidate solutions' evolution : Shows the number of candidate architectures and the order of magnitude of RMSE errors for the candidate architectures with and without TL-DSS

Finally, the results show that, although DE excels in accuracy with and without TL-DSS, its differential mutation strategy involves a high number of fitness assessments, resulting in a longer CPU time. Thus, the choice of methodology depends not only on the resources available (search time) but also on the accuracy of the model.

Figures 3.5 to 3.8 show the search space's normal evolution of the four candidate architectures. The approach proposes architectures with more controlled evaluation results, contrary to the non-enhanced approach.

These figures show that the proposed methodology achieves the following :

- Converges more quickly : Most of the error reduction occurs within the first 20-30 iterations for the proposed method. In contrast, the basic method often requires more than 50 iterations or even double that to achieve a comparable level of performance.
- Presents reduced variance : The red curves fluctuate much less and have a narrower envelope, reflecting more controlled and reliable progress. In contrast, the blue curves (approach without TL-DSS) frequently show declines and peaks of degradation, indicating ineffective evaluation.
- Achieves a more reliable final RMSE : In each of the figures, the end point of the red curve (approach with TL-DSS) is below that of the blue curve (approach without TL-DSS). This result shows that TL-DSS not only speeds up the search but also produces a more accurate architecture.

The results presented in these figures confirm that integrating transfer learning and dynamically adapting the search space leads to more efficient and stable NAS trajectories than the non-enhanced approach.

3.5.4 Comparison with other research

Tables 3.10 and 3.11 presents a comparison of different neural architecture search (NAS) methods, highlighting the diversity of approaches and application areas covered by current research.

Tableau 3.10 Comparison between the proposed approach and other related research (1/2)

Article / Method	**Field of application**	**NAS method / Main algorithm**	**Major innovations**	**Efficiency / Main performance**
ESC-NAS (Ranmal et al., 2024)	Classification of environmental sounds on the edge	NAS hardware-aware, Bayesian search	Cell search optimized for edge, taking into account hardware constraints	85,78% (FSC22), 81,25% (UrbanSound8K), compact models for edge
EGNAS (Jwa et al., 2024)	Graph Neural Networks (GNN)	Evolutionary NAS, parameter sharing	Fast evolutionary algorithm, weight sharing, step training	Up to 40× faster than SOTA methods, better accuracy on Cora, Citeseer, PubMed
Multi-Objective Evolutionary NAS (Liang et al., 2024)	Image classification (generalized)	Multi-lens evolutionary NAS, supernet	Weight-sharing supernet, MOEA/D bi-population, inter-population communication	Outperforms SOTA on various datasets, increasing diversity and efficiency
TrajectoryNAS (Sharifi et al., 2024)	Trajectory prediction (autonomous vehicles)	Multi-objective NAS, metaheuristics	End-to-end optimization, precision/latency function, NAS on each component	+4,8 % precision, 1.1× less latency on NuScenes compared to SOTA

Tableau 3.11 Comparison between the proposed approach and other related research (2/2)

Article / Method	**Field of application**	**NAS method / Main algorithm**	**Major innovations**	**Efficiency / Main performance**
The proposed approach : ENAS-TL-DSS	Time series prediction	Enhanced NAS, evolutionary algorithms, LSTM	Dynamic Search space, learning transfer, learning curve extrapolation	Up to 89.09% of search time reduction, up to 99% prediction accuracy, increasing efficiency

Each method is distinguished by specific innovations tailored to various needs : ESC-NAS (Ranmal et al., 2024) targets the optimization of sound classification on edge devices by integrating hardware constraints. EGNAS (Jwa et al., 2024) proposes an approach to accelerate architecture search for graph networks using evolutionary algorithms and weight sharing. Multi-objective approaches, such as that of Liang et al., promote the discovery of efficient and diverse architectures through weight sharing and advanced evolutionary strategies. TrajectoryNAS (Sharifi et al., 2024), meanwhile, illustrates the importance of end-to-end optimization for real-time trajectory prediction, balancing accuracy and latency. Although these approaches have proven effective in their respective fields, none of them address the issue of search space, which can introduce dimensioning biases. Furthermore, search space optimization remains a common problem across all application domains. As a result, the method proposed in this study not only improves knowledge sharing but also dynamically optimizes the search space as the search evolves. It also avoids evaluation overtime, thanks to its learning curve extrapolation approach. This approach reduces search time by up to 89% while ensuring an accuracy of around 99%.

3.6 Conclusion

The trend prediction of global horizontal irradiance data was used to validate the approach proposed in this study, involving the design of LSTM models by neural architecture search (NAS). This approach implements evolutionary methods to explore the search space using four different algorithms : artificial bee colony (ABC), genetic algorithm (GA), differential evolution (DE), and particle swarm optimization (PSO). The results show that using neural architecture search combined with the application of evolutionary algorithms yields excellent results, achieving an RMSE and MAE evaluation of over 99% within a 24-hour prediction window. However, this approach remains very restrictive in terms of its time requirements. To address this issue, a hybrid learning approach was proposed, incorporating transfer learning and dynamic adaptation of the research space (TL-DSS). The results obtained when using this enhanced approach demonstrated that it is possible to significantly reduce research time while achieving equally efficient models. Incorporating TL-DSS can reduce the search time previously required for the ABC and GA algorithms by 21.44% and 13.75%, respectively. The reduction in search time reached 81.01% for DE and 89.09% for PSO.

In summary, this study makes three key contributions :

- Dynamic search space (DSS) : Progressively refining the search space based on interim best models ;
- Speed-up via transfer learning (TL) and learning curve extrapolation : Significantly reducing the NAS run time ;
- High-performance architecture design through intelligent adaptive exploration : Balancing speed and predictive accuracy.

These contributions demonstrate the feasibility and effectiveness of the proposed approach for GHI forecasting while paving the way for future extensions.

Building on these contributions, several promising directions emerge :

- Extending dynamic NAS to Transformer-based time-series models, leveraging their self-attention mechanisms for long-range dependencies ;

- Investigating conditional NAS for hybrid CNN–RNN or GNN architectures, allowing the search to jointly select model families and hyperparameters.

The obtained results suggest that exploring these avenues will further optimize the efficiency of searches and reveal powerful architectures in a wide range of application areas.

CHAPITRE 4

DEEP REINFORCEMENT LEARNING APPROACH FOR HYBRID RENEWABLE ENERGY SYSTEMS OPTIMIZATION

Inoussa Legrene[1] , Tony Wong[1] , Louis-A. Dessaint[2]

[1] Département de Génie des Systèmes,
[2] Département de Génie Électrique,
École de Technologie Supérieure,
1100 Notre-Dame Ouest, Montréal, Québec, Canada H3C 1K3

Article publié dans la revue « Engineering Applications of Artificial Intelligence », juillet 2025
DOI : https://doi.org/10.1016/j.engappai.2025.111650

4.1 Abstract

The sizing of hybrid renewable energy systems (HRES) is a major challenge faced in contemporary energy research. The optimal configuration based on the specific consumption requirements is essential for strategic energy planning. Effective sizing must balance the investment costs, reliability, environmental impacts, and greenhouse gas emissions while satisfying the expected energy requirements. This study proposes a novel multi-criteria sizing approach based on deep reinforcement learning (DRL). The DRL agent is guided by a reward function that integrates three essential performance metrics : energy cost (LCOE), renewable energy fraction (REF), and the Loss of power supply probability (LPSP). A penalty function is also included to consider the reliance on external sources, such as diesel generators and the public grid, promoting greater autonomy and renewable usage. The DRL-based approach was implemented and tested on three distinct demand profiles, using hourly data for one year. A comparative analysis was conducted against three established methods : particle swarm optimization (PSO), multi-objective PSO (MOPSO), and non-dominated sorted genetic algorithm (NSGA-II). The results indicate that DRL significantly outperforms all the benchmark methods in terms of economic efficiency. DRL achieves a significant reduction in the energy costs, ranging from 21.33% to 30.09% when compared with PSO, 27.89% to 30.27% when compared with MOPSO, and 27.63% to 28.47% when compared with NSGA-II. These findings demonstrate that DRL presents a robust

and adaptive framework for the sizing and operational control of HRES. DRL presents more autonomous, cost-effective, and scalable renewable energy solutions by minimizing the energy costs while maintaining the system reliability.

4.2 Introduction

Hybrid renewable energy systems (HRES) are being increasingly implemented owing to the need to reduce greenhouse gas (CO_2) emissions and the diversification of energy sources. However, the process of sizing a hybrid energy system remains a complex challenge owing to the variability of renewable sources and the specific requirements of each consumer. Consequently, several approaches have been developed, including the use of metaheuristic methods such as particle swarm optimization (PSO) (Faria et al., 2023; Musa and Ibrahim, 2015), genetic algorithm (GA) (Medghalchi Taylan, 2023), and grey wolf optimization (GWO) (Mahmoud et al., 2022), along with the use of simulation tools such as HOMER/HOMER Pro (Bazzi et al., 2024 ; Lilienthal, 2005). These methods present excellent performance in the various contexts in which they have been used. However, they face several limitations, which are given below :

- Sensitivity to the initial optimization parameters—metaheuristics require precise, algorithm-specific parameter adjustments to avoid being trapped in the local optima.
- Partial consideration of dynamic variations—variation in the loads and generation sources must be considered to ensure a system that is robust against the intermittent nature of the generation sources.
- High computational cost—some approaches, such as dynamic programming and simulation tools, require a considerable amount of time and resources to optimize large ensembles.

Therefore, in this study, we proposed a method based on a deep reinforcement learning (DRL) approach.

The application of DRL presents significant advantages in terms of the adaptability to varying conditions, thereby creating a balance between exploration and exploitation, multi-criteria

management, and flexibility for different configurations. By applying Deep RL, this study promotes four key aspects : adaptability and continuous learning, a balance between exploration and exploitation, flexibility and generalization, and reward-based learning.

Since HRES face constant variations in the production and demand, DRL enables real-time adaptation to these variations, thereby improving the system efficiency by continuously adjusting the energy management strategies. Exploration and exploitation must be balanced to achieve better interplay between energy consumption and maximizing the long-term efficiency. The proposed approach can be applied to various HRES to integrate new technologies (thermal storage, gas generators) or facilitate adaptation at different scales (from microgrids to large-scale grids). Reward-based learning helps in achieving the perfect compromise between multiple objectives, which is crucial since different and often conflicting objectives (system cost, energy efficiency, emission reduction) must be considered for the sizing of a reliable HRES. Reinforcement learning makes it possible to model these trade-offs using a reward function, enabling an efficient multi-criteria optimization that considers the variability of renewable energy sources.

Based on these observations, this study addresses four issues that have not yet been addressed in the previous studies conducted on HRES. (i) Adaptive sizing : component capacities (PV, WT, BESS, DG) are learned online using a deep reinforcement learning policy, addressing the conventional "sizing-dispatch" dichotomy. (ii) Multi-criteria cumulative reward : a unified reward signal simultaneously reduces the levelized cost of energy (LCOE) and Loss of power supply probability (LPSP), while maximizing the fraction of renewable energy (REF), without requiring the prior heuristic weighting or a posteriori Pareto front sorting. (iii) Flexible simulator-agnostic framework : the algorithm interacts with the environment only through state-action pairs, enabling a high-fidelity digital twin or a data-driven metamodel to be freely interchanged. (iv) Direct integration of generator-grid constraints : generator ramp limits and grid purchase/sale quotas are encoded in the Markov decision process, thereby ensuring operational feasibility in the island, grid-coupled, or hybrid modes. These four factors constitute the novelty of this study and pave the way for real-time, multi-criteria, and scalable optimization of HRES.

The main contributions of this study can be summarized as follows :

- **Adaptive and Autonomous Sizing of Renewable Energy Systems Using Deep Reinforcement Learning (DRL)**—Unlike conventional metaheuristic approaches that require manual parameter tuning, DRL learns autonomously from system interactions, making it more adaptable to variations in the energy demand and renewable resource availability. This extends beyond fixed-rule optimization by enabling self-learning strategies that improve with time.
- **Multi-Criteria Cumulative Reward Modeling for Hybrid Renewable Energy Systems Optimization**—One of the major challenges in HRES sizing involves balancing conflicting objectives, such as cost minimization, renewable energy utilization, and system reliability. This study presents a reward-based framework that dynamically evaluates the trade-offs between these factors, enabling the DRL model to optimize the energy dispatch and storage decisions in real time while ensuring a cost-effective and reliable system configuration.
- **Flexible and Scalable Optimization Framework for Hybrid Renewable Energy Systems**—The proposed DRL-based methodology is designed to be adaptable to various HRES architectures, from off-grid microgrids to large-scale grid-connected systems.

The remainder of this article is organized as follows. Section 4.3 presents an overview of recent studies on the design of hybrid renewable energy systems, including their methodologies and types of systems. Section 4.4 presents the modeling of the HRES, the problem formulation, and the proposed systematic DRL approach. Section 4.5 presents the results, discusses the methods developed in this study, and compares the results with those reported in previous studies. Lastly, Section 4.6 presents the conclusion and future research implications.

4.3 Related reviews

Extensive research has been conducted on HRES. However, there is no unanimity on the components (photovoltaic (PV) solar panels, wind turbines (WT), batteries as an energy storage system (BESS)) that constitute these hybrid systems (Faria et al., 2023; Samy et al., 2018),

the best algorithm or optimization tool (Baidas et al., 2022; Musa and Ibrahim, 2015), or the cost, reliability, and feasibility evaluation factors required for system performance analysis (Kushwaha and Bhattacharjee, 2024; Kushwaha, Ray, and Bhattacharjee, 2022). The diversity of these systems can be attributed to the uniqueness of each problem, which is characterized by a proprietary consumption profile in various weather conditions that affect the availability of the exploitable energy sources.

Kushwaha and Bhattacharjee (2024) reported various systems based on PV solar panels, WT, BESS, and biogas (BG) and diesel (DG) generators as an external compensation system for the difference in production. Following several evaluations, they obtained an optimal PV-WT-BESS-BG-DG system based on social, economic, technological, and environmental criteria, with an energy cost of 0.1799 $\$/kWh$ for a village in India. Mokhtara et al. (2021) also proposed an optimal design approach for PV/WT/BESS/DG hybrid systems for the electrification of residential buildings in rural areas, considering the energy performance of the buildings and the climatic conditions.Medghalchi and Taylan (2023) addressed the sizing of a system comprising PV, WT, BESS, and a fuel cell electrolyzer [16]. They reported that a combination of PV, WT, and BESS is the most favorable system, with an energy cost of 0.1838 Euro/kWh. Bouafia et al. (2023) evaluated various combinations comprising PV and WT in 12 localities in Morocco. They reported that the best system is obtained by integrating PV and WT. Lastly, several studies, including the analyses conducted by Samy et al. (2021), demonstrated that green energy systems (PV/WT) can improve the reliability of unstable power grids while highlighting the economic implications.

Various methods have been developed in the previous studies. Simulation tools such as HOMER/HOMER Pro (Bazzi, El Hafdaoui, Khallaayoun, Mehta, Ouazzani, and Zörner, 2024; Lilienthal, 2005) and PVGIS (Lemaire et al., 2024) have been used to simulate the typical examples of predefined systems (configurations). Several works have highlighted the economic and feasibility factors of this simulation approach as the criteria for selecting the optimal system (Bahgaat, 2023; Baidas et al., 2022; Lu et al., 2017). Baidas et al. (2022) simulated various configurations using HOMER, which were then evaluated and compared. The comparison

criterion was the net present cost (NPC), with the most profitable configuration from an economic and environmental perspective involving integrating WTs and batteries. Similarly, several studies have adopted metaheuristic algorithms, such as PSO and its derivatives, including MOPSO, instead of simulation tools (Bouafia et al., 2023; Faria et al., 2023; Mansouri Kouhestani et al., 2020; Medghalchi and Taylan, 2023; Musa and Ibrahim, 2015; Samy et al., 2021; Ukoima, Okoro, Obi, Akuru, and Davidson, 2024), GA (Medghalchi and Taylan, 2023) and its derivatives, such as the non-dominated sorted genetic algorithm II (NSGA-II) (Sandeep and Nandihalli, 2020; Ukoima et al., 2024), Salp Swarm Algorithm (SSA), GWO and its derivatives (Mahmoud et al., 2022), and social spider optimization (SSO) and opposite social spider optimization (OSSO) (Sandeep and Nandihalli, 2020).Faria et al. (2023) analyzed MOPSO to analyze the shared energy management between several consumers, also known as community management. Economic and technical criteria, such as the energy costs and self-sufficiency ratios, were in direct conflict in this work, and based on the analytical approach adopted, the so-called optimal configuration varies between the members of the community and between the approaches used to exploit the energy produced (Bahgaat, 2023). In (Kushwaha and Bhattacharjee, 2024), several metaheuristic algorithms are used to determine the best approach, including the marine predator algorithm (MPA), GA, PSO, and SSA. The MPA is significant due to its ability to evade local minimums while obtaining the best energy cost, at 0.1799 $\$/kWh$, for the best configuration. Similarly, Mahmoud et al. (2022) compared SSA, GWO, and improved GWO (IGWO). In they study, they primarily focused on energy production using PV panels and WTs, BESS, and external energy production using a diesel generator. Consequently, they demonstrated that the IGWO method presented the best performance when compared with the other approaches.

A wide range of factors can be considered as the selection criteria. Typically, various factors, such as the algorithm or simulation tool used, performance evaluation criteria, components of the HRES, weather conditions affecting the choice of renewable sources, and energy requirements to be met, significantly affect the final system to be adopted. Although the metaheuristic methods present good performance when the parameters are well defined, they can also underperform and get trapped in the local optima (Kushwaha and Bhattacharjee, 2024) if the environmental

parameters are not defined precisely. Essentially, the solution approach depends on the problem to be solved and requires adjusting the hyperparameters for each problem instance.

4.4 System and Problem Formulation

In this study, we addressed the sizing of HRES, as shown in Figure 1 (Legrene et al., 2025). PV panels and WTs have been used as the main sources of energy production in various research projects (Al-Quraan and Al-Mhairat, 2024; Baidas et al., 2022). These renewable sources are supported by generators running on natural gas or diesel (DG). In particular, generators are included to ensure the system reliability, particularly in the event of extreme weather conditions or grid outages. This study minimizes their usage to reduce the carbon footprint and maximize the use of renewable energies. Additionally, these systems are typically combined with BESS to make them robust (Baidas et al., 2022; Mahmoud et al., 2022). Consequently, we considered four different types of HRES (based on the principle depicted in Figure 4.1) :

- PV solar panels coupled with BESS : PV+BESS ;
- PV solar panels coupled with BESS and generators : PV+BESS+DG ;
- PV solar panels and WTs coupled with BESS : PV+WT+BESS ; and
- PV solar panels and WTs coupled with BESS and generators : PV+WT+BESS+DG.

The following subsection present the mathematical approaches applied to the system elements (PV solar panels, WTs, BESS, DG, and hybrid converter), the problem formulation, and the optimization strategy.

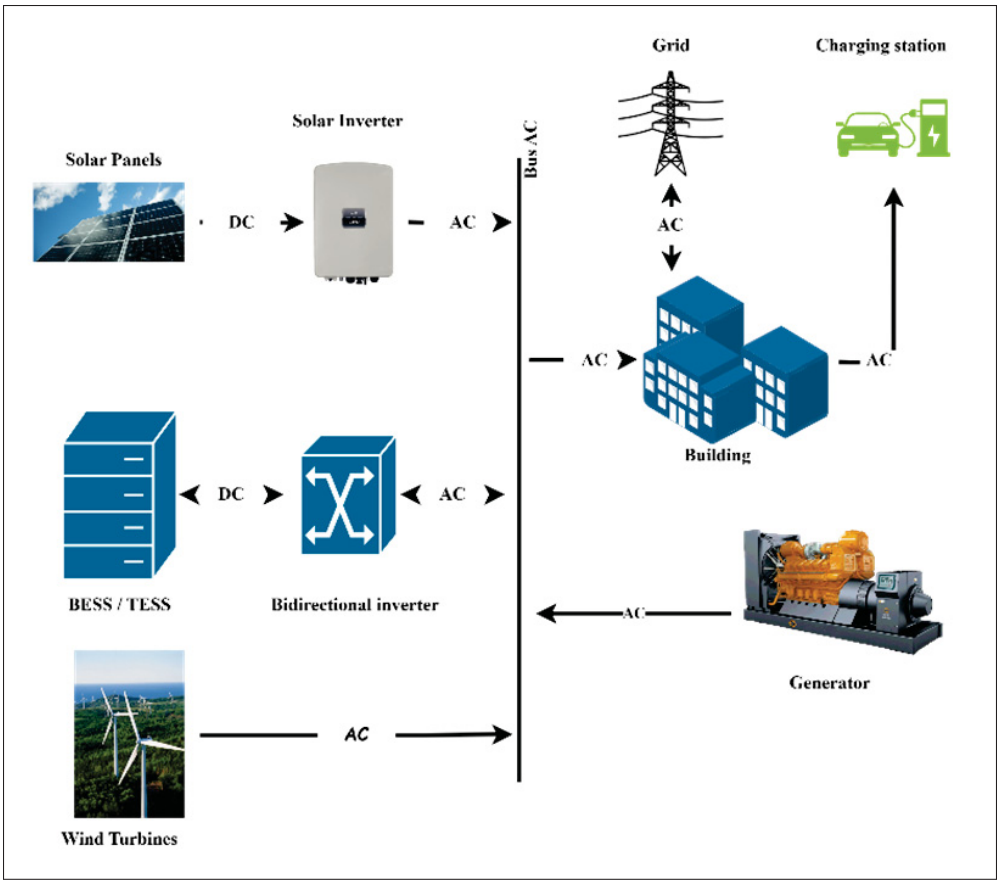

Figure 4.1 Hybrid Renewable Energy System (HRES) (Legrene et al., 2025)

4.4.1 System Modeling

4.4.1.1 Solar panel model

Several factors must be considered when producing energy through PV systems, including solar irradiance, ambient temperature, and panel efficiency (Mahmoud et al., 2022; Tabak et al., 2017; Memon et al., 2021). The energy produced depends on the number of panels in the system, which is an optimization problem parameter. An optimization method is implemented to determine the minimum number of PVs that help achieve the ideal compromise between the amount of energy

produced and the cost. The amount of energy produced is defined as follows :

$$P_{\mathrm{PV}} = \eta_{\mathrm{PV}} \times S_{\mathrm{PV}} \times I(t) \tag{4.1}$$

where η_{PV} and S_{PV} denote the instantaneous efficiency and the installation area of the panels (in m^2), respectively, and are defined as follows (Mahmoud et al., 2022; Memon et al., 2021) :

$$\begin{gathered} \eta_{\mathrm{PV}} = \eta_r \times (1 - \beta_T \left(T_c(t) - T_{\mathrm{nom}}\right) \\ \beta_T = \frac{k_p}{100} \\ T_c(t) = T_a + \left[\left(\frac{\mathrm{NOCT}-20}{800}\right) \times I(t)\right] \end{gathered} \tag{4.2}$$

$$S_{\mathrm{PV}} = \frac{N_{\mathrm{PV}} \times P_{\mathrm{PV}}^{\mathrm{rated}} \times \eta_{\mathrm{cab}}}{I_{\mathrm{nom}}} \tag{4.3}$$

Here, η_r denotes the effectiveness of the panel, T_{nom} and I_{nom} denote the standard operating conditions (T_{nom}=25 °C and I_{nom}=1000 W/m^2), T_a and T_c denotes the ambient temperature (based on the locality) and the temperature, respectively, of the panel (in °C). Additionally, k_p denotes the maximum power coefficient of temperature (in %/°C), and NOCT denotes the nominal operating temperature of the PV cells, which is provided by the manufacturer. I(t) denotes the solar irradiance at time t (in W/m^2), $P_{\mathrm{PV}}^{\mathrm{rated}}$ denotes the nominal output power of the panels, and η_{cab} denotes the efficiency of the wiring, which are considered as the input data of the optimization problem. N_{PV} denotes the number of solar panels that need to be installed to satisfy the load demand, the principal solar parameter of the optimization problem. Lastly, P_{PV} (in W) denotes the amount of energy produced by the installed solar system. In this study, we considered monofacial solar panels, with the parameters defined in Table 4.1 (Energy, 2023).

Tableau 4.1 PV specifications

Parameters	Symbols	Value	Unit
Nominal Output	$P_{\text{PV}}^{\text{rated}}$	200	W
Cell efficiency	η_r	22.90	%
NOCT	NOCT	45	°C
PV Cost	-	367	\$/unit
Installation cost	-	1.27	$\$/W$
Maintenance and Operation Cost	-	0.015	$\$/W$
CO_2 Emission	-	0.0338	$kgCO_2/kWh$
Irradiance at SC	-	1000	W/m^2
Temperature at SC	-	25	°C
Temp. Coef of Voc	k_p	-0.29	%/°C
PV Lifetime	-	25	years
Cabling efficiency	η_{cab}	95	%

4.4.1.2 Wind turbine model

The energy production process using WTs involves converting the kinetic energy (due to the speed) of the wind into electrical energy. The energy production of a wind turbine installation is expressed as follows (Memon et al., 2021; Tabak et al., 2017) :

$$P_{\text{WT}} = N_{\text{WT}} \times \eta_{\text{WT}} \times \begin{cases} 0 \text{ if } v(t) < v_{ci}, \quad v(t) > v_{co} \\ P_{\text{WT}}^{\text{rated}} \times \frac{v^3 - v_{ci}^3}{v_r^3 - v_{ci}^3}, \quad v_{ci} < v(t) < v_r \\ P_r, \quad v_r \leq v(t) \leq v_{co} \end{cases} \tag{4.4}$$

where N_{WT}, η_{WT}, and $P_{\text{WT}}^{\text{rated}}$ denote the number of WTs, turbine efficiency, and rated power output, respectively, of each turbine (in kW or MW). These parameters are typically provided

by the manufacturer. The variables, v_{ci}, v_{co}, and v_r denote the wind cut-off speed (in m/s) at which the turbine produces power, the cut-off speed at which the turbine is stopped, preventing damage, and thus ceases to produce energy, and the rated speed at which the turbine produces energy equivalent to its rated power output, respectively. The v_{ci} and v_{co} values are typically provided by the manufacturer. v denotes the speed of the WT at the hub and is defined as follows (Al-Ghussain et al., 2020; Memon et al., 2021) :

$$v(t) = v_{rf}(t) \times \left(\frac{h_{rf}}{\mathrm{h_{hub}}} \right)^{\alpha} \tag{4.5}$$

where v_{rf}, h_{rf}, and h_{hub} denote the speed at the reference height (in m/s), reference height at which the data are available, and height of the WT hub, respectively, and α denotes the coefficient of friction. The BWC XL-1 model was used for the experiments ; Table 2 presents its technical description (Al-Quraan and Al-Mhairat, 2024; Faria et al., 2023).

Tableau 4.2 WT Specifications (Faria et al., 2023)

Parameters	**Symbols**	**Value**	**Unit**
Rated power	P_r	1	kW
Turbine efficiency	η_{WT}	96	%
Cut-in Speed	v_{ci}	2.5	m/s
Cut-out Speed	v_{co}	20	m/s
Rated speed	v_r	11	m/s
Height at WT hub	h_{hub}	10	m
Height at reference	h_r	20	m
Lifetime	-	30	$years$
Capital cost	-	1800	$\$/kW$
Op. & Maint. Cost	-	15	$\$/kW/year$
Friction coef.	α	0.35	-

4.4.1.3 Battery energy storage system

The batteries in HRES conserve the surplus produced from renewable sources (solar, wind) when all the energy that is produced is not consumed by the loads. This energy, which is stored during overproduction, is used when the energy demand is greater than the energy produced by the system. Defining the battery capacity size to be used in HRES depends on several factors, including the battery life, acceptable battery discharge threshold, and ambient temperature (Ismail, Moghavvemi, and Mahlia, 2013; Mahmoud et al., 2022). The state of charge (SOC), or the ratio of stored energy to battery capacity, is an essential parameter during the charging and discharging of batteries (Mahmoud et al., 2022).

- BESS charging process

Battery charging in HRES occurs when the energy production by renewable sources is greater than the demand at a given time, t. The battery charge is defined as follows (Al-Quraan and Al-Mhairat, 2024; Memon et al., 2021) :

$$E_{\text{ch}} = \frac{\left[\left(P_{\text{WT}}(t) + \eta_{\text{PV}}^{\text{conv}} \times P_{\text{PV}}(t)\right) - P_L(t)\right]}{\eta_{\text{BESS}}^{\text{conv}}} \times \eta_{\text{ch}} \tag{4.6}$$

$$\text{SOC}(t) = \text{SOC}(t-1)(1-\delta) + E_{\text{ch}}(t) \tag{4.7}$$

where $\eta_{\text{PV}}^{\text{conv}}$, $\eta_{\text{BESS}}^{\text{conv}}$, and η_{ch} denote the efficiency of the solar converter and battery and charging efficiency of the battery system, respectively. $P_L(t)$ and E_{ch} are the load demand and the load energy at time t, and $\text{SOC}(t)$ and $\text{SOC}(t-1)$ in equation 4.7 represent the battery's state of charge at times t and $t-1$, respectively.

- BESS discharge process

The battery discharge process must be automatic when the total energy produced by renewable sources in the system (in this case, PV and WT) cannot sufficiently meet the load demand. The battery discharge must consider the allowable depth of discharge (DoD) and the self-discharge coefficient. The discharge is expressed as follows (Al-Quraan and Al-Mhairat, 2024; Memon et al., 2021) :

$$E_{\text{dis}} = \frac{\left[P_L(t) - \left(P_{\text{WT}}(t) + \eta_{\text{PV}}^{\text{conv}} \times P_{PV}(t)\right)\right]}{\eta_{\text{BESS}}^{\text{conv}}} \times \eta_{\text{dis}} \tag{4.8}$$

$$\text{SOC}(t) = \text{SOC}(t-1)(1-\delta) - E_{\text{dis}}\,(t) \tag{4.9}$$

where η_{dis} denotes the discharge efficiency of the battery (accounting for the accepted discharge threshold), and δ denotes the self-discharge coefficient. E_{dis} denotes the energy available in the battery that can be applied to the power loads.

Table 4.3 presents the specifications of the Elios EA12-200 battery model, which was used in this study (energies, 2023).

Tableau 4.3 BESS Specifications

Parameters	Symbols	Value	Unit
State of Charge min	SOC_{min}	10	%
State of Charge max	SOC_{max}	100	%
Charge-Discharge efficiency	$\eta_{\text{ch-dis}}$	92	%
Auto discharge rate	δ	0.01	%
Power rating	-	200, 12	Ah, V
Lifetime	-	15	$years$
Capital Cost	-	495	$\$/unit$
Operation & Maintenance Cost	-	5	$\$/year/unit$

4.4.1.4 Diesel generators

In this context, energy was produced using diesel-powered generators. A generator is used only when the energy produced by renewable sources added to the energy available in the storage sources cannot sufficiently meet the load demand. However, this study, which also focuses on limiting the greenhouse gas emissions, defines a production limit for the generator (e.g., it is not allowed to produce more than 20% of the total load demand). The energy output of a diesel generator corresponds to the amount of fuel consumed, C_{DG}, which is defined as follows (Ismail et al., 2013; Mahmoud et al., 2022) :

$$C_{\mathrm{DG}} = \alpha_{\mathrm{DG}} \times P_{\mathrm{DG}}(t) + \theta_{\mathrm{DG}} \times P_{\mathrm{DG}}^{\mathrm{rated}} \tag{4.10}$$

where $P_{\mathrm{DG}}(t)$ and $P_{\mathrm{DG}}^{\mathrm{rated}}$ denote the average and the nominal power of the generator, respectively. The variables, α_{DG} and θ_{DG}, denote the coefficients of the consumption curve and are equal to 0.246 and 0.08145 l/kWh, respectively. We considered the Generac generators in the context of these experiments ; Table 4.4 presents the specifications of these generators (Mahmoud et al., 2022).

Tableau 4.4 Generator Specifications

Parameters	Value	Unit
Capacities	7.5, 10, 13, 14, 16, 18, 20, 22, 24	kW
Fuel consumption	(2.07, 3.31), (2.86, 3.60), (4.36, 6.37), (5.52, 7.25), (5.15, 6.94), (4.79, 6.99), (5.78, 8.52), (6.46, 9.26), (5.75, 8.66)	(50%, 100%)
Operation load	95	%
Capital cost	370	$\$/kW$
Operation & Maintenance Cost	3	%
Fuel cost	1.2	$\$/L$
Carbon emission	66	kg/kW
Carbon emissions from fuel	2.6	kg/L
Lifetime	25	$Years$

4.4.1.5 Hybrid converter

The HRES considered in this study requires the use of solar converters, which can convert the electricity produced by the PV panels in direct current (DC) into alternating current (AC), suitable for consumption by devices and injectable into the electricity grid, while protecting against overvoltage incidents and short circuits. On the energy storage side, a bidirectional converter converts the AC electricity from the system into DC to recharge the batteries. It converts the DC energy stored in the batteries into AC to be consumed by the loads. We used the 12 kW ELIOS hybrid converter that is suitable for both PV and BESS. Table 4.5 presents its specifications (energies, 2023).

Tableau 4.5 12 kW ELIOS Hybrid Converter Specifications

Parameters	**Value**	**Unit**
Maximum charging/discharging current	250/250	A
Maximum charging/discharging power	12	kW
Battery charging efficiency	95	%
Battery discharging efficiency	94.50	%
Capital cost	300	$\$/kW$
Operation & Maintenance cost	5	$\$/year$
Nominal AC Voltage	120/240	V
Nominal DC Voltage	360	V
Lifetime	15	$year$

4.4.2 Energy management strategies

Different scenarios can affect the economic factors, feasibility, and reliability of HRES (Faria et al., 2023). Figure 4.2 depicts the process of managing HRES. In this process, we considered two renewable sources of energy production (solar and wind), an energy storage system (lithium battery), and a diesel generator (Figure 2.4).

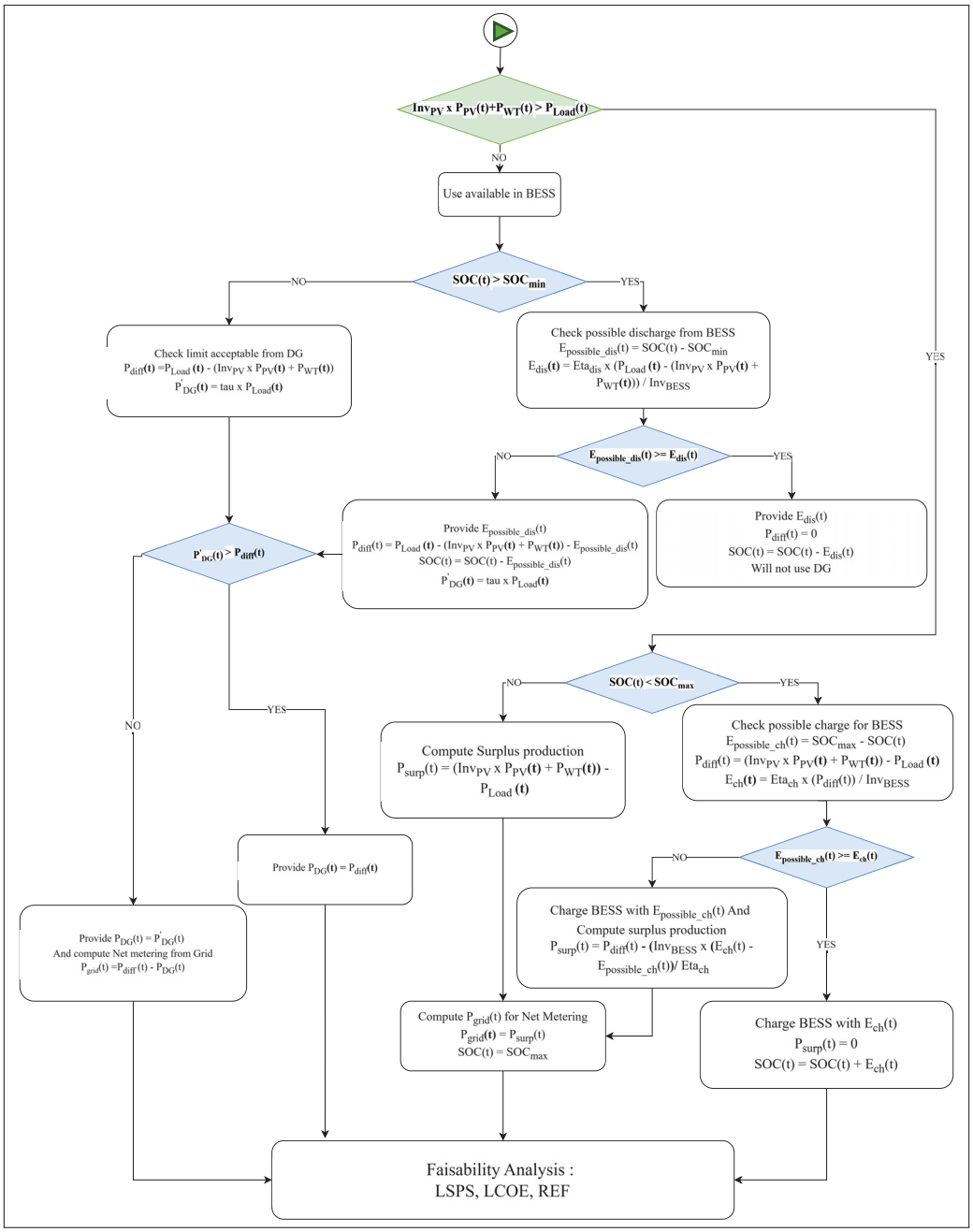

Figure 4.2 Energy management process

At each given time, t, the total energy produced by the system (solar and wind) is calculated and compared with the load demand. When production is sufficient, two possible scenarios are observed : 1) When the energy produced is equivalent to the demand : In this case, the load

consumes all the energy produced, and no amount of energy is imported from the batteries or the grid, nor used to charge the batteries or injected into the grid.

2) When the energy produced is greater than the demand : In this case, the difference in the production and load demand that represents the surplus is initially used to charge the battery until the maximum allowable SOC is reached. When the surplus production is not exhausted after charging the storage system to the maximum allowable, it is fed into the grid at the defined rate, μ. When the storage system is unable to take any amount of surplus, all of it is injected into the grid at the set rate.

Two scenarios are observed when the production cannot meet the load demand at time t.

1) The energy storage system contains sufficient energy to cover the difference : The storage system (the battery) is discharged to satisfy the difference in energy between the demand and production.

2) The storage system does not contain sufficient energy to cover the difference : The generator is used to produce energy, considering its production condition. Here, τ denotes the limit of permissible energy obtained from the generator. This approach presents two forms of management. The first is if the limit imposed on the generator enables the amount of power to cover the demand. The second is if the energy produced by the generator does not cover the difference in the energy demand, considering the imposed limit. In this case, after using the energy stored in the storage system and the amount safely generated by the generator, the remaining demand is imported from the grid at the set rate, ϑ.

The rates, ϑ and μ, are calculated as 0.14 and 0.05 $\$/kWh$, respectively (Al-Ghussain et al., 2020; Bouafia et al., 2023; Medghalchi and Taylan, 2023).

4.4.3 System analysis factors

Previous studies considered the net present cost (NPC) (Bahgaat, 2023; Mansouri Kouhestani et al., 2020), LCOE (Bouafia et al., 2023; Legrene, Wong, and Dessaint, 2024b), and weighted

average cost of energy (waCOE) (Medghalchi and Taylan, 2023) as factors to evaluate the economics of HRES. Similarly, Baidas et al. (2022); Al-Quraan and Al-Mhairat (2024) used the REF to analyze the integration of renewable sources in a hybrid system. Since the reliability of the system is equally important, Mansouri Kouhestani et al. (2020)) employed LPSP to evaluate the reliability of these systems. Baghaee et al. (2016) proposed the use of the human development index (HDI) to determine the system reliability. Since different factors can be used to analyze HRES, the sizing process evaluated here considers the LCOE, REF, and LPSP.

4.4.3.1 Levelized cost of energy

The LCOE is the measurement factor used to define the cost (in $\$/kWh$) of the energy produced by a system. This coefficient must be minimized while sizing HRES. The total cost of a system is determined based on the ratio of the HRES LCOE $\mathbb{C}_{\text{Total}}$ (in \$) to the total load for a year (in kWh), which is given as follows (equation 4.11) :

$$\text{LCOE} = \frac{\mathbb{C}_{\text{Total}}}{\sum_{t=1}^{8760} P_L(t)} \tag{4.11}$$

The total cost of a system includes the initial investment capital, $\mathbb{C}_{\text{Capital}}$, costs associated with replacements, $\mathbb{C}_{\text{Remp}}$, and the operations and maintenance costs, $\mathbb{C}_{\text{Op\&Maint}}$ (Coban, Lewicki, and Brelik, 2024). Additionally, for HRES connected to the electricity grid, the cost of the energy purchased from the grid and the total cost of sales must also be considered (Coban et al., 2024). The total cost, $\mathbb{C}_{\text{Total}}$ is expressed as follows (Coban et al., 2024; Memon et al., 2021) :

$$\mathbb{C}_{\text{Total}} = \mathbb{C}_{\text{Capital}} + \mathbb{C}_{\text{Remp}} + \mathbb{C}_{\text{Op\&Maint}} + E_a \times \tau_a - E_v \times \min(\tau_a, \tau_v) \tag{4.12}$$

where E_a, E_v , τ_a, and τ_v denote the quantities of energy bought and sold and the rates of purchases and sales on the grid, respectively.

- Capital cost

The total cost of capital involves the sum of the product of the initial cost of each piece of equipment, j, $\mathbb{C}^{j}_{\text{Initial}}$, multiplied by its recovery factor, $\text{CRF}\left(r, m_j\right)$. This initial cost is defined as follows :

$$\begin{aligned} \mathbb{C}_{\text{Capital}} &= \sum \mathbb{C}^{j}_{\text{Initial}} \times \text{CRF}\left(r, m_j\right) \\ \text{CRF}\left(r, m_j\right) &= \frac{r(1+r)^{m_j}}{(1+r)^{m_j}-1} \\ \mathbb{C}^{j}_{\text{Initial}} &= \text{Cap}_j \times \mathbb{C}_{uj} \end{aligned} \tag{4.13}$$

where Cap_j and $\mathbb{C}_{uj}$ denote the capacity of the PV, WT, DG, and BESS components (in W for PV and WT and in Wh for BESS and DG) and the unit cost of each component (in \$/kW or \$/W for PV and WT and in $\$/kWh$ or $\$/Wh$ for ESS and DG), respectively, and where r and m_j denote the interest rates (in %) and the life of the component, j.

- Replacement cost

The replacement cost helps in preventing a component from malfunctioning during the lifetime of the system, m_s. This cost is introduced for each component when m_s is greater than the lifetime of the component, m_j ($m_s > m_j$), and can be expressed as follows :

$$\mathbb{C}_{\text{Remp}} = \sum \mathbb{C}^{j}_{\text{Initial}} \times \frac{\left(m_s - m_j\right)}{m_j} \tag{4.14}$$

- Maintenance and operation cost

The cost of operation and maintenance, $\mathbb{C}_{\text{Op\&Maint}}$, represents the main cost of the operation of HRES (Mahmoud et al., 2022). When this cost cannot be determined annually, it can be calculated based on the product of the operating (or maintenance) cost per hour of each component ($\mathbb{C}^{j}_{\text{Op\&Maint}}$) and the duration of operation and maintenance ($t^{j}_{\text{Op\&Maint}}$), as shown below :

$$\mathbb{C}_{\text{Op\&Maint}} = \sum \mathbb{C}^{j}_{\text{Op\&Maint}} \times t^{j}_{\text{Op\&Maint}} \tag{4.15}$$

4.4.3.2 Loss of power supply probability - LPSP

The reliability of HRES is measured based on the value of the LPSP (in %) (Mansouri Kouhestani et al., 2020). This probability helps in quantifying the underproduction of energy by the system (LPS) when compared with the load demand, P_L. This probability is expressed as follows :

$$\begin{gathered} \mathrm{LPSP} = \frac{\sum_{t=1}^{8760} \mathrm{LPS}(t)}{\sum_{t=1}^{8760} P_L(t)} = \frac{\sum_{t=1}^{8760} (P_L(t) - P_{\mathrm{Total}}(t))}{\sum_{t=1}^{8760} P_L(t)} \\ \mathrm{LPSP}(\%) = \mathrm{LPSP} \times 100 \end{gathered} \tag{4.16}$$

where $P_L(t)$ and $\mathrm{LPS}(t)$ denote the load demand and energy loss at the instant t, respectively.

LPS loss occurs only when all the energy produced (PV+WT) is added to that available in the storage systems, and when these amounts, combined with the additional energy produced by the generator, cannot satisfy the load demand. The acceptable reliability threshold for HRES is 5% (Mansouri Kouhestani et al., 2020).

4.4.3.3 Renewable energy fraction

The REF is designed to help in selecting HRES whose main production sources are solar and wind. Thus, in HRES that employs a diesel generator, the REF (in %) is defined as follows (Baidas et al., 2022) :

$$\begin{gathered} \mathrm{REF} = \frac{\sum_{t=1}^{8760} P_{\mathrm{renewable}}(t)}{\sum_{t=1}^{8760} P_{\mathrm{Total}}(t)} = \frac{\sum_{t=1}^{8760} (P_{\mathrm{WT}}(t) + \eta_{\mathrm{PV}} \times P_{\mathrm{PV}}(t))}{\sum_{t=1}^{8760} (P_{\mathrm{WT}}(t) + \eta_{\mathrm{PV}} \times P_{\mathrm{PV}}(t) + P_{\mathrm{GRID}}(t) + P_{\mathrm{DG}}(t))} \\ \mathrm{REF}(\%) = \mathrm{REF} \times 100 \end{gathered} \tag{4.17}$$

where $P_{\mathrm{WT}}(t)$ and $\eta_{\mathrm{PV}} \times P_{\mathrm{PV}}(t)$ denote the energy production from the wind and solar sources, respectively, at time t. The variables, $P_{\mathrm{GRID}}(t)$ and $P_{\mathrm{DG}}(t)$, represent the quantities of energy taken from the electricity grid and produced by the diesel generator, respectively, for the same period t. In a hybrid renewable energy system, the fraction of renewable energy must be maximized, thereby reducing the greenhouse gas emissions.

4.4.3.4 Constraints

The feasibility constraints affect the reliability criterion, the energy produced by the diesel generator, and the amount of energy taken from the grid. These constraints are summarized in equation 4.18, respectively. The impact of these constraints on the search for the optimal system is determined based on a set of values considered within the framework of the study.

We set $\varepsilon = 0.05$ (Mansouri Kouhestani et al., 2020), conducted different experiments with γ and τ values of [0.1,0.2,0.3,0.4], and proposed a methodical evaluation of the parameters that can affect the performance of the HRES. The selection of the values helps in isolating the effects of the different parameters and in identifying the sensitivities that enable more efficient optimization of the system, owing to a good understanding of the impact of each constraint.

$$\begin{gathered} \mathrm{LPSP} \leq \mathrm{LPSP}^{\max} = \varepsilon \\ P_{\mathrm{DG}} \leq P_{\mathrm{DG}}^{\max} = \tau \times P_L \\ P_{\mathrm{GRID}} \leq P_{\mathrm{GRID}}^{\max} = \gamma \times P_L \\ \varepsilon = 0.05, \gamma \in [0.1, 0.2, 0.3, 0.4], \tau \in [0.1, 0.2, 0.3, 0.4] \end{gathered} \tag{4.18}$$

4.4.4 Problem formulation

The optimization of a hybrid renewable energy system in this framework is a multi-criteria optimization problem under the previously defined constraints, as shown below :

$$\begin{cases} \min f_1 = \min \mathrm{LCOE} \\ \min f_2 = \min \mathrm{LPSP} \\ \max f_3 = \max \mathrm{REF} \end{cases} \tag{4.19}$$

In the framework of the proposed method, we proposed a DRL optimization approach in which a reward function is defined based on the above objective functions. This reward function in the

sizing process is expressed as follows :

$$\mathrm{R} = \sum_{i=0}^{n} \left[\sum_{j=1}^{k} \frac{\pm\left(f_j^{\text{best}} - f_j^i\right)}{\max\left(\left\{\left|f_j^{\text{best}} - f_j^i\right|, j=1,2,\ldots,k\right\}\right)} + \Phi \right]$$
$$\begin{cases} f_j^{\text{best}} = f_j^i, & \text{if } i = 0 \\ f_j^{\text{best}} = f_j^i, & \text{if } f_j^{\text{best}} \leq f_j^i \\ f_j^{\text{best}} = f_j^{\text{best}}, & \text{else} \end{cases} \tag{4.20}$$

where n and k denote the number of iterations and number of objective functions, respectively. Normalizing the differences between new and best values by maximizing them helps avoid prioritizing a single goal function. Additionally, Φ denotes a cost function corresponding to the search constraints, which is defined as follows :

$$\Phi = \frac{P_{\text{sys}}^{\max} - P_{\text{sys}}^i}{\max\left(\left\{\left|P_{\text{sys}}^{\max} - P_{\text{sys}}^i\right|\right\}, P_{\text{sys}} \epsilon \left\{\mathrm{P}_{\text{GRID}}, P_{\text{DG}}\right\}\right)} + \left(\mathrm{LPSP}^{\max} - \mathrm{LPSP}^i\right) \tag{4.21}$$

Applying Φ enables the adjustment of the objectives. Normalization between -1 and 1 helps in avoiding maximization or minimization at the expense of other objectives. Thus, the proposed method aims to maximize the cumulative reward, R.

4.4.5 Research approach

This section presents the proposed approach and the methods used as a benchmark. Furthermore, we define the framework, including the case studies considered and the values of the parameters.

4.4.5.1 Deep reinforcement learning

We used DRL with greedy epsilon to optimize the HRES.

Reinforcement learning is a major breakthrough in the fields of machine learning and artificial intelligence for the development of intelligent, autonomous, and emerging technology (Du and

Ding, 2021; Le, Rathour, Yamazaki, Luu, and Savvides, 2022; Mnih, Kavukcuoglu, Silver, Rusu, Veness, Bellemare, Graves, Riedmiller, Fidjeland, Ostrovski, Petersen, Beattie, Sadik, Antonoglou, King, Kumaran, Wierstra, Legg, and Hassabis, 2015; Nguyen, Nguyen, and Nahavandi, 2020). DRL helps in overcoming the inability of conventional reinforcement learning methods to obtain a better understanding of environments with high variability and adapt to complex state systems owing to the usage of neural network models in the reinforcement learning process (Zhu, Lin, Jain, and Zhou, 2023). Advances in the use of deep reinforcement learning models have helped in solving previously unsolvable problems, such as learning to play video games from pixel inputs (Arulkumaran, Deisenroth, Brundage, and Bharath, 2017; Mnih et al., 2015).

Various DRL models have been developed for solving various problems. Three of these ar : deep Q-network (DQN), which approximates the value of the Q-value function, enabling agents to learn policies from inputs (Mnih et al., 2015) ; trust region policy optimization (TRPO) (Arulkumaran et al., 2017), which ensures that policy optimization is achieved stably and efficiently without deviating significantly from the current policy ; and asynchronous advantage actor-critic (A3C), which involves parallelizing several agents, promoting stability, and accelerating the learning process that enables it to adapt to complex environments (Kiran, Sobh, Talpaert, Mannion, Sallab, Yogamani, and Pérez, 2022).

These models have been analyzed in other areas, such as automatic driving (Kiran et al., 2022), in multi-agent systems, enabling better communication and collaboration in complex tasks, such as non-stationarity and partial observability problems (Kiran et al., 2022; Nguyen et al., 2020), and in neuroscience (Botvinick, Wang, Dabney, Miller, and Kurth-Nelson, 2020).

4.4.5.2 Approach

Figure 4.3 depicts the reinforcement learning approach adopted in this study, which is based on TD3 with the epsilon-greedy approach. This approach comprises five main steps : state

initialization, agent decision-making, HRES evaluation, agent reward calculation, and agent management and training on the buffer.

- Initial state

Defining the initial state helps in assigning a state to the system, i.e., a set of values that enables the system to be defined at time 0 of the process. The system state settings always remain unchanged. The values are only updated during the training process, enabling the changes caused by a particular decision of the agent to be known at any given time. The state of the system, $\mathcal{S}$, is then defined as follows :

$$\mathcal{S} = \left\{N_{\mathrm{PV}}, N_{\mathrm{WT}}, C_{\mathrm{BESS}}, C_{\mathrm{DG}}, E_{\mathrm{np}}, E_{l}, \mathrm{LCOE}, \mathrm{LPSP}, \mathrm{REF}\right\} \tag{4.22}$$

where N_{PV} and N_{WT} denote the number of photovoltaic solar panels and wind turbines, respectively. $\mathrm{Cap}_{\mathrm{BESS}}$ and $\mathrm{Cap}_{\mathrm{DG}}$ denote the capacity of the storage system (battery) and the diesel generator. E_{np} and E_{l} denote the amount of energy not supplied and the amount of energy lost over the entire evaluation period, respectively, and LCOE, LPSP,and REF denote the values obtained for this evaluation. The first four parameters represent the decisions made by the agent, and the agent's decision directly impacts the last five.

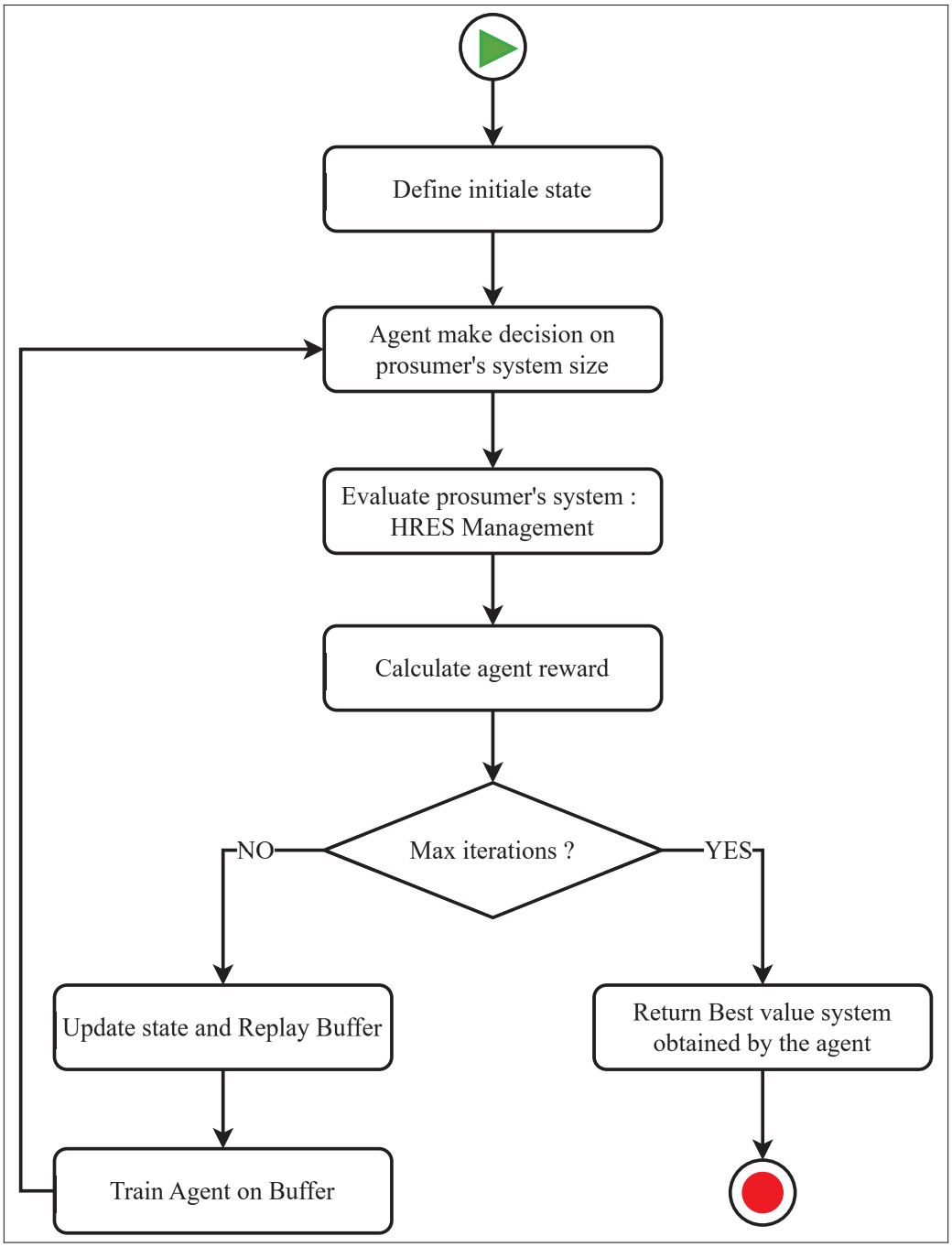

Figure 4.3 Proposal approach steps

- Decision-making agent

Starting from the initial state or the updated state, the agent selects the value of the parameters of the previous state. The agent considers the state of the system following his previous decision or the initial state. Consequently, four probability values are predicted between 0 and 1 from the actor of the system (the agent), or a sequence of 4 random values is generated between 0 and 1 based on the value of the epsilon at the time of the decision. The values thus obtained are then recalibrated between the maximum and the minimum to determine the values corresponding to the number of PV panels and WTs, capacity of the battery (BESS), and the capacity of the diesel generator (DG). Here, p denotes the predicted probability value for a parameter, P, and the corresponding value, x, can be defined as follows :

$$x = \left\lfloor x_{\min} + (x_{\max} - x_{\min}) \times \frac{p+1}{2} \right\rfloor \tag{4.23}$$

where $x_{\min}$ and $x_{\max}$ denote the minimum and maximum values of P.

- System evaluation

The evaluation of the system involves estimating the amount of energy produced at each moment and the management of the system at each moment over the entire duration (a full year). Based on the state of the system, the LCOE, LPSP, and REF are calculated to determine the impact of each decision. Lastly, the corresponding cumulative agent reward is calculated. This total agent reward, R, is calculated (equation 4.20) without considering P_{GRID} in the calculation of the REF and is calculated based on the difference between the demand and production for the HRES. The new final state obtained is then added to the buffer for the replay phases.

- Update States and Replay Buffer—Agent Training

When the maximum number of iterations, i.e., the stop condition, is not reached, the system state is updated for the agent with the new values that the agent would have considered as an action and the new cumulative reward based on that decision. The replay buffer, which contains

the past decisions and reward history of an agent, is updated with the current decision and the earned reward. The agent is then trained on minibatches of these decisions and the rewards obtained at the end of these past decisions. In particular, a mini-batch of T random transactions is taken from the replay buffer (equation 4.24).

$$\left\{\left(s_j, a_j, r_j, s_{j+1}, \mathrm{d}_j\right)\right\}_{j=1}^{T} \tag{4.24}$$

For each of the transactions of T, the target value, y_j, is calculated as shown in equation 4.25, where ζ denotes the discount factor and $Q\left(s, a; \theta^{-}\right)$ denotes the target shares value function parameterized by θ^{-}. θ^{-} represents the weight of the target network, which is a delayed copy of θ. The model parameters are then updated using the gradient descent method (equation 4.27), where α denotes the learning rate and $L(\theta)$, which is defined by equation 4.26, represents the minimization of the loss function corresponding to θ.

$$y_j = \begin{cases} r_j + \zeta \max_{a'} Q\left(s_{j+1}, a'; \theta^{-}\right), & d_j = 0 \\ r_j, & d_j = 1 \end{cases} \tag{4.25}$$

$$L(\theta) = \frac{1}{T} \sum_{j=1}^{T} \left(y_j - Q\left(s_j, a_j; \theta\right)\right)^2. \tag{4.26}$$

$$\theta = \theta - \alpha \nabla_{\theta} L(\theta) \tag{4.27}$$

Table 4.6 presents the parameter values used to train the DRL agent.

Tableau 4.6 DRL train and decision parameters

Batch size	Learning rate	Policy noise	Policy update frequency	Epsilon decay	Epsilon min	Epsilon
64	0.001	0.2	10	0.995	0.01	0.1

The replay buffer is used to break the correlations between the sequential data along with the target network, enabling it to stabilize learning (Mnih et al., 2015). The agent makes a new decision at the end of this training phase, and the evaluation process is resumed. This process enables the agent to improve their understanding of the system and the environment and conform to it as the training is continued.

4.4.5.3 Particle swarm optimization

The PSO is a robust and commonly used optimization algorithm. This algorithm was first proposed by Kennedy and Eberhart (1995). It is based on the social behavior of birds in flight or fish in schools (Mohamed et al., 2016). Since its inception, PSO has been successfully applied in various fields, addressing a wide range of complex optimization problems. The PSO algorithm was used for the sizing process of the HRES (Kushwaha and Bhattacharjee, 2024; Mansouri Kouhestani et al., 2020). The search process for this problem begins with defining several particles, P, which collaborate during T iterations (generations) to determine the system that satisfies the defined optimality criteria. Each particle has a position $\mathrm{x}_i^{(t)}$ at each moment t representing a generation (iteration) (equation 4.29). For the particle, the position constitutes the set of values required to define the system. Essentially, each position in the framework comprises two (PV-BESS) to four (PV-WT-BESS-DG) values to determine the number of panels, number of turbines, battery capacity, and capacity of the diesel generator based on the system type. The particle also has a velocity $\mathrm{v}_i^{(t)}$, which defines the rate of change and the direction when analyzing the search space for each particle (equation 4.28).

$$v_i^{(t+1)} = \omega v_i^{(t)} + c_1 a_1 \left(\text{pbest}_{\,i} - x_i^{(t)} \right) + c_2 a_2 \left(\text{gbest}^{\,(t)} - x_i^{(t)} \right), \tag{4.28}$$

$$x_i^{(t+1)} = x_i^{(t)} + v_i^{(t+1)} \tag{4.29}$$

Generation after generation, each particle stores the values of the parameters required for its solution, $x_i^{(t)}$, in the memory. Thus, the best value is obtained from the goal function and is represented by $\text{pbest}_{\,i}$. With each generation, the algorithm updates the best position of all the particles, $\text{gbest}^{\,(t)}$. The coefficients of inertia, ω, confidence, c_1 and c_2, and random values, a_1 and a_2, enable the algorithm to define the adjustments that must be made to the various parameters, generation after generation. Apart from the decision-making method on the values of the optimization problem parameters, the procedure for evaluating the system remains identical to applying DRL.

PSO is used as the reference method in this study since it is one of the most commonly used methods in HRES optimization (Bouafia et al., 2023; Faria et al., 2023). However, this analysis also includes a discussion of other metaheuristics, such as GA and SSA, along with simulation tools such as HOMER Pro to place the proposed approach in a broader context. The PSO algorithm used here is based on the "global best" algorithm proposed by Miranda (2018).

Table 4.7 presents the values of some specific PSO parameters assumed in this study.

Tableau 4.7 PSO Parameter specifications

Population size	Iteration	Inertia coefficient	Confidence coefficient	
			c_1	c_2
10	100	0.9	0.5	0.3

4.4.5.4 Multi-objective Particle Swarm Optimization

MOPSO is an extension of the previously reported PSO algorithm. MOPSO was developed specifically for multi-objective, often conflicting, optimization problems, such as the discounted energy cost, REF, and system reliability. MOPSO algorithms depend on the Pareto dominance mechanisms and the use of external archives to store non-dominated solutions. This approach guides the search for well-distributed Pareto fronts, thereby ensuring the diversity of the solutions (Cui, Meng, and Qiao, 2022; Samy et al., 2021). The effectiveness of MOPSO algorithms has been demonstrated in various applications, from standardized test functions to real-life industrial applications, such as industrial process optimization and energy system optimization (Agarwal, Agrawal, and Kaur, 2022; Cui et al., 2022). The results indicate that MOPSO outperforms other evolutionary algorithms in terms of the speed of convergence, quality, and diversity of solutions (Cui et al., 2022).

In this study, we applied MOPSO as one of the comparison methods for its ability to generate diversified solution sets that are well distributed on the Pareto front, as well as its demonstrated performance on benchmarks and real applications (Cui et al., 2022; Shu, Liu, Liu, Yang, and Zhang, 2023). Figure 4.4 depicts the application of MOPSO in this 6-stage research.

In the context of HRES, MOPSO is used as a reference method for simultaneously optimizing the conflicting objectives of the discounted cost of energy (LCOE), energy reliability (LPSP), and renewable energy share (REF). Each particle represents a possible technological configuration of the system (number of PVs, number of WTs, battery capacity, generator capacity) and is developed in the decision space based on its past experiences and those of others via a leader selection mechanism. During the process, MOPSO maintains a dynamic archive of the Pareto optimal solutions, thereby ensuring a good balance between exploration and exploitation. MOPSO presents a robust benchmark for evaluating the performance of advanced optimization approaches in sustainable energy systems owing to its ability to rapidly converge on various Pareto fronts.

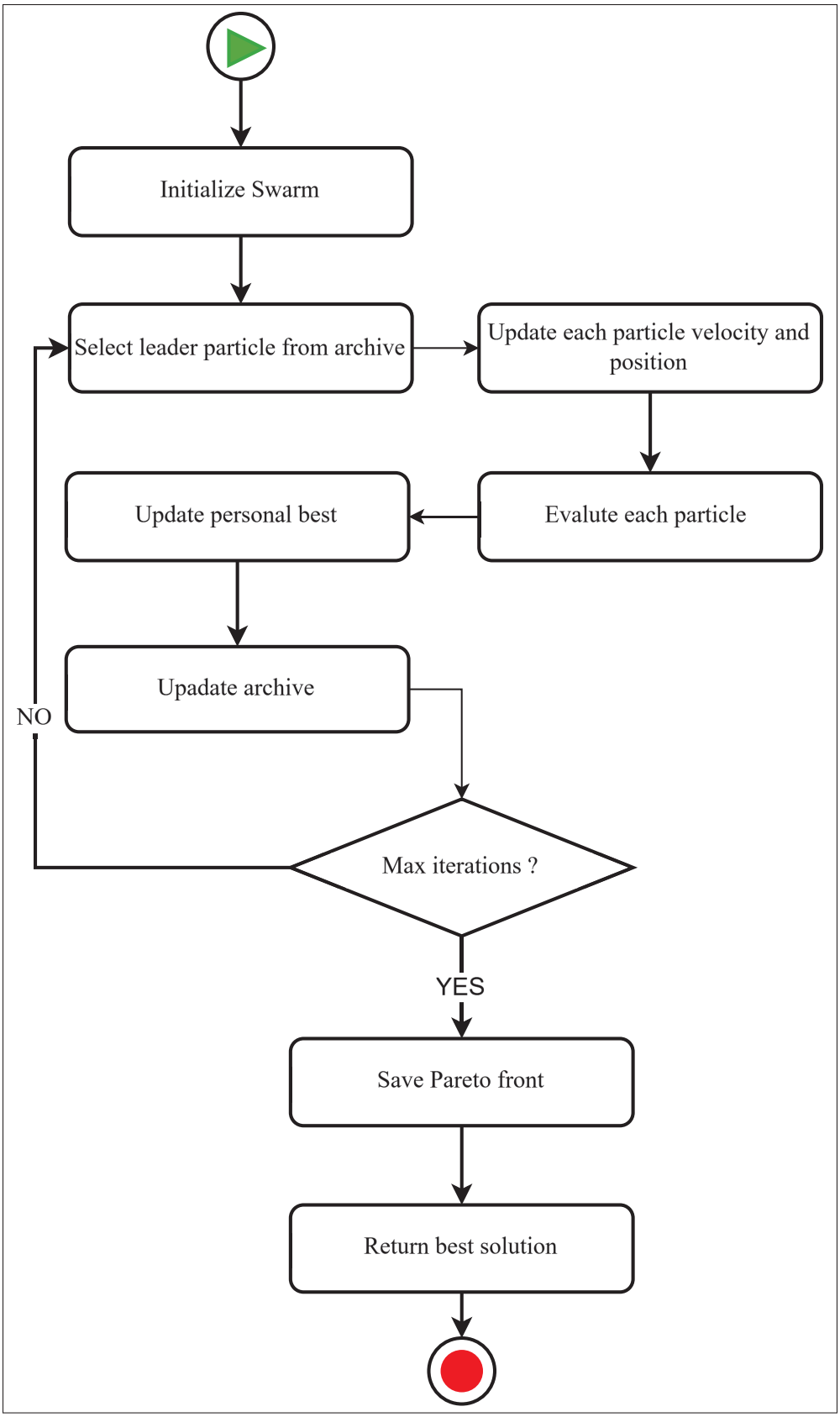

Figure 4.4 MOPSO approach steps

Table 4.8 presents the values of the MOPSO parameters assumed in this study (Cui et al., 2022; Nshimirimana, Abraham, and Nothnagel, 2021).

Tableau 4.8 MOPSO Parameter specifications

Population size	Iteration	Inertia weight	Cognitive coefficient	Social coefficient
20	50	0.5	1.5	1.5

4.4.5.5 Non-dominated Sorting Genetic Algorithm II

NSGA-II is a multi-objective evolutionary algorithm that is widely used owing to its ability to efficiently solve multi-objective optimization problems. Proposed by Kalyanmoy Deb in 2002, the excellent performance of NSGA-II was demonstrated in several fields, from engineering and architectural design to water resource management and bioinformatics (Bailey and Caldas, 2023; He, Du, Bai, Yang, and Ma, 2024; Shirajuddin, Muhammad, and Abdullah, 2022).

In this study, each individual represents a system configuration (number of PVs, number of WTs, battery capacity, generator capacity), which is evaluated based on the conflicting criteria of this study : LCOE, LPSP, and REF. The NSGA-II algorithm generates a solution through crossover and mutation and classifies the population based on the Pareto fronts and a density distance to preserve the diversity, as shown in Figure 4.5. NSGA-II stands out from other multi-objective optimization algorithms owing to its fast, non-dominated sorting, elitism, and diversity without sharing parameters. NSGA-II introduces a more efficient non-dominated sorting method, thereby reducing the computational complexity to $O(MN^2)$, where M denotes the number of objectives and N denotes the population size (Deng, Zhang, Zhou, Liu, Zhou, Chen, and Zhao, 2021)

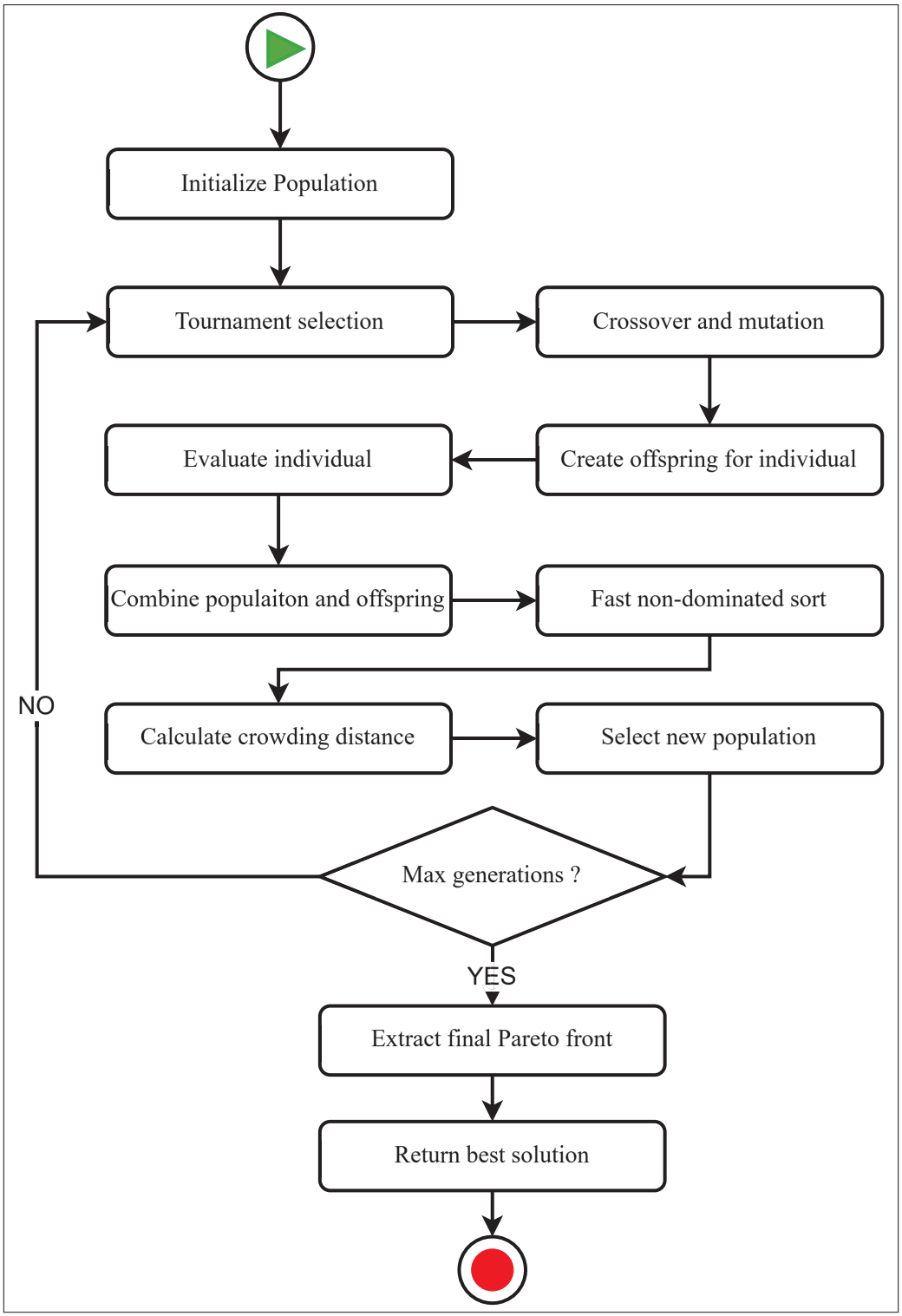

Figure 4.5 NSGA-II approach steps

Therefore, NSGA-II can identify the reliable trade-offs between the economic, energy, and environmental performance owing to its efficient non-dominated sorting mechanism and its ability to produce a well-distributed Pareto front (Deng et al., 2021). Furthermore, its elliptical design combines parental and child populations to select the best configurations, which ensures that high-quality solutions are preserved over generations (Bailey and Caldas, 2023; Bora, Mariani, and Coelho, 2019; Shirajuddin et al., 2022).

Table 4.9 presents the values of the NSGA-II parameters assumed in this study (Ferreira, Antunes, Carriço, and Covas, 2023; Wang, Wang, Huang, Wang, Liu, and Savić, 2019).

Tableau 4.9 NSGA-II Parameter specifications

Population size	**Generation**	**Mutation probability**	**Crossover probability**
20	50	0.1	0.9

4.5 Results and discussions

This section presents the case studies regarding the energy consumption profiles, type of system, different scenarios, and the imposed constraints.

4.5.1 Study data

Three energy consumption profiles, P1 [Building 1 consumption], P2 [Building 2 consumption], and P3 [Building 3 consumption], were considered for the significant variability that exists between them from the perspective of total consumption and the average monthly distribution, as shown in Figure 6 for each of the profiles. These profiles were previously selected at random from the National Renewable Energy Laboratory (NREL) database of energy consumption profiles (Wilson, Parker, Fontanini, Present, Reyna, Adhikari, Bianchi, CaraDonna, Dahlhausen, Kim, LeBar, Liu, Praprost, White, Zhang, DeWitt, Merket, Speake, Hong, Li, Mims Frick,

Wang, Blair, Horsey, Roberts, Trenbath, Adekanye, Bonnema, El Kontar, Gonzalez, Horowitz, Jones, Muehleisen, Platthotam, Reynolds, Robertson, Sayers, and Li, 2021). The datasets present hourly consumption profiles over 1 year (8760 rows of values).

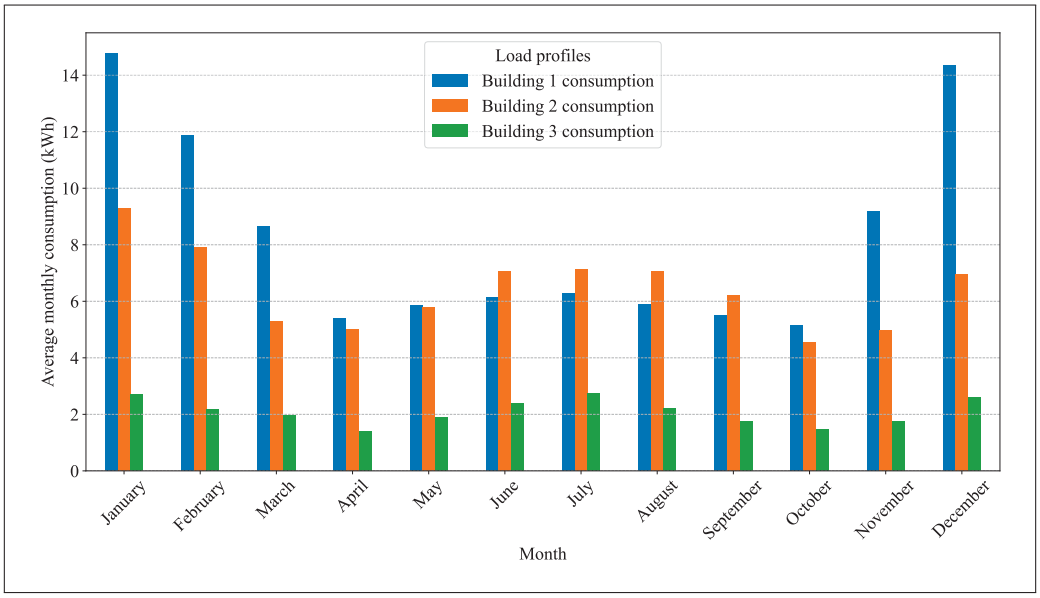

Figure 4.6 Average monthly energy consumption

Figure 4.6 depicts the differences between the different profiles (in kWh). The most important requests occur in December and January for most of these profiles. The periods of low demand are typically recorded in April, May, September, and October.

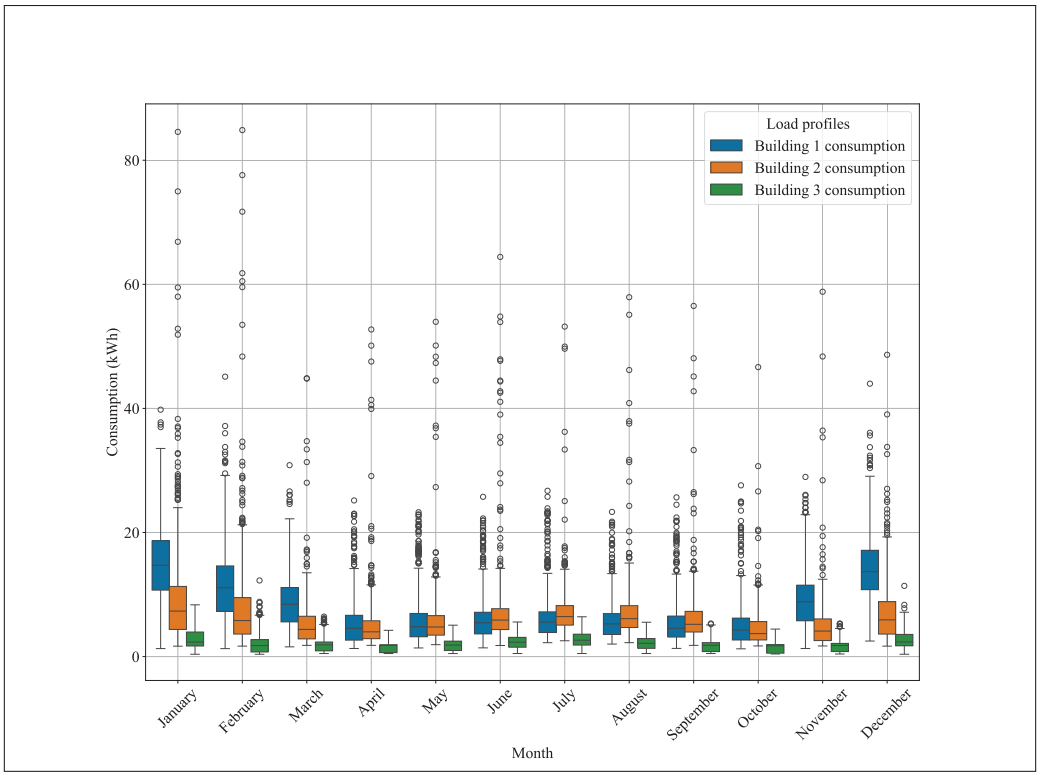

Figure 4.7 Profiles comparative boxplots

Comparatively, the boxplots in Figure 4.7 show that the consumption profile P3 is more stable throughout the year. Additionally, the consumption profiles, P1 and P2, demonstrate significant variability in the summer and peaks in demand in the winter (December and January). The boxplots show that some values in the P1 and P2 profiles could be outliers. A comparison with Figure 4.6, which presents the monthly average consumption, indicates that the profile with the highest demand is P1, totaling 72,157.99 kWh, whereas P2 and P3 register 56,341.69 and 18,317.89 kWh, respectively.

This study considers the available Typical Meteorological Year (TMY) data of the region (Wilson et al., 2021) since the profiles were randomly extracted from the same region. Table 4.10 presents a descriptive analysis of this data.

Tableau 4.10 Descriptive analysis of time series data

	Temperature [°C]	**Wind Speed [m/s]**	**Solar Irradiance [W/m^2]**
Count		8760	
Mean	14.8257	3.4460	169.0066
Std.	10.1880	1.9379	256.6405
Min	-14.0000	0.0000	0.0000
25%	7.0000	2.1000	0.0000
50%	16.0000	3.1000	0.0000
75%	22.8000	4.6000	253.0000
Max	39.0000	12.8000	993.0000

Moderate temperature variability can be observed over the year, with an average value of 14.8 C and a standard deviation of 10.2 C. Furthermore, the wind conditions are typically moderate, with an average speed of 3.45 m/s; however, there are a few extreme episodes, with gusts reaching up to 12.8 m/s. The solar irradiance demonstrates a large variation between the sunny and cloudy days, with an average of 169 W/m^2, a maximum value of 993 W/m^2, and a minimum value of 0 W/m^2.

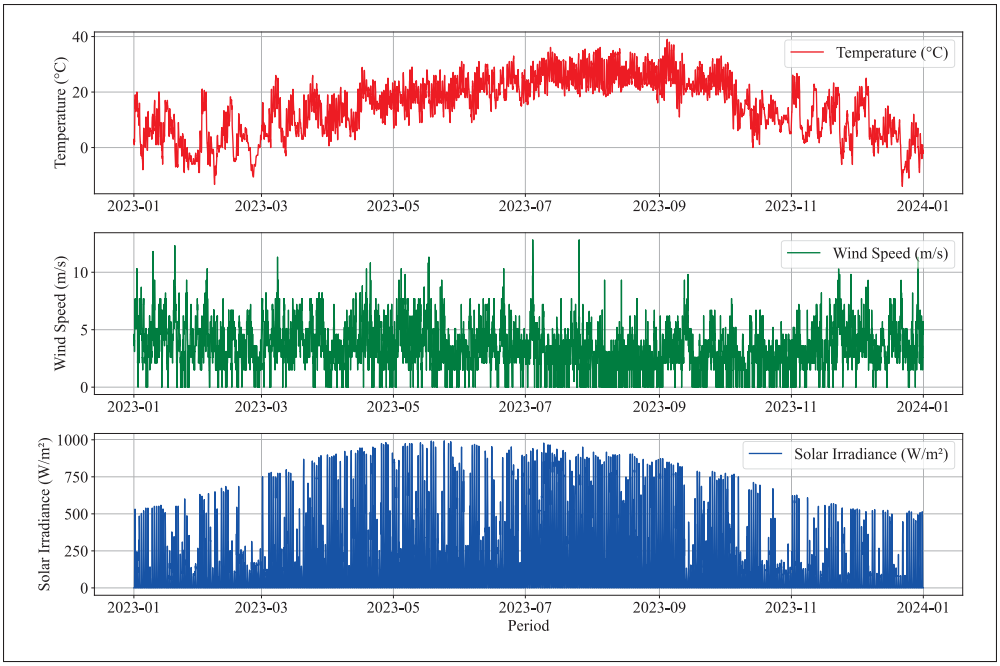

Figure 4.8 Time Series Data

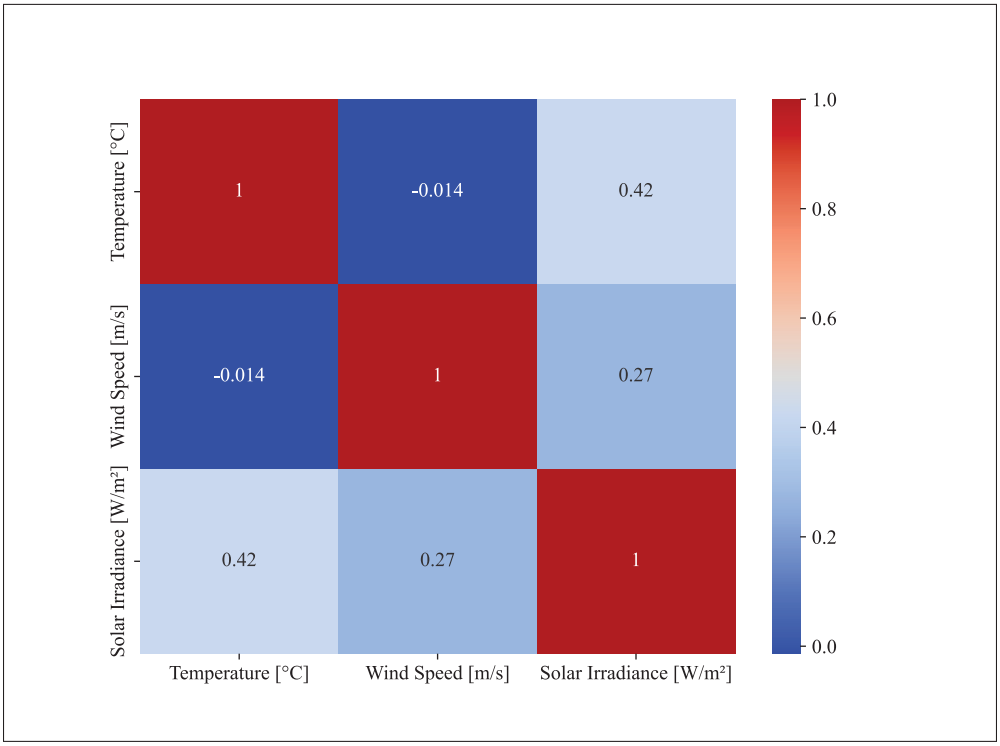

Figure 4.9 Correlation matrix of time series data

The graph in Figure 4.8 demonstrates significant temperature variations in the summer (from June to September), which is a phenomenon of seasonal variations. The minimum temperatures are reached during the winter months (December to February). Meanwhile, the wind speed plot demonstrates significant variations throughout the year, with somewhat larger variations in the winter. The peak periods could represent periods of strong winds, such as storms or gusts. Part 03 of this graph depicts the distribution of solar irradiance over the entire year. A high intensity of solar irradiation can be observed in the summer due to the longer days and direct sunlight, whereas it is minimal in the winter owing to the lower levels of the sun and shorter days. Periods of low intensity could indicate cloudy episodes or storms.

Additionally, the correlation matrix in Figure 4.9 depicts the relationships between the different variables (temperature, wind speed, and solar irradiance). The value scale from 0.0 to 1.0 demonstrates the degree of correlation (relationships) between the variables. The darker blue color represents weaker correlation, whereas the darker red color represents stronger correlation, where each variable is strongly correlated with itself and is represented on the diagonal. Sunny days are typically associated with higher temperatures, which presents a positive correlation between the temperature and solar irradiance (0.42). The negative correlation of -0.014 between the wind speed and temperature indicates that windy days tend to be cool. This could explain the windchill factor. Additionally, a positive correlation of 0.27 between wind speed and solar irradiance can be noted. This could be explained by the fact that sunny days, besides having less cloud cover, are typically characterized by moderate wind conditions.

4.5.2 Study systems

This approach was analyzed using four different types of systems for each profile. Additionally, the analysis was performed with constraints imposed on both the tau (τ) rate of energy permissible by the generator when it is part of the system and the gamma (γ) rate of energy permissible via the electrical grid (equation 4.30). The four types of systems are :

- Case 1 : PV-WT-BESS-DG

- Case 2 : PV-WT-BESS
- Case 3 : PV-BESS-DG
- Case 4 : PV-BESS

In each of the above cases, the battery is used for storage when the energy production exceeds the demand at a given time. Consequently, the energy stored in the battery fulfills the energy demand when production cannot meet the demand. Additionally, when it exists, the generator provides the difference up to the limit imposed when the battery energy cannot sufficiently compensate for the demand.

$$\gamma, \tau \in [0.1, 0.2, 0.3, 0.4] \tag{4.30}$$

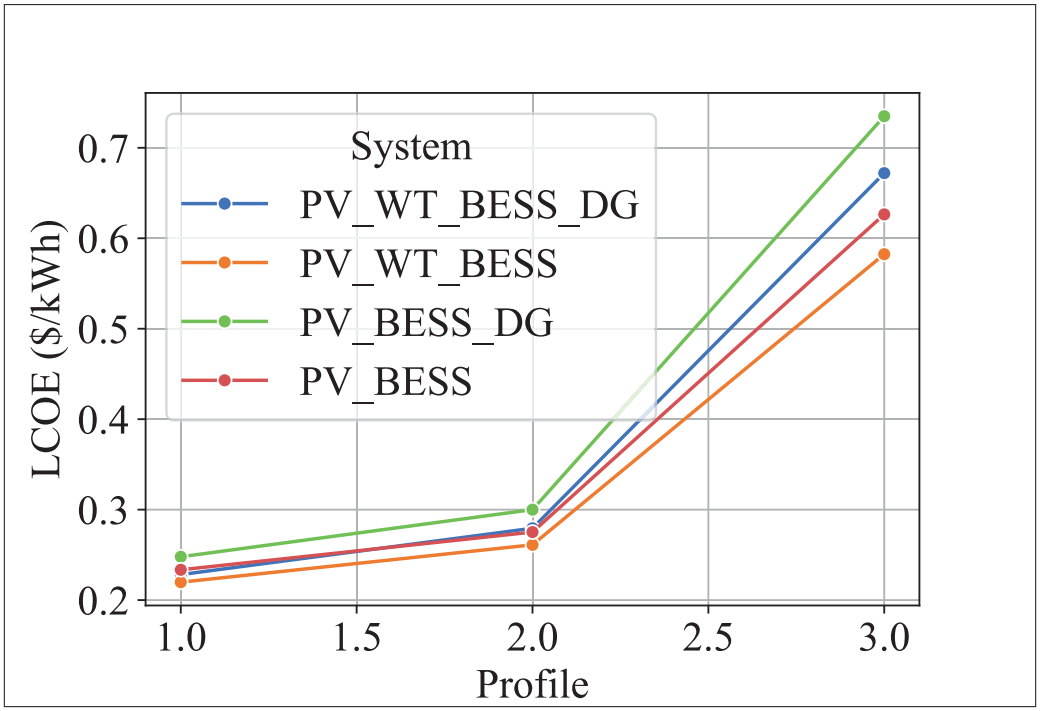

Figure 4.10 LCOE vs. Profile for Different Systems

An optimal renewable energy hybrid system is defined based on several factors. A sensitivity analysis demonstrates the behavior of four typical systems on different energy demand profiles under stress to determine the characteristics of the systems that would best meet the energy, cost, and reliability requirements.

Each system was evaluated annually on each profile while varying the energy production constraint from the generator and the constraint of the energy admissible via the grid. This evaluation approach helps in capturing the seasonal and climatic variability. Renewable sources are strongly influenced by seasonality ; however, the energy demand of a consumer is also variable between the seasons. This year-long assessment enables these variations to be captured to provide a realistic estimate of the system performance. Table 4.14 summarizes the best parameter values for each system and profile and the values obtained for each objective.

The results presented in Table 4.14 demonstrate that the P1 profile obtains the lowest energy costs (between 0.2198 and 0.2479 $\$/kWh$) when compared with the P2 and P3 profiles (Figure 4.10). This indicates that the specific characteristics of the P1 profile, such as the energy demand and environmental conditions, are better aligned with all the configurations (scenarios studied) of the optimized renewable energy hybrid system. This analysis demonstrates the importance of customizing the energy systems based on the demand profiles and environmental conditions. This approach minimizes the overall costs and the system's cost per kWh. The search intervals typically defined for all the profiles could also explain this result. Based on this analysis, it can be concluded that applying management and optimization strategies to each profile's specificities can considerably reduce the energy expenditure in real-life scenarios.

The scenario-oriented analysis with and without generators as backup demonstrates that the absence of generators in the system (PV-WT-BESS and PV-BESS) significantly reduces the cost of energy. This indicates that the integration of renewable sources, such as PV panels and WTs, in addition to being beneficial for the environmental footprint, is also economically advantageous in certain cases (Figure 4.10). However, this increases the dependence on the intermittent renewable sources, thereby requiring more robust storage sources (BESS) to maintain the system

stability (Tables 4.11, 4.12 and 4.13). This observation concurs with the requirement for an optimized design that comprehensively evaluates the need for a generator based on the variability of demand and available resources.

Tableau 4.11 DRL vs. PSO, MOPSO and NSGA-II comparison table, P1

Profile	**Method**	**Scenario**	**LCOE** ($\$/kWh$)
Load Profile 1	DRL	PV–WT–BESS–DG	0.2282
		PV–WT–BESS	0.2198
		PV–BESS–DG	0.2479
		PV–BESS	0.2335
	PSO	PV–WT–BESS–DG	0.2895
		PV–WT–BESS	0.2800
		PV–BESS–DG	0.2892
		PV–BESS	0.2806
	MOPSO	PV–WT–BESS–DG	0.3048
		PV–WT–BESS	0.3445
		PV–BESS–DG	0.4021
		PV–BESS	0.4149
	NSGA-II	PV–WT–BESS–DG	0.3073
		PV–WT–BESS	0.3712
		PV–BESS–DG	0.3726
		PV–BESS	0.4457

Tableau 4.12 DRL vs. PSO, MOPSO and NSGA-II comparison table, P2

Profile	**Method**	**Scenario**	**LCOE** ($\$/kWh$)
Load Profile 2	DRL	PV–WT–BESS–DG	0.2794
		PV–WT–BESS	0.2611
		PV–BESS–DG	0.3000
		PV–BESS	0.2752
	PSO	PV–WT–BESS–DG	0.3504
		PV–WT–BESS	0.3323
		PV–BESS–DG	0.3487
		PV–BESS	0.3319
	MOPSO	PV–WT–BESS–DG	0.3899
		PV–WT–BESS	0.3786
		PV–BESS–DG	0.4707
		PV–BESS	0.5465
	NSGA-II	PV–WT–BESS–DG	0.3836
		PV–WT–BESS	0.4472
		PV–BESS–DG	0.5004
		PV–BESS	0.5599

Tableau 4.13 DRL vs. PSO, MOPSO and NSGA-II comparison table, P3

Profile	**Method**	**Scenario**	**LCOE** ($\$/kWh$)
Load Profile 3	DRL	PV–WT–BESS–DG	0.6720
		PV–WT–BESS	0.5826
		PV–BESS–DG	0.7349
		PV–BESS	0.6264
	PSO	PV–WT–BESS–DG	0.9490
		PV–WT–BESS	0.8498
		PV–BESS–DG	0.9269
		PV–BESS	0.8333
	MOPSO	PV–WT–BESS–DG	1.0364
		PV–WT–BESS	0.9435
		PV–BESS–DG	1.0539
		PV–BESS	0.8879
	NSGA-II	PV–WT–BESS–DG	1.0155
		PV–WT–BESS	0.9244
		PV–BESS–DG	0.9720
		PV–BESS	0.8724

Additionally, Figure 4.10 also shows that scenarios without WTs, such as PV-BESS-DG and PV-BESS, typically present a higher LCOE. This is more evident for P3, where the costs increase drastically. This analysis indicates an overload on the battery energy storage (BESS) or an oversizing of resources caused by predefined confidence intervals, presenting higher setup and operating costs and less efficient energy management.

This observation corresponds to the definition of discrete values used to determine the optimal values for the generator (between 7.5 and 24 kWh), which may not be adequate for all the energy profiles. The capacity of the generator in each of the scenarios where it exists demonstrates that

defining the discrete values for these capacities could significantly affect the total cost of the system and, by extension, the LCOE (the cost per kWh). Defining an inappropriate granularity of values can present additional costs owing to the undersizing or oversizing of the generators based on the actual requirements of a system. Therefore, the values of this complex must be adapted based on the specific characteristics of the consumption profile and the surface area of the building (the available installation space). The proposed approach considers a typical case study, which could present suboptimal results for specific cases. It can also help in minimizing the costs without compromising system performance. This analysis highlights the importance of a carefully calibrated optimization approach.

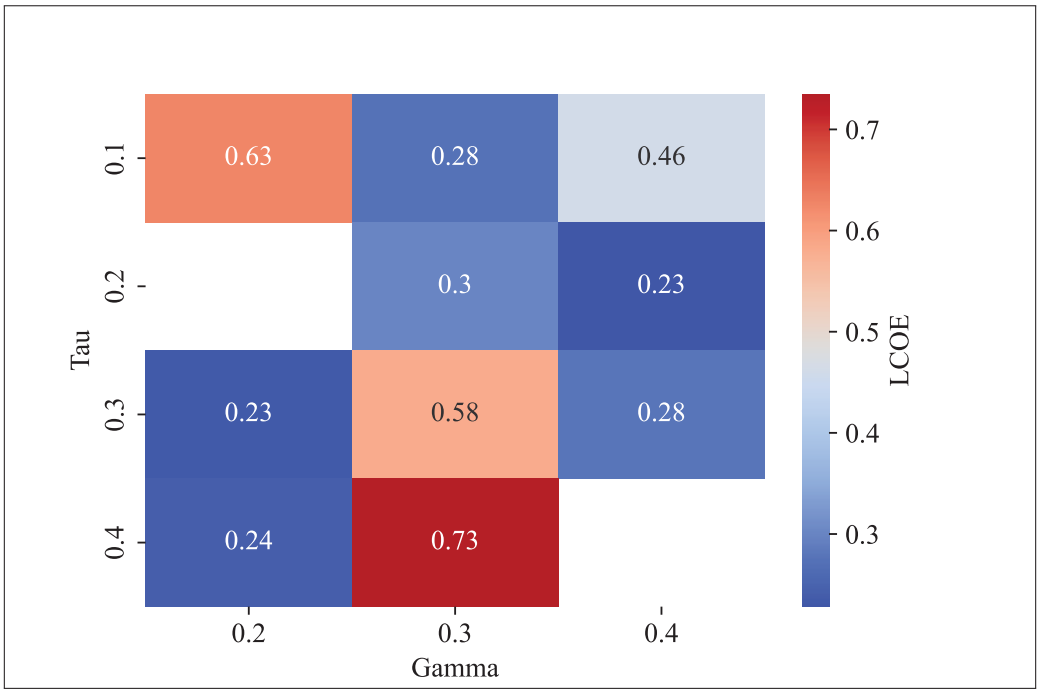

Figure 4.11 Heatmap of LCOE

Tableau 4.14 DRL Simulation results

Profile	Scenario	Parameters				Constrants		Criteria		
		PV	**WT**	**BESS** (kWh)	**DG** (kW)	γ	τ	**LCOE** $(\$/kWh)$	**LPSP** (%)	**REF** (%)
P1	Case 1	81	23	16.8	7.5	0.4	0.2	0.2282	0.53	33
	Case 2	79	25	19.2	–	0.2	–	0.2198	0.69	34
	Case 3	76	–	36.0	10.0	0.4	0.1	0.2479	0.68	13
	Case 4	76	–	36.0	–	0.2	–	0.2335	0.87	13
P2	Case 1	85	24	16.8	7.5	0.4	0.3	0.2794	0.49	42
	Case 2	84	24	16.8	–	0.2	–	0.2611	0.65	41
	Case 3	85	–	36.0	7.5	0.3	0.2	0.3000	0.63	19
	Case 4	82	–	31.2	–	0.3	–	0.2752	0.82	18
P3	Case 1	74	23	19.2	7.5	0.4	0.1	0.6720	0.26	79
	Case 2	76	25	16.8	–	0.3	–	0.5824	0.34	80
	Case 3	80	–	33.6	7.5	0.3	0.4	0.7349	0.44	49
	Case 4	74	–	36.0	–	0.2	–	0.6264	0.59	46

One significant observation is the improvement in the REF in scenarios that include both the PV panels and WTs (Table 4.14). This demonstrates the positive impact of these technologies on the sustainability of an energy system by increasing the contribution of renewable sources. This analysis indicates that the PV and WT must be integrated within the same system wherever possible, particularly in contexts where the reduction of CO_2 emissions and dependence on fossil fuels are major issues, to maximize the usage of clean energy.

Figure 4.11 shows that the dynamic management of energy flows between the renewable sources, public grid, and generator is crucial. The τ and γ factors could contribute to the definition of adaptive strategies that present a balance between the local exploration and external supply, accounting for the actual demand conditions and the associated costs. The LCOE values (0.63 and 0.58 $\$/kWh$) were obtained in generator-free scenarios for P3. These costs are the lowest energy costs for P3. This indicates that the absence of WT and a high percentage of supply allowed by the generator in that scenario contribute to the increase in the energy cost (0.67 and 0.73 $\$/kWh$).

Furthermore, the areas with the lowest LCOE of 0.23 and 0.24 $\$/kWh$ (blue colors) demonstrate that a moderate proportion of qualifying energy from the generator, combined with a balanced use of qualifying energy via the grid, reduces the energy costs. The energy cost will likely increase when there is a low dependence on the generator, as shown in Figure 4.11. This could indicate that when there is insufficient generation, taking energy from the grid is relatively more expensive than obtaining it from the generator.

The grid integration improves energy reliability. Additionally, hydroelectricity could be a viable renewable alternative based on the region. Therefore, the proposed approach could be extended to model the impact of different sources of the energy mix of the grid. Furthermore, the difference between the purchase and sale rates of energy significantly affects the overall cost of the system. An increase in the purchase price of electricity tends to increase the dependence on batteries. Conversely, reducing the grid sale price could limit the interest in injecting surplus energy. In

future works, sensitivity analysis must be conducted to evaluate these impacts and optimize the energy management.

4.5.2.1 Comparison between Deep Reinforcement Learning and Benchmarks

This section presents a comparative analysis of the results obtained by the proposed DRL method and the three conventional optimization algorithms : PSO, MOPSO, and NSGA-II. The comparison is based on three performance indicators : discounted cost of energy (LCOE), load satisfaction ratio (LPSP), and renewable energy penetration ratio (REF). Simulations were performed on the three different load and generation profiles presented above, representing the energy contexts of increasing complexity.

- Economic evaluation using LCOE

The results presented in Figure 4.12 demonstrate that the DRL method consistently achieves the best LCOE scores for profiles 1 and 2. For profile 1, DRL achieves an average value of 0.23 $\$/kWh$ with wide variations, when compared with 0.37 $\$/kWh$ for MOPSO and NSGA-II and 0.28 for PSO. This adaptability of DRL can also be observed in profile 2, where DRL maintains a relatively low LCOE of 0.28 $\$/kWh$, whereas the other methods exceed 0.34 $\$/kWh$. These results demonstrate the effectiveness of DRL in reducing the costs by learning optimal policies in a dynamic environment.

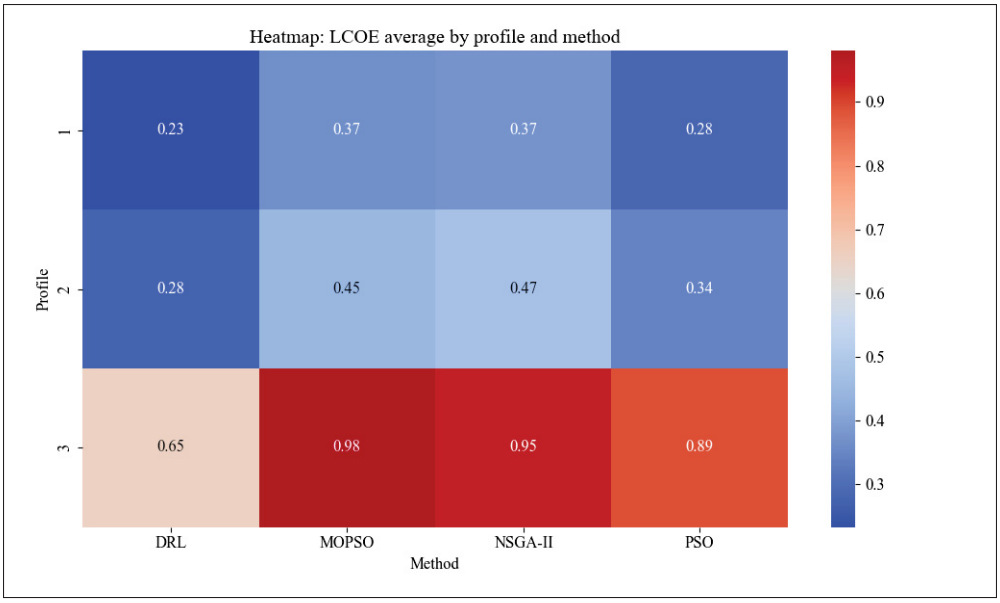

Figure 4.12 Heatmap of LCOE average by profile and method

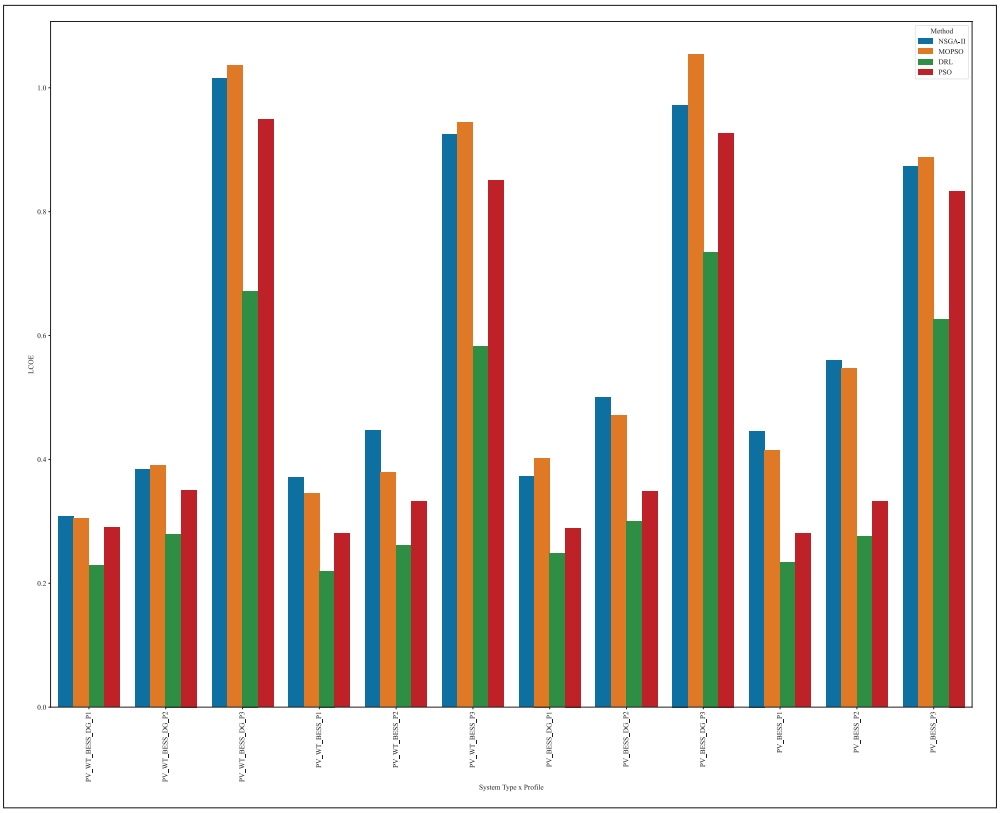

Figure 4.13 Comparison of systems by profile and method (DRL vs. PSO vs. MOPSO vs. NSGA-II)

All the LCOEs increased in profile 3, corresponding to a relatively constant profile. However, DRL maintains a significant advantage (0.65 $\$/kWh$) when compared with 0.98 $\$/kWh$ for MOPSO, 0.95 $\$/kWh$ for NSGA-II, and 0.89 $\$/kWh$ for PSO. This result demonstrates the economic resilience of DRL in unfavorable environments, where the coordinated management of sources is essential.

The results presented in Figure 4.13 demonstrate the superiority of DRL in reducing the costs of the system, regardless of the profile and type of the system (PV-BESS, PV-WT-BESS, PV-BESS-DG, and PV-WT-BESS-DG).

- Reliability assessment using LPSP

The DRL method demonstrates a high average LPSP when compared with other methods for profiles 1 and 2 (0.69 and 0.65, respectively), relatively close to the acceptable limit of 0.50, as shown in Figure 4.14. This highlights the ability of DRL to provide a system with a reliable power supply. The results obtained by DRL are comparable to those of PSO (0.65 for profile 1 and 0.60 for profile 2), whereas the evolutionary methods (MOPSO and NSGA-II) obtain mean values significantly below the threshold, at approximately 0.40.

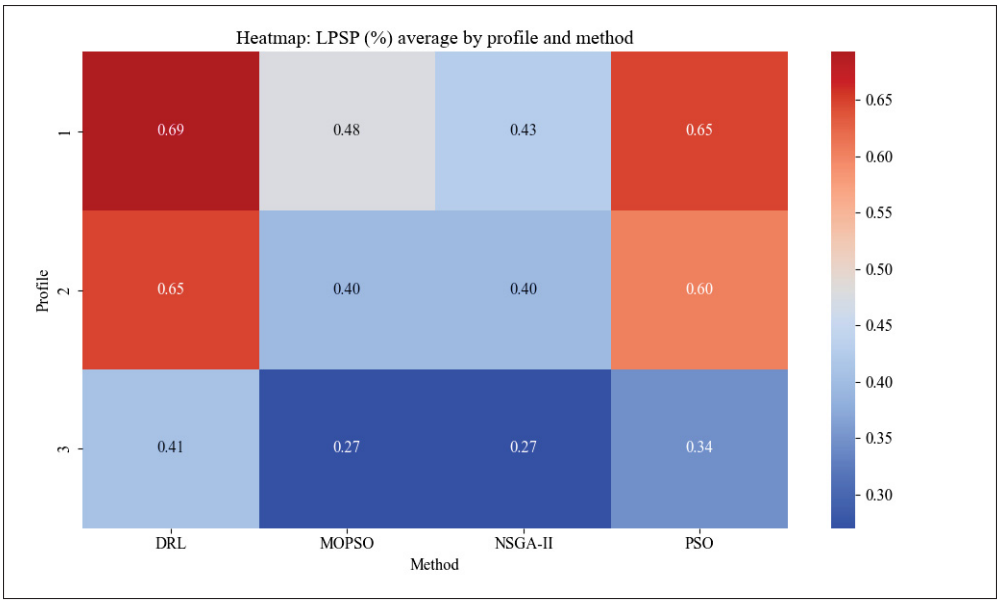

Figure 4.14 Heatmap of LPSP average by profile and method

In profile 3 - where profile incompatibility naturally limits the overall performance of the DRL - the PSO, MOPSO, and NSGA-II methods achieve average LPSP values below the threshold. These results demonstrate the ability of the DRL to anticipate load fluctuations and adapt control decisions accordingly.

- Sustainability analysis using REF

Contrary to the two indicators (LCOE and LPSP), Figure 4.15 shows that DRL does not achieve the best performance in terms of the REF for profiles 1 and 2, achieving an average value of 23.25% and 30.00%, respectively. Although this seems low, it could be a strategic compromise where DRL prioritizes economic optimization and load satisfaction over the maximum usage of renewables, which may be desirable in some real-life situations where renewable sources are insufficient or unstable.

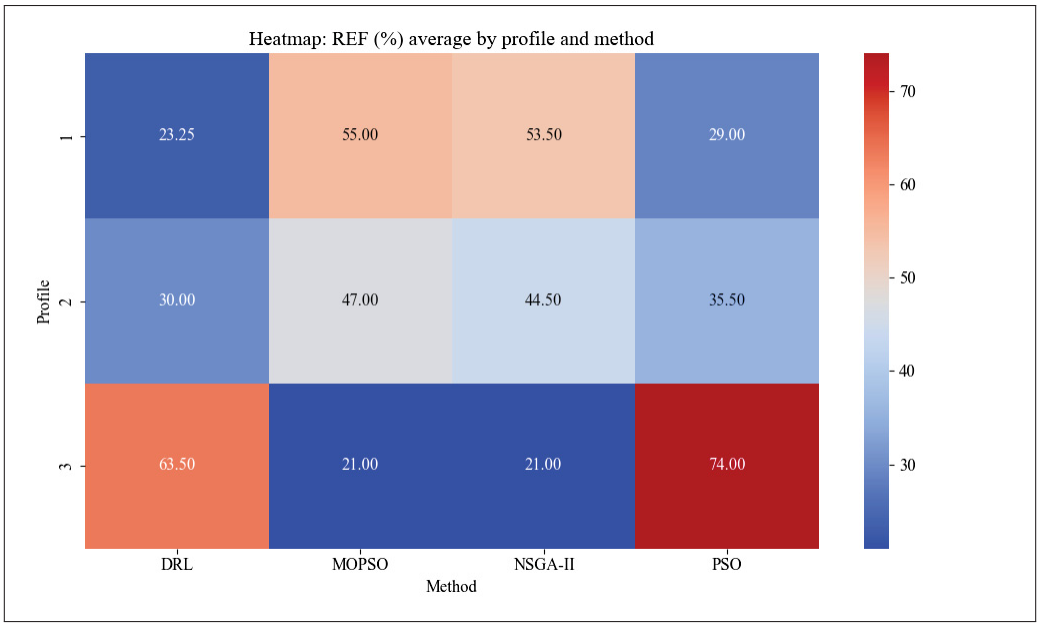

Figure 4.15 Heatmap of REF average by profile and method

However, in profile 3, DRL achieves an average REF of 63.50%. This result demonstrates that DRL can effectively integrate renewable sources in contexts where the renewable potential is sufficient and highly exploitable.

- Discussions

The results demonstrate the significant advantages of the DRL method :

- Economic performance : DRL minimizes the LCOE for all profiles and system types, making it particularly suitable in contexts with significant budgetary considerations.
- Reliability : The load satisfaction rates demonstrate that the DRL can maintain an adequate supply, regardless of the context (small, medium, or large load demand).
- Adaptive compromise : Although the REF is sometimes lower, it can be adjusted based on systemic priorities. In this way, DRL can learn multi-objective management policies in real time, unlike conventional evolutionary methods, which are typically limited by a rigid search structure and static heuristics.

Although the PSO, MOPSO, and NSGA-II methods present a high capacity to maximize the use of renewables, they demonstrate a considerable net degradation in terms of the discounted cost of the system. Therefore, the DRL approach, as presented in this study, stands out for its ability to provide a balanced solution between economic performance, operational reliability, and environmental sustainability. This approach is observed to be effective in the dynamic and uncertain environments that are typically observed in HRES owing to its ability to adapt and learn continuously. The results demonstrate that using DRL for HRES optimization presents a significant reduction in the energy cost, of 21.33% to 30.09% when compared with the PSO, of 27.89% to 30.27% when compared with the MOPSO, and of 27.63% to 28.47% when compared with the NSGA-II, as shown in Table 4.13. Dynamic and adaptive learning for optimizing hybrid renewable energy systems could guide future choices in designing and operating more robust, reliable, and economically viable systems.

4.5.2.2 Comparison of the proposed DRL approach with other works

Several works and various contexts have been considered in this study, such as the maritime transport sector analyzed by Iqbal et al. (2024) (Table 4.15). However, these works evaluate different hybrid system configurations and optimization methods based on several criteria, such as the LCOE, waCOE, REF, and LPSP. Some studies have focused on the PSO and GA methods and their variants.

When compared with the DRL approach, whose energy cost varies between 0.2198 and 0.7349 $\$/kWh$ based on the simulated systems and profiles, the proposed approach achieves a minimum LCOE that is better than or almost equivalent to that reported in previous studies (Iqbal, Liu, Zeng, Zhang, and Zeeshan, 2024; Medghalchi and Taylan, 2023), which employed the HOMER Pro and PSO+GA approach. However, Vaka and Matam (2023), who performed a 24-h evaluation, reported that optimization over a short period of time could better satisfy the requirements and help in defining a more optimal system.

Medghalchi and Taylan (2023) reported a REF of 60.1%, which highlights the significant contribution of renewable resources to the energy mix. The proposed DRL approach obtains values between 13% and 80 % based on the profile and the system, which demonstrates that this approach can define a system that effectively considers the renewable sources. Additionally, Medghalchi and Taylan (2023) reported that the hybrid PSO+GA method helped in sizing a system that can satisfy almost half of the demand based on the energy generated and stored, with a DSF value of 44.63 %. The DRL approach helps in obtaining a demand satisfaction of approximately 34 % by the locally generated energy in the case of the best LCOE.

Considering the results of Mansouri Kouhestani et al. (2020), whose approach is based on optimizing the LPSP, the proposed approach obtains high reliability results of between 0.26 and 0.87%.

Several types of configurations were covered, from simple combinations (PV+WT+BESS) to complex configurations that integrate BG and EFCS. The results of this study demonstrate that the use of advanced technologies such as EFCS or resource technology, such as lithium-ion batteries or lead-acid batteries (Iqbal et al., 2024), could improve the cost and reliability indicators (Kushwaha et al., 2022; Medghalchi and Taylan, 2023; Vaka and Matam, 2023). These results present avenues for improving the DRL method by optimizing the operating points of the different technologies integrated into the system.

Tableau 4.15 Comparison with other research

Systems/Resources	Methods	Criteria (Results)	References
PV, WT, BESS	PSO	LPSP (1–30%)	Mansouri Kouhestani et al. (2020)
PV, WT, BG, DG	MPA, PSO, SSA, GA	LCOE ($0.1799/kWh)	Kushwaha and Bhattacharjee (2024)
PV, WT, BESS, EFCS	Hybrid PSO+GA	waCOE (0.1838 Euro/kWh), DSF (44.63%), F_{res} (60.1%)	Medghalchi and Taylan (2023)
PV, WT, BESS, DG	PSO, ϵ-PSO	LCOE ($0.0148/kWh), PSRF (0.0730)	Vaka and Matam (2023)
PV, WT, BESS (LIB/LAB), FC, DG	HOMER Pro	LCOE ($0.295/$0.284/kWh)	Iqbal et al. (2024)

4.6 Conclusion

This study demonstrates that DRL can achieve cost-effective, reliable, and highly renewable hybrid energy systems. Four complementary innovations highlight the proposed framework. (1) Adaptive sizing mitigates enumerative searches by letting the agent learn optimal capacities directly through interactions ; (2) a cumulative, explicitly multi-objective reward helps in achieving concurrent gains in the LCOE, LPSP, and REF ; (3) a simulation-agnostic interface decouples the optimizer from a specific modelling engine, thereby expanding its applicability ; and (4) the explicit embedding of generator ramp-rate and grid-quota constraints yields operating strategies that are feasible under stringent real-world limits.

Applied to three highly variable demand profiles, this approach reduces the LCOE by 30.27%, outperforming PSO, MOPSO, and NSGA-II in all the scenarios. These results demonstrate the potential of DRL as a suitable technique for the dynamic, multi-criteria optimization of HRES.

We presented several graphical illustrations to analyze the results. The experimental results demonstrated the superior adaptability of DRL when compared with the benchmark methods in several scenarios.

Subsequently, the main outcomes of this study can be summarized as follows :

- The DRL reduces the energy costs by 21.33% to 30.27%, demonstrating its efficiency in minimizing the total costs of the system.
- Renewable energy sources are effectively integrated through the application of DRL, which increases the dependence on sustainable generation over fossil-fuel-based alternatives.
- The DRL model dynamically adapts to fluctuations in the energy demand and resource reliability, thereby ensuring greater system resilience.
- The sensitivity analysis demonstrates that variation between the amount of energy obtained from external sources and the renewable energy system affects the overall system profitability, highlighting the importance of economic factors in HRES design.

When implementing optimal HRES, the electricity supplier's permissible injection limit must be considered in the system design.

Although DRL is an effective approach for HRES optimization, it faces certain limitations and presents areas for future improvements. These include :

- Multi-agent reinforcement learning (MARL) for component-level optimization : Rather than using a single DRL agent to manage all the system components, a multi-agent approach could enhance the efficiency by enabling independent agents to optimize the PV panels, WTs, BESS, and backup generators while interacting collaboratively.

- Incorporating tariff policies and grid injection limits : Future works must further analyze regulatory and economic constraints, such as grid energy purchase prices, dynamic tariffs, and restrictions on the renewable energy injection into the power grid. These factors directly affect profitability and system configuration and must be dynamically integrated into the DRL framework.
- Extending the proposed model to alternative configurations : Future works must also analyze additional HRES configurations, including offshore wind power, hydrogen storage, and hybrid systems with thermal energy storage to demonstrate the scalability and robustness of the DRL-based approach across a broader range of applications.

Based on these aspects, the DRL framework can be refined to enhance the intelligence, adaptability, and economic feasibility of HRES, paving the way for next-generation autonomous energy management solutions.

CONCLUSION ET RECOMMANDATIONS

Les travaux présentés dans cette thèse s'inscrivent dans une problématique centrale de la transition énergétique : dimensionner et piloter efficacement des systèmes hybrides d'énergies renouvelables (HRES) malgré des ressources intermittentes (solaire, éolien). Dans ce contexte, la performance du système dépend de la capacité à anticiper, dimensionner et gérer les ressources de manière réactive et optimisée.

L'objectif général de la thèse est ainsi de proposer une méthodologie évolutive et adaptative, capable de répondre à des contraintes réalistes liées à l'intégration massive des énergies renouvelables. Cette intégration impose plusieurs défis structurants :

- intermittence et variabilité temporelle : absence de production (sans soleil/vent) et fluctuations multi-échelles, qui rendent les approches figées insuffisantes et nécessitent une adaptation aux conditions dynamiques.
- variabilité de la demande : profils de consommation horaires et saisonniers qui exigent des décisions réactives pour éviter le surdimensionnement tout en satisfaisant la charge.
- contraintes économiques et fiabilité : minimiser le coût actualisé de l'énergie (LCOE) tout en maintenant une faible probabilité de perte de puissance (LPSP), ce qui implique une optimisation multiobjectif.
- contraintes environnementales : maximiser la fraction d'énergie renouvelable (REF) et limiter l'usage des générateurs fossiles afin de réduire l'empreinte carbone.
- contraintes réseau (systèmes connectés) : bornes d'injection et de prélèvement liées aux politiques tarifaires, aux règles d'interconnexion et aux limites techniques de l'infrastructure locale.

Face à ces contraintes simultanées, il apparaît nécessaire de construire une démarche séquentielle et apprenante, capable d'évoluer avec les contextes d'exploitation et les conditions météorologiques.

C’est précisément l’ambition poursuivie dans cette thèse, structurée autour de trois contributions complémentaires.

Cette thèse répond au besoin d’un dimensionnement plus rapide, de données d’entrée plus fiables et d’une optimisation plus adaptative des HRES. Elle apporte trois contributions complémentaires :

- accélération de la sélection des topologies (Objectif I). Une méthode hybride Branch-and-Bound et kNN réduit le temps d’évaluation des configurations de 45,85% à 94,68%, tout en conservant une précision de sélection de 83,36% à 97,25%.
- réduction d’incertitude via la prévision du GHI (Objectif II). Un NAS enrichi (TL et DSS) diminue le temps de recherche jusqu’à 89,09% et améliore la précision (jusqu’à ~99% vs. NAS classique selon les scénarios étudiés).
- dimensionnement dynamique multicritère (Objectif III). Une approche DRL optimise simultanément coût (LCOE), fraction renouvelable (REF) et fiabilité (LPSP), avec une réduction de coût énergétique de 21,33% à 30,09% selon les profils, tout en améliorant les indicateurs énergétiques et de stabilité.

C’est dans cette vision que se sont déroulée les approches présentées dans cette thèse. Dans un premier temps, nos recherches se sont orientées vers la réduction des temps de sélection de topologies optimales pour les micro-réseaux. À travers le chapitre 2, nous avons démontré l’intérêt d’une approche hybride combinant les méthodes Branch and Bound (BB) et K-Nearest Neighbors (KNN). Ce choix méthodologique initial a permis de réduire drastiquement le temps nécessaire à l’évaluation exhaustive des configurations potentielles, tout en garantissant une précision suffisante dans la sélection finale. Ce résultat constitue une avancée méthodologique intéressante, puisqu’il met en évidence comment l’hybridation d’approches déterministes (BB) et de classification automatique (KNN) peut optimiser l’efficacité computationnelle.

Toutefois, cette stratégie présentait des limites, notamment liées à la dépendance aux modèles complets de simulation, et à une faible capacité d'adaptation dynamique face à l'évolution des conditions opérationnelles et météorologiques. Afin de lever ces limites, une étape cruciale s'imposait. Il était nécessaire d'estimer de manière précise les ressources solaires disponibles, condition indispensable à une meilleure évaluation du rendement énergétique des différentes configurations. Ainsi, la prédiction du GHI est devenue un levier fondamental permettant de renforcer la pertinence des choix technico-économiques dans le dimensionnement des HRES.

C'est dans cette optique que cette thèse propose l'approche présentée dans le chapitre 3, basée sur une stratégie innovante de recherche d'architecture neuronale (NAS), combinée au transfert d'apprentissage (TL) et à l'adaptation dynamique de l'espace de recherche (DSS) pour une prédiction précise du GHI. Cette seconde phase de nos travaux représente une transition décisive vers une conception dynamique et automatisée des modèles neuronaux, réduisant ainsi considérablement le temps de calcul tout en améliorant la précision des prédictions.

L'intérêt majeur de cette approche réside dans sa capacité à s'adapter dynamiquement aux changements dans les données disponibles, minimisant ainsi le besoin d'intervention humaine répétée. Ce résultat constitue une avancée importante par rapport aux approches statiques existantes, en offrant à la fois agilité méthodologique et flexibilité opérationnelle face à la variabilité des données climatiques.

Finalement, nous voulions un mécanisme de dimensionnement adaptatif au contexte de chaque besoin. Non seulement les besoins énergétiques diffèrent, mais plus importants encore étaient de pouvoir considérer plusieurs critères d'optimisations, à savoir : le coût énergétique, la fiabilité du système et la fraction énergétique renouvelable. En plus de ces objectifs contradictoires, nous devions également tenir compte des incertitudes existantes liées à la variabilité des sources de production. C'est dans le but de répondre à cette problématique que le chapitre 4 présente une méthodologie par apprentissage par renforcement profond (Deep Reinforcement Learning –

DRL) permettant un dimensionnement dynamique et une gestion optimale en temps réel des HRES.

Dans cette approche, l'innovation réside d'une part dans l'intégration directe des critères multiples (coût énergétique, fiabilité, fraction d'énergie renouvelable) au sein d'une politique décisionnelle automatisée, et d'autre part, la capacité de gérer efficacement l'intermittence inhérente aux énergies renouvelables. Cette approche, par la souplesse et la robustesse offertes par l'apprentissage profond, répond efficacement aux limites identifiées lors des phases précédentes. En effet, elle élimine non seulement la dépendance à une modélisation exhaustive et coûteuse, mais elle permet également une adaptation en temps réel, alignée aux contraintes du marché et aux conditions météorologiques variables.

La progression méthodologique qui émerge clairement à travers ces travaux illustre parfaitement une démarche scientifique cohérente et intégrée : débutant par une optimisation locale du temps de sélection (chapitre 2), elle évolue vers la prédiction précise des facteurs environnementaux (chapitre 3), puis aboutit à une stratégie globale d'optimisation adaptative en temps réel (chapitre 4). Cette approche progressive met en évidence la pertinence d'une méthodologie de recherche évolutive, capable d'intégrer les progrès technologiques récents en intelligence artificielle et en apprentissage automatique pour répondre efficacement aux défis actuels de la gestion énergétique.

Il convient toutefois de noter certaines limites intrinsèques à ces travaux. Bien que le DRL se soit révélé extrêmement performant en termes de gestion adaptative, sa mise en œuvre pratique nécessite encore de résoudre des problématiques liées à l'interprétabilité des décisions automatisées et à la sécurité opérationnelle des systèmes énergétiques complexes. De plus, les expérimentations menées, bien que robustes, restent conditionnées par les jeux de données et scénarios testés, et pourraient nécessiter des validations plus poussées en conditions réelles ou semi-réelles afin d'assurer une applicabilité plus large.

Dans ce prolongement, plusieurs perspectives de recherche se dessinent :

- approches hybrides ML–DRL : combiner l'extrapolation de performances ML (pour éliminer rapidement les mauvaises architectures) et le DRL (pour la prise de décision en temps réel), afin d'obtenir des agents plus rapides à entraîner et plus robustes.
- dimensionnement dynamique avec prix spot : développer des agents DRL capables de négocier l'achat et la revente d'électricité sur des marchés en temps réel, en modulant simultanément l'utilisation du générateur diesel et le recours au réseau principal.
- intégration systématique de l'analyse de sensibilité : inclure la variabilité simultanée de plusieurs paramètres dans la phase d'entraînement DRL, pour développer des politiques résistantes aux incertitudes extrêmes.
- dimensionnement participatif et acceptabilité sociale : associer l'opérateur du microréseau, la communauté locale et les régulateurs pour définir des objectifs partagés (tarifs sociaux, quotas d'énergie renouvelable), et intégrer ces dimensions dans le cadre de décision DRL.

Malgré ces limites, les contributions méthodologiques présentées dans cette thèse ouvrent de nombreuses perspectives. La stratégie globale adoptée illustre comment l'innovation en intelligence artificielle peut être exploitée pour une transition énergétique réussie, adaptative et durable.

BIBLIOGRAPHIE

Steven Adriaensen, Herilalaina Rakotoarison, Samuel Müller, and Frank Hutter. Efficient bayesian learning curve extrapolation using prior-data fitted networks. *Advances in neural information processing systems*, 36, 2024.

Parul Agarwal, R. K. Agrawal, and Baljeet Kaur. Multi-objective particle swarm optimization with guided exploration for multimodal problems. *Applied Soft Computing*, 120 :108684, May 2022. ISSN 1568-4946. doi : https://doi.org/10.1016/j.asoc.2022.108684.

Mehdi Ahmadi Jirdehi and Vahid Sohrabi Tabar. Risk-aware energy management of a microgrid integrated with battery charging and swapping stations in the presence of renewable resources high penetration, crypto-currency miners and responsive loads. *Energy*, 263 : 125719, January 2023. ISSN 0360-5442. doi : https://doi.org/10.1016/j.energy.2022.125719.

E. F. Akmam, T. Siswantining, S. M. Soemartojo, and D. Sarwinda. Multiple Imputation with Predictive Mean Matching Method for Numerical Missing Data. pages 1–6, October 2019. doi : https://doi.org/10.1109/ICICoS48119.2019.8982510.

Loiy Al-Ghussain, Remember Samu, Onur Taylan, and Murat Fahrioglu. Sizing renewable energy systems with energy storage systems in microgrids for maximum cost-efficient utilization of renewable energy resources. *Sustainable Cities and Society*, 55 :102059, 2020. ISSN 2210-6707.

A. Al-Quraan and B. Al-Mhairat. Sizing and energy management of grid-connected hybrid renewable energy systems based on techno-economic predictive technique. *Renewable Energy*, 228 :120639, July 2024. ISSN 0960-1481. doi : https://doi.org/10.1016/j.renene.2024.120639.

N. C. Alluraiah and P. Vijayapriya. Optimization, Design, and Feasibility Analysis of a Grid-Integrated Hybrid AC/DC Microgrid System for Rural Electrification. *IEEE Access*, 11 :67013–67029, 2023. ISSN 2169-3536. doi : https://doi.org/10.1109/ACCESS.2023.3291010.

Cristhian Aranguren. Reducing Simulation Time in a Huff-And-Puff Gas Injection Project in Complex Shale Reservoirs : Sequence-Based Proxy Multi-Porosity Reservoir Simulator, 2023.

K. Arulkumaran, M. P. Deisenroth, M. Brundage, and A. A. Bharath. Deep Reinforcement Learning : A Brief Survey. *IEEE Signal Processing Magazine*, 34(6) :26–38, 2017. ISSN 1558-0792. doi : https://doi.org/10.1109/MSP.2017.2743240.

Ahmed Bilal Awan, Muhammad Zubair, Guftaar Ahmad Sardar Sidhu, Abdul Rauf Bhatti, and Ahmed G. Abo-Khalil. Performance analysis of various hybrid renewable energy systems using battery, hydrogen, and pumped hydro-based storage units. *International Journal of Energy Research*, 43 :6296 – 6321, 2018. doi : https://doi.org/10.1002/er.4343.

H. R. Baghaee, M. Mirsalim, G. B. Gharehpetian, and H. A. Talebi. Reliability/cost-based multi-objective Pareto optimal design of stand-alone wind/PV/FC generation microgrid system. *Energy*, 115 :1022–1041, 2016. ISSN 0360-5442.

Naglaa K. Bahgaat. Estimation of renewable energy systems for mobile network based on real measurements using HOMER software in Egypt. *Scientific Reports*, 13(1) :16713, October 2023. ISSN 2045-2322. doi : https://doi.org/10.1038/s41598-023-43877-2.

Mohammed W. Baidas, Mastoura F. Almusailem, Rashad M. Kamel, and Sultan Sh Alanzi. Renewable-energy-powered cellular base-stations in Kuwait's rural areas. *Energies*, 15 (7) :2334, 2022. ISSN 1996-1073. doi : https://doi.org/10.3390/en15072334.

Elnaz Tafrihi Bailey and Luisa Caldas. Operative generative design using non-dominated sorting genetic algorithm II (NSGA-II). *Automation in Construction*, 155 :105026, November 2023. ISSN 0926-5805. doi : https://doi.org/10.1016/j.autcon.2023.105026.

Bowen Baker, Otkrist Gupta, Ramesh Raskar, and Nikhil Naik. Accelerating neural architecture search using performance prediction, 2017.

Muhammad Paend Bakht, Mohd Norzali Haji Mohd, Usman Ullah Shaikh, and Nuzhat Khan. Optimal Design and Performance Analysis of Hybrid Renewable Energy System for Ensuring Uninterrupted Power Supply During Load Shedding. *IEEE Access*, 12 : 5792–5813, 2024. doi : https://doi.org/10.1109/ACCESS.2024.3349594.

Kasun Bandara, Rob J. Hyndman, and Christoph Bergmeir. MSTL : A Seasonal-Trend Decomposition Algorithm for Time Series with Multiple Seasonal Patterns. *arXiv preprint arXiv :2107.13462*, 2021. doi : https://doi.org/10.1504/IJOR.2025.143957.

Farzan Banihashemi, Manuel Weber, and Werner Lang. Model order reduction of building energy simulation models using a convolutional neural network autoencoder. *Building and Environment*, 207 :108498, January 2022. ISSN 0360-1323. doi : https://doi.org/10.1016/j.buildenv.2021.108498.

Ahmed Bazzi, Hamza El Hafdaoui, Ahmed Khallaayoun, Kedar Mehta, Kamar Ouazzani, and Wilfried Zörner. Optimization Model of Hybrid Renewable Energy Generation for Electric Bus Charging Stations. *Energies*, 17(1), 2024. ISSN 1996-1073. doi : https://doi.org/10.3390/en17010053.

Natalie Best, Jordan Ott, and Erik J. Linstead. Exploring the efficacy of transfer learning in mining image-based software artifacts. *Journal of Big Data*, 7(1) :59, August 2020. ISSN 2196-1115. doi : https://doi.org/10.1186/s40537-020-00335-4.

T. Blenk and Christian Weindl. Development of Methods for Sensitivity Analysis of Electrical Energy Networks and Systems within State Space. *Energies*, September 2024. doi : https://doi.org/10.3390/en17174489.

Teodoro Cardoso Bora, Viviana Cocco Mariani, and Leandro dos Santos Coelho. Multi-objective optimization of the environmental-economic dispatch with reinforcement learning based on non-dominated sorting genetic algorithm. *Applied Thermal Engineering*, 146 : 688–700, January 2019. ISSN 1359-4311. doi : https://doi.org/10.1016/j.applthermaleng.2018.10.020.

Matthew Botvinick, Jane X. Wang, Will Dabney, Kevin J. Miller, and Zeb Kurth-Nelson. Deep Reinforcement Learning and Its Neuroscientific Implications. *Neuron*, 107(4) :603–616, August 2020. ISSN 0896-6273. doi : https://doi.org/10.1016/j.neuron.2020.06.014.

Mohammed Bouafia, Amine El Fathi, Azeddine El-Hammouchi, and Nabil El Akchioui. Deep analysis on Sizing Renewable Energy System at 12 Locations in Morocco Using Particle Swarm Optimization. *International Journal of Renewable Energy Research (IJRER)*, 13(3) :1386–1397, 2023. ISSN 1309-0127. doi : https://doi.org/10.20508/ijrer.v13i3.14116.g8811.

J. P. Casey. BNEF : Fixed-tilt PV LCOE to fall to US$35/MWh by the end of 2025, 2025.

Akshay Chandrashekaran and Ian R. Lane. Speeding up Hyper-parameter Optimization by Extrapolation of Learning Curves Using Previous Builds. pages 477–492. Springer International Publishing, 2017. ISBN 978-3-319-71249-9. doi : https://doi.org/10.1007/978-3-319-71249-9_29.

Shuai Chen, Jian Liu, Zhenwei Cui, Zhiyu Chen, Hua Wang, and Wendong Xiao. A Deep Reinforcement Learning Approach for Microgrid Energy Transmission Dispatching. *Applied Sciences*, 14(9), 2024. ISSN 2076-3417. doi : https://doi.org/10.3390/app14093682.

Xiuhong Chen, Xianglei Huang, Yifan Cai, Haoming Shen, and Jiayue Lu. Intra-day forecast of ground horizontal irradiance using long short-term memory network (LSTM). *Journal of the Meteorological Society of Japan. Ser. II*, 98(5) :945–957, 2020. ISSN 0026-1165. doi : https://doi.org/10.2151/jmsj.2020-048.

Perawut Chinnavornrungsee, Songkiate Kittisontirak, Nuwong Chollacoop, Sasiwimon Songtrai, Kobsak Sriprapha, Piti Uthong, Jun Yoshino, and Tomonao Kobayashi. Solar irradiance prediction in the tropics using a weather forecasting model. *Japanese Journal of Applied Physics*, 62(SK) :SK1050, June 2023. ISSN 1347-4065 0021-4922. doi : https://doi.org/10.35848/1347-4065/acd4c8.

K. T. Chitty-Venkata, M. Emani, V. Vishwanath, and A. K. Somani. Neural Architecture Search for Transformers : A Survey. *IEEE Access*, 10 :108374–108412, 2022. ISSN 2169-3536. doi : https://doi.org/10.1109/ACCESS.2022.3212767.

K. T. Chitty-Venkata, M. Emani, V. Vishwanath, and A. K. Somani. Neural Architecture Search Benchmarks : Insights and Survey. *IEEE Access*, 11 :25217–25236, 2023. ISSN 2169-3536. doi : https://doi.org/10.1109/ACCESS.2023.3253818.

Pinar Civicioglu and Erkan Besdok. A conceptual comparison of the Cuckoo-search, particle swarm optimization, differential evolution and artificial bee colony algorithms. *Artificial Intelligence Review*, 39(4) :315–346, April 2013. ISSN 1573-7462. doi : https://doi.org/10.1007/s10462-011-9276-0.

Hasan Huseyin Coban, Wojciech Lewicki, and Agnieszka Brelik. Modeling environmental and economic factors in regional energy optimization. *Economics and Environment*, 89(2) : 748, 2024. doi : https://doi.org/10.34659/eis.2024.89.2.748.

Ying Cui, Xi Meng, and J. Qiao. A multi-objective particle swarm optimization algorithm based on two-archive mechanism. *Appl. Soft Comput.*, 119 :108532, February 2022. doi : https://doi.org/10.1016/j.asoc.2022.108532.

Paulo Vitor de Campos Souza. Fuzzy neural networks and neuro-fuzzy networks : A review the main techniques and applications used in the literature. *Applied Soft Computing*, 92 : 106275, 2020. ISSN 1568-4946. doi : https://doi.org/10.1016/j.asoc.2020.106275.

Association Canadienne de l'énergie renouvelable. Communiqué du 31 janvier 2024. 2024.

Wu Deng, Xiaoxiao Zhang, Yongquan Zhou, Yi Liu, Xiangbing Zhou, Huiling Chen, and Huimin Zhao. An enhanced fast non-dominated solution sorting genetic algorithm for multi-objective problems. *Inf. Sci.*, 585 :441–453, November 2021. doi : https://doi.org/10.1016/j.ins.2021.11.052.

Conseil des ministres de l'Énergie. Plan d'action – Solutions énergétiques intégrées pour les collectivités, 2009.

Z. Ding, Y. Chen, N. Li, D. Zhao, Z. Sun, and C. L. P. Chen. BNAS : Efficient Neural Architecture Search Using Broad Scalable Architecture. *IEEE Transactions on Neural Networks and Learning Systems*, 33(9) :5004–5018, 2022. ISSN 2162-2388. doi : https://doi.org/10.1109/TNNLS.2021.3067028.

Tansel Dokeroglu, Ender Sevinc, and Ahmet Cosar. Artificial bee colony optimization for the quadratic assignment problem. *Applied Soft Computing*, 76 :595–606, 2019. ISSN 1568-4946. doi : https://doi.org/10.1016/j.asoc.2019.01.001.

David Domínguez-Barbero, Javier García-González, Miguel Á Sanz-Bobi, and Aurelio García-Cerrada. Energy management of a microgrid considering nonlinear losses in batteries through Deep Reinforcement Learning. *Applied Energy*, 368 :123435, August 2024. ISSN 0306-2619. doi : https://doi.org/10.1016/j.apenergy.2024.123435.

Zhipeng Dou, Jianqiang Qian, Yingzi Li, Rui Lin, Jianhai Wang, Peng Cheng, and Zeyu Xu. Reducing molecular simulation time for AFM images based on super-resolution methods. *Beilstein Journal of Nanotechnology*, 12(1) :775–785, 2021. ISSN 2190-4286. doi : https://doi.org/10.3762/BJNANO.12.61.

Wei Du and Shifei Ding. A survey on multi-agent deep reinforcement learning : from the perspective of challenges and applications. *Artificial Intelligence Review*, 54(5) :3215–3238, June 2021. ISSN 1573-7462. doi : https://doi.org/10.1007/s10462-020-09938-y.

Jikai Duan, Hongchao Zuo, Yulong Bai, Mingheng Chang, Xiangyue Chen, Wenpeng Wang, Lei Ma, and Bolong Chen. A multistep short-term solar radiation forecasting model using fully convolutional neural networks and chaotic aquila optimization combining WRF-Solar model results. *Energy*, 271 :126980, 2023. ISSN 0360-5442. doi : https://doi.org/10.1016/j.energy.2023.126980.

M. R. Elkadeem, Kotb M. Kotb, Khaled Elmaadawy, Zia Ullah, Emad Elmolla, Bingchuan Liu, Shaorong Wang, András Dán, and Swellam W. Sharshir. Feasibility analysis and optimization of an energy-water-heat nexus supplied by an autonomous hybrid renewable power generation system : An empirical study on airport facilities. *Desalination*, 504 : 114952, May 2021. ISSN 0011-9164. doi : https://doi.org/10.1016/j.desal.2021.114952.

Thomas Elsken, Jan Hendrik Metzen, and Frank Hutter. Neural architecture search : A survey. *The Journal of Machine Learning Research*, 20(1) :1997–2017, 2019. ISSN 1532-4435.

Ali M. Eltamaly and Abdullrahman A. Al-Shamma'a. Optimal configuration for isolated hybrid renewable energy systems. *Journal of Renewable and Sustainable Energy*, 8(4), 2016. doi : https://doi.org/10.1063/1.4960407.

Volts energies. 18KW All in one Volts Energies Hybrid Solar Inverter Charger | ELIOS, 2023.

Eco Green Energy. Helios Plus 445Wc 450Wc 455Wc Module photovoltaïque Monocristallin, 2023.

João Faria, Carlos Marques, José Pombo, Sílvio Mariano, and Maria do Rosário Calado. Optimal Sizing of Renewable Energy Communities : A Multiple Swarms Multi-Objective Particle Swarm Optimization Approach. *Energies*, 16(21) :7227, 2023. ISSN 1996-1073. doi : https://doi.org/10.3390/en16217227.

Bruno Ferreira, A. Antunes, N. Carriço, and D. Covas. NSGA-II parameterization for the optimal pressure sensor location in water distribution networks. *Urban Water Journal*, 20 :738–750, May 2023. doi : https://doi.org/10.1080/1573062X.2023.2209553.

Raimondo Gallo, Marco Castangia, Alberto Macii, Enrico Macii, Edoardo Patti, and Alessandro Aliberti. Solar radiation forecasting with deep learning techniques integrating geostationary satellite images. *Engineering Applications of Artificial Intelligence*, 116 : 105493, 2022. ISSN 0952-1976. doi : https://doi.org/10.1016/j.engappai.2022.105493.

Youyang Gao, Dechun Yin, Xiaoliang Zhao, Yu Wang, and Yan Huang. Prediction of Telecommunication Network Fraud Crime Based on Regression-LSTM Model. *Wireless Communications and Mobile Computing*, 2022 :3151563, August 2022. ISSN 1530-8669. doi : https://doi.org/10.1155/2022/3151563.

Abdelkader Gourbi, Imen Bousmaha, Mostefa Brahami, and Amar Tilmatine. Numerical Study of a Hybrid Photovoltaic Power Supply System. *Journal of Power Technologies*, (2) : 137–144%V 96, July 2016. ISSN 2083-4195.

J. Grollier, D. Querlioz, K. Y. Camsari, K. Everschor-Sitte, S. Fukami, and M. D. Stiles. Neuromorphic spintronics. *Nature Electronics*, 3(7) :360–370, July 2020. ISSN 2520-1131. doi : https://doi.org/10.1038/s41928-019-0360-9.

Syed Altan Haider, Muhammad Sajid, Hassan Sajid, Emad Uddin, and Yasar Ayaz. Deep learning and statistical methods for short-and long-term solar irradiance forecasting for Islamabad. *Renewable Energy*, 198 :51–60, 2022. ISSN 0960-1481. doi : https://doi.org/10.1016/j.renene.2022.07.136.

Sheikh Md Nahid Hasan, Shameem Ahmad, A. Liaf, A. Mustayen, M. Hasan, T. Ahmed, Sujan Howlader, Mahamudul Hassan, and Mohammad Rafiqul Alam. Techno-Economic Performance and Sensitivity Analysis of an Off-Grid Renewable Energy-Based Hybrid System : A Case Study of Kuakata, Bangladesh. *Energies*, March 2024. doi : https://doi.org/10.3390/en17061476.

Hamid HassanzadehFard, Fatemeh Tooryan, Vahid Dargahi, and Shuangshuang Jin. A cost-efficient sizing of grid-tied hybrid renewable energy system with different types of demands. *Sustainable Cities and Society*, 73 :103080, October 2021. ISSN 2210-6707. doi : https://doi.org/10.1016/j.scs.2021.103080.

Bo-Hu He, Xiu-Li Du, Ming-Zhou Bai, Jin-Wen Yang, and Dong Ma. Inverse analysis of geotechnical parameters using an improved version of non-dominated sorting genetic algorithm II. *Computers and Geotechnics*, 171 :106416, July 2024. ISSN 0266-352X. doi : https://doi.org/10.1016/j.compgeo.2024.106416.

Hydro-Québec. Stratégie de développement éolien. 2024.

Hydro-Québec. Une approche évolutive pour une ambition de 3 000 MW d'énergie solaire au Québec. 2025.

Rashid Iqbal, Yancheng Liu, Yuji Zeng, Qinjin Zhang, and Muhammad Zeeshan. Comparative study based on techno-economics analysis of different shipboard microgrid systems comprising PV/wind/fuel cell/battery/diesel generator with two battery technologies : A step toward green maritime transportation. *Renewable Energy*, 221 :119670, February 2024. ISSN 0960-1481. doi : https://doi.org/10.1016/j.renene.2023.119670.

Mahmoud S. Ismail, Mahmoud Moghavvemi, and T. M. I. Mahlia. Techno-economic analysis of an optimized photovoltaic and diesel generator hybrid power system for remote houses in a tropical climate. *Energy Conversion and Management*, 69 :163–173, 2013. ISSN 0196-8904. doi : https://doi.org/10.1016/j.enconman.2013.02.005.

Etoju Jacob and Hooman Farzaneh. Dynamic modeling and experimental validation of a standalone hybrid microgrid system in Fukuoka, Japan. *Energy Conversion and Management*, 274 :116462, December 2022. ISSN 0196-8904. doi : https://doi.org/10.1016/j.enconman.2022.116462.

Muhammad Shahzad Javed, Tao Ma, Jakub Jurasz, and Jerzy Mikulik. A hybrid method for scenario-based techno-economic-environmental analysis of off-grid renewable energy systems. *Renewable and Sustainable Energy Reviews*, 139 :110725, April 2021. ISSN 1364-0321. doi : https://doi.org/10.1016/j.rser.2021.110725.

L. Ji, Xiaolin Liang, Yulei Xie, G. Huang, and Bing Wang. Optimal design and sensitivity analysis of the stand-alone hybrid energy system with PV and biomass-CHP for remote villages. *Energy*, March 2021. doi : https://doi.org/10.1016/J.ENERGY.2021.120323.

Younkyung Jwa, Chang Wook Ahn, and Man-Je Kim. EGNAS : Efficient Graph Neural Architecture Search Through Evolutionary Algorithm. *Mathematics*, 12(23) :3828, 2024. ISSN 2227-7390.

D. Karaboga and B. Basturk. On the performance of artificial bee colony (ABC) algorithm. *Applied Soft Computing*, 8(1) :687–697, January 2008. ISSN 1568-4946. doi : https://doi.org/10.1016/j.asoc.2007.05.007.

Sourabh Katoch, Sumit Singh Chauhan, and Vijay Kumar. A review on genetic algorithm : past, present, and future. *Multimedia Tools and Applications*, 80(5) :8091–8126, February 2021. ISSN 1573-7721. doi : https://doi.org/10.1007/s11042-020-10139-6.

Kosmas A. Kavadias and Panagiotis Triantafyllou. Hybrid Renewable Energy Systems' Optimisation. A Review and Extended Comparison of the Most-Used Software Tools. *Energies*, 14(24), 2021. ISSN 1996-1073. doi : https://doi.org/10.3390/en14248268.

James Kennedy and Russell Eberhart. Particle swarm optimization. volume 4, pages 1942–1948. IEEE, 1995. ISBN 0-7803-2768-3. doi : https://doi.org/10.1109/ICNN.1995.488968.

M. Y. Khan, M. Ali, S. Qaisar, M. Naeem, C. Chrysostomou, and M. Iqbal. Placement Optimization for Renewable Energy Sources : Ontology, Tools, and Wake Models. *IEEE Access*, 8 :72781–72800, 2020. ISSN 2169-3536. doi : https://doi.org/10.1109/ACCESS.2020.2984901.

B. R. Kiran, I. Sobh, V. Talpaert, P. Mannion, A. A. A. Sallab, S. Yogamani, and P. Pérez. Deep Reinforcement Learning for Autonomous Driving : A Survey. *IEEE Transactions on Intelligent Transportation Systems*, 23(6) :4909–4926, 2022. ISSN 1558-0016. doi : https://doi.org/10.1109/TITS.2021.3054625.

Pujari Harish Kumar, R. Gopi, R. Rajarajan, N. Vaishali, K. Vasavi, and Sunil Kumar P. Prefeasibility Techno-Economic Analysis of Hybrid Renewable Energy System. *e-Prime - Advances in Electrical Engineering, Electronics and Energy*, January 2024. doi : https://doi.org/10.1016/j.prime.2024.100443.

Vikas Kumar and Manoranjan Sahu. Evaluation of nine machine learning regression algorithms for calibration of low-cost PM2. 5 sensor. *Journal of Aerosol Science*, 157 :105809, 2021. ISSN 0021-8502.

Pawan Kumar Kushwaha and Chayan Bhattacharjee. Socio-techno-economic-environmental sizing of hybrid renewable energy system using metaheuristic optimization approaches. *Environmental Progress & Sustainable Energy*, 43(3) :e14386, 2024. ISSN 1944-7442. doi : https://doi.org/10.1002/ep.14386.

Pawan Kumar Kushwaha, Priyanka Ray, and Chayan Bhattacharjee. Optimal Sizing of a Hybrid Renewable Energy System : A Socio-Techno-Economic-Environmental Perspective. *Journal of Solar Energy Engineering*, 145(3), 2022. ISSN 0199-6231. doi : https://doi.org/10.1115/1.4055196.

Willem Lambrichts and Mario Paolone. Analytical Computation of the Sensitivity Coefficients in Hybrid AC/DC Networks. *IEEE Transactions on Smart Grid*, 15 :5459–5471, November 2024. doi : https://doi.org/10.1109/TSG.2024.3404552.

Ngan Le, Vidhiwar Singh Rathour, Kashu Yamazaki, Khoa Luu, and Marios Savvides. Deep reinforcement learning in computer vision : a comprehensive survey. *Artificial Intelligence Review*, 55(4) :2733–2819, April 2022. ISSN 1573-7462. doi : https://doi.org/10.1007/s10462-021-10061-9.

I. Legrene, T. Wong, and L. A. Dessaint. Horizontal Global Solar Irradiance Prediction Using Genetic Algorithm and LSTM Methods. pages 1–5, August 2024a. ISBN 2158-2297. doi : https://doi.org/10.1109/ICIEA61579.2024.10665041.

I. Legrene, T. Wong, and L. A. Dessaint. Practical Cost Effectiveness Analysis for Solar Energy Systems : Case Study of Stand-Alone Retail Building. pages 1–5, June 2024b. ISBN 2166-9546. doi : https://doi.org/10.1109/CPE-POWERENG60842.2024.10604314.

Inoussa Legrene, Tony Wong, Nicolas Mary, and Louis-A. Dessaint. Reduction in Microgrid Topology Selection Time via Hybrid Branch and Bound and k-Nearest Neighbors Techniques. *Mathematics*, 13(3) :360, 2025. ISSN 2227-7390. doi : https://doi.org/10.3390/math13030360.

Julien Lemaire, Rui Castro, and Fátima Montemor. Empowering Remote and Off-Grid Renewable Energy Communities : Case Studies in Congo, Australia, and Canada. *Energies*, 17(19), 2024. ISSN 1996-1073. doi : https://doi.org/10.3390/en17194848.

Guoqiang Li and Ning Yang. A Hybrid SARIMA-LSTM Model for Air Temperature Forecasting. *Advanced Theory and Simulations*, 6(2) :2200502, 2023. ISSN 2513-0390. doi : https://doi.org/10.1002/adts.202200502.

Junchao Liang, Ke Zhu, Yuan Li, Yun Li, and Yuejiao Gong. Multi-Objective Evolutionary Neural Architecture Search with Weight-Sharing Supernet. *Applied Sciences*, 14(14) : 6143, 2024. ISSN 2076-3417.

Peter Lilienthal. HOMER® micropower optimization model. Technical report, National Renewable Energy Lab.(NREL), Golden, CO (United States), 2005.

Hanxiao Liu, Karen Simonyan, Oriol Vinyals, Chrisantha Fernando, and Koray Kavukcuoglu. Hierarchical representations for efficient architecture search. *arXiv preprint arXiv :1711.00436*, 2017. doi : https://doi.org/10.48550/arXiv.1711.00436.

Xiaoming Liu, Liang Wang, Yongji Cao, Ruicong Ma, Yao Wang, Changgang Li, R. Liu, and Shihao Zou. Renewable Scenario Generation Based on the Hybrid Genetic Algorithm with Variable Chromosome Length. *Energies*, 2023a. doi : https://doi.org/10.3390/en16073180.

Y. Liu, Y. Sun, B. Xue, M. Zhang, G. G. Yen, and K. C. Tan. A Survey on Evolutionary Neural Architecture Search. *IEEE Transactions on Neural Networks and Learning Systems*, 34(2) : 550–570, 2023b. ISSN 2162-2388. doi : https://doi.org/10.1109/TNNLS.2021.3100554.

Jiaxin Lu, Weijun Wang, Yingchao Zhang, and Song Cheng. Multi-objective optimal design of stand-alone hybrid energy system using entropy weight method based on HOMER. *Energies*, 10(10) :1664, 2017. doi : https://doi.org/10.3390/en10101664.

Fayza S. Mahmoud, Ahmed A. Zaki Diab, Ziad M. Ali, Abou-Hashema M. El-Sayed, Thamer Alquthami, Mahrous Ahmed, and Husam A. Ramadan. Optimal sizing of smart hybrid renewable energy system using different optimization algorithms. *Energy Reports*, 8 : 4935–4956, November 2022. ISSN 2352-4847. doi : https://doi.org/10.1016/j.egyr.2022.03.197.

Ashis K. Mandal, Rikta Sen, Saptarsi Goswami, and Basabi Chakraborty. Comparative Study of Univariate and Multivariate Long Short-Term Memory for Very Short-Term Forecasting of Global Horizontal Irradiance. *Symmetry*, 13(8), 2021. ISSN 2073-8994. doi : https://doi.org/10.3390/sym13081544.

Jeremy Mange and Annette G. Skowronska. Autonomy and mobility simulation time reduction through machine learning while considering uncertainty and reliability prediction. *Optical Engineering*, 62(3) :031214–031214, 2023. ISSN 0091-3286. doi : https://doi.org/10.1117/1.OE.62.3.031214.

Fariborz Mansouri Kouhestani, James Byrne, Daniel Johnson, Locke Spencer, Bryson Brown, Paul Hazendonk, and Jeremy Scott. Multi-criteria PSO-based optimal design of grid-connected hybrid renewable energy systems. *International Journal of Green Energy*, 17 (11) :617–631, 2020. ISSN 1543-5075. doi : https://doi.org/10.1080/15435075.2020.1779072.

Jaime Martínez-Turégano, Salvador Añó-Villalba, Soledad Bernal-Perez, and Ramon Blasco-Gimenez. Aggregation of Type-4 Large Wind Farms Based on Admittance Model Order Reduction. *Energies*, 12(9) :1730, 2019. ISSN 1996-1073. doi : https://doi.org/10.3390/en12091730.

Zahra Medghalchi and Onur Taylan. A novel hybrid optimization framework for sizing renewable energy systems integrated with energy storage systems with solar photovoltaics, wind, battery and electrolyzer-fuel cell. *Energy Conversion and Management*, 294 :117594, October 2023. ISSN 0196-8904. doi : https://doi.org/10.1016/j.enconman.2023.117594.

Usama Mehboob, Junaid Qadir, Salman Ali, and Athanasios Vasilakos. Genetic algorithms in wireless networking : techniques, applications, and issues. *Soft Computing*, 20(6) :2467–2501, June 2016. ISSN 1433-7479. doi : https://doi.org/10.1007/s00500-016-2070-9.

Shebaz A. Memon, Darshit S. Upadhyay, and Rajesh N. Patel. Optimal configuration of solar and wind-based hybrid renewable energy system with and without energy storage including environmental and social criteria : A case study. *Journal of Energy Storage*, 44 :103446, 2021. ISSN 2352-152X. doi : https://doi.org/10.1016/j.est.2021.103446.

Lester James Miranda. PySwarms : a research toolkit for Particle Swarm Optimization in Python. *Journal of Open Source Software*, 3(21) :433, 2018. ISSN 2475-9066.

Tsvetelina Mladenova and Irena Valova. Classification with K-Nearest Neighbors Algorithm : Comparative Analysis between the Manual and Automatic Methods for K-Selection. *International Journal of Advanced Computer Science and Applications*, 14(4), 2023. ISSN 2158-107X. doi : https://doi.org/10.14569/IJACSA.2023.0140444.

Volodymyr Mnih, Koray Kavukcuoglu, David Silver, Andrei A. Rusu, Joel Veness, Marc G. Bellemare, Alex Graves, Martin Riedmiller, Andreas K. Fidjeland, Georg Ostrovski, Stig Petersen, Charles Beattie, Amir Sadik, Ioannis Antonoglou, Helen King, Dharshan Kumaran, Daan Wierstra, Shane Legg, and Demis Hassabis. Human-level control through deep reinforcement learning. *Nature*, 518(7540) :529–533, February 2015. ISSN 1476-4687. doi : https://doi.org/10.1038/nature14236.

Mohamed A. Mohamed, Ali M. Eltamaly, and Abdulrahman I. Alolah. PSO-based smart grid application for sizing and optimization of hybrid renewable energy systems. *PloS one*, 11(8) :e0159702, 2016. ISSN 1932-6203. doi : https://doi.org/10.1371/journal.pone.0159702.

Charafeddine Mokhtara, Belkhir Negrou, Noureddine Settou, Belkhir Settou, and Mohamed Mahmoud Samy. Design optimization of off-grid Hybrid Renewable Energy Systems considering the effects of building energy performance and climate change : Case study of Algeria. *Energy*, 219 :119605, March 2021. ISSN 0360-5442. doi : https://doi.org/10.1016/j.energy.2020.119605.

Mostafa H. Mostafa, Shady H. E. Abdel Aleem, Samia G. Ali, Ziad M. Ali, and Almoataz Y. Abdelaziz. Techno-economic assessment of energy storage systems using annualized life cycle cost of storage (LCCOS) and levelized cost of energy (LCOE) metrics. *Journal of Energy Storage*, 29 :101345, June 2020. ISSN 2352-152X. doi : https://doi.org/10.1016/j.est.2020.101345.

H. Musa and S. B. Ibrahim. A review of particle swarm optimization (PSO) algorithms for optimal distributed generation placement. *International Journal of Energy and Power Engineering*, 4(4) :232–239, 2015.

Chinna Alluraiah Nallolla and Vijayapriya P. Optimal Design of a Hybrid Off-Grid Renewable Energy System Using Techno-Economic and Sensitivity Analysis for a Rural Remote Location. *Sustainability*, November 2022. doi : https://doi.org/10.3390/su142215393.

Ressources naturelle Canada. Qu'est-ce que l'énergie renouvelable ?, 2024.

J. Nesamalar, S. Suruthi, S. Raja, and K. Tamilarasu. Techno-economic analysis of both on-grid and off-grid hybrid energy system with sensitivity analysis for an educational institution. *Energy Conversion and Management*, July 2021. doi : https://doi.org/10.1016/J.ENCONMAN.2021.114188.

T. T. Nguyen, N. D. Nguyen, and S. Nahavandi. Deep Reinforcement Learning for Multiagent Systems : A Review of Challenges, Solutions, and Applications. *IEEE Transactions on Cybernetics*, 50(9) :3826–3839, 2020. ISSN 2168-2275. doi : https://doi.org/10.1109/TCYB.2020.2977374.

Alessandro Niccolai, Seyedamir Orooji, Andrea Matteri, Emanuele Ogliari, and Sonia Leva. Irradiance Nowcasting by Means of Deep-Learning Analysis of Infrared Images. *Forecasting*, 4(1) :338–348, 2022. ISSN 2571-9394. doi : https://doi.org/10.3390/forecast4010019.

R. Niu, H. Li, Y. Zhang, and Y. Kang. Neural Architecture Search Based on Particle Swarm Optimization. pages 319–324, October 2019. doi : https://doi.org/10.1109/ICDSBA48748.2019.00073.

R. Nshimirimana, A. Abraham, and G. Nothnagel. A multi-objective particle swarm for constraint and unconstrained problems. *Neural Computing and Applications*, 33 :11355–11385, January 2021. doi : https://doi.org/10.1007/s00521-020-05555-6.

M. Nurunnabi, N. Roy, Eklas Hossain, and H. Pota. Size Optimization and Sensitivity Analysis of Hybrid Wind/PV Micro-Grids- A Case Study for Bangladesh. *IEEE Access*, 7 : 150120–150140, October 2019. doi : https://doi.org/10.1109/ACCESS.2019.2945937.

OpenWeather. History Bulk weather data - OpenWeatherMap, 2021.

Y. Pei, Y. Yao, J. Zhao, F. Ding, and J. Wang. Deep Reinforcement Learning for Microgrid Cost Optimization Considering Load Flexibility. pages 1–5, July 2024. ISBN 1944-9933. doi : https://doi.org/10.1109/PESGM51994.2024.10688837.

Radio-Canada. Hydro-Québec veut développer 3000 MW d'énergie solaire, 2025.

Dakshina Ranmal, Piumini Ranasinghe, Thivindu Paranayapa, Dulani Meedeniya, and Charith Perera. ESC-NAS : Environment Sound Classification Using Hardware-Aware Neural Architecture Search for the Edge. *Sensors*, 24(12) :3749, 2024. ISSN 1424-8220.

Laila A. Rtemi, Wedad El-Osta, and Ahmad Attaiep. Hybrid System Modeling for Renewable Energy Sources. *Solar Energy and Sustainable Development Journal*, 2023.

Chaitanya Sampat, Yukteshwar Baranwal, and Rohit Ramachandran. Accelerating multi-dimensional population balance model simulations via a highly scalable framework using GPUs. *Computers & chemical engineering*, 140 :106935, September 2020. ISSN 0098-1354. doi : https://doi.org/10.1016/j.compchemeng.2020.106935.

M. M. Samy and S. Barakat. Hybrid Invasive Weed optimization - Particle Swarm optimization Algorithm for Biomass/PV Micro-grid Power System. pages 377–382, December 2019. doi : https://doi.org/10.1109/MEPCON47431.2019.9008156.

M. M. Samy, H. H. Sarhan, S. Barakat, and S. A. Al-Ghamdi. A Hybrid PV-Biomass Generation Based Micro-Grid for the Irrigation System of a Major Land Reclamation Project in Kingdom of Saudi Arabia (KSA) - Case Study of Albaha Area. pages 1–8, June 2018. doi : https://doi.org/10.1109/EEEIC.2018.8494543.

M. M. Samy, M. I. Mosaad, M. F. El-Naggar, and S. Barakat. Reliability Support of Undependable Grid Using Green Energy Systems : Economic Study. *IEEE Access*, 9 :14528–14539, 2021. ISSN 2169-3536. doi : https://doi.org/10.1109/ACCESS.2020.3048487.

S. R. Sandeep and Rudranna Nandihalli. Optimal sizing in hybrid renewable energy system with the aid of opposition based social spider optimization. *Journal of Electrical Engineering & Technology*, 15 :433–440, 2020. ISSN 1975-0102. doi : https://doi.org/10.1007/s42835-019-00184-z.

Yashwant Sawle, Siddharth Jain, Sanjana Babu, A. Nair, and B. Khan. Prefeasibility Economic and Sensitivity Assessment of Hybrid Renewable Energy System. *IEEE Access*, 9 : 28260–28271, 2021. doi : https://doi.org/10.1109/ACCESS.2021.3058517.

Vivek Saxena, Narendra Kumar, Saibal Manna, Saurabh Kumar Rajput, Kusum Lata Agarwal, Sourav Diwania, and Varun Gupta. Modelling, solution and application of optimization techniques in HRES : From conventional to artificial intelligence. *Applied Energy*, 380 : 125047, February 2025. ISSN 0306-2619. doi : https://doi.org/10.1016/j.apenergy.2024.125047.

Sebastian Scher and Gabriele Messori. Predicting weather forecast uncertainty with machine learning. *Quarterly Journal of the Royal Meteorological Society*, 144(717) :2830–2841, 2018. ISSN 0035-9009. doi : 10.1002/qj.3410.

Zainullah Serat, Massoud Danishmal, and Fida Mohammad Mohammadi. Optimizing hybrid PV/Wind and grid systems for sustainable energy solutions at the university campus : Economic, environmental, and sensitivity analysis. *Energy Conversion and Management : X*, August 2024. doi : https://doi.org/10.1016/j.ecmx.2024.100691.

Ali Asghar Sharifi, Ali Zoljodi, and Masoud Daneshtalab. TrajectoryNAS : A Neural Architecture Search for Trajectory Prediction. *Sensors*, 24(17) :5696, 2024. ISSN 1424-8220.

Shubhkirti Sharma and Vijay Kumar. A Comprehensive Review on Multi-objective Optimization Techniques : Past, Present and Future. *Archives of Computational Methods in Engineering*, 29(7) :5605–5633, November 2022. ISSN 1886-1784. doi : 10.1007/s11831-022-09778-9.

N. Shawki, R. R. Nunez, I. Obeid, and J. Picone. On Automating Hyperparameter Optimization for Deep Learning Applications. pages 1–7, December 2021. ISBN 2473-716X. doi : https://doi.org/10.1109/SPMB52430.2021.9672266.

Talhah Mohamad Shirajuddin, N. Muhammad, and J. Abdullah. Optimization problems in water distribution systems using Non-dominated Sorting Genetic Algorithm II : An overview. *Ain Shams Engineering Journal*, August 2022. doi : https://doi.org/10.1016/j.asej.2022.101932.

Xiaoli Shu, Yanmin Liu, Jun Liu, Meilan Yang, and Qian Zhang. Multi-objective particle swarm optimization with dynamic population size. *Journal of Computational Design and Engineering*, 10(1) :446–467, 2023. ISSN 2288-5048. doi : https://doi.org/10.1093/jcde/qwac139.

Sarangthem Sanajaoba Singh and E. Fernandez. Modeling, size optimization and sensitivity analysis of a remote hybrid renewable energy system. *Energy*, 143 :719–731, January 2018. doi : https://doi.org/10.1016/J.ENERGY.2017.11.053.

Pirapong Singsathid, Pikul Puphasuk, and Jeerayut Wetweerapong. Adaptive differential evolution algorithm with a pheromone-based learning strategy for global continuous optimization. *Foundations of Computing and Decision Sciences*, 48(2) :243–266, 2023. doi : https://doi.org/10.2478/fcds-2023-0010.

Humberto Sossa, Beatriz A. Garro, Juan Villegas, Carlos Avilés, and Gustavo Olague. Automatic Design of Artificial Neural Networks and Associative Memories for Pattern Classification and Pattern Restoration. pages 23–34. Springer Berlin Heidelberg, 2012. ISBN 978-3-642-31149-9. doi : https://doi.org/10.1007/978-3-642-31149-9_3.

Wilson Trigueiro de Sousa Junior, José Arnaldo Barra Montevechi, Rafael de Carvalho Miranda, Mona Liza Moura de Oliveira, and Afonso Teberga Campos. Shop floor simulation optimization using machine learning to improve parallel metaheuristics. *Expert Systems with Applications*, 150 :113272, July 2020. ISSN 0957-4174. doi : https://doi.org/10.1016/j.eswa.2020.113272.

Abdülsamed Tabak, Mehmet Özkaymak, Muhammet Tahir Güneser, and Hüseyin Oktay Erkol. Optimization and evaluation of hybrid PV/WT/BM system in different initial costs and LPSP conditions. *International Journal of Advanced Computer Science and Applications*, 8(11), 2017. ISSN 2158-107X. doi : https://doi.org/10.14569/IJACSA.2017.081116.

Hamed Taherdoost and Mitra Madanchian. Multi-Criteria Decision Making (MCDM) Methods and Concepts. *Encyclopedia*, 3(1) :77–87, 2023. ISSN 2673-8392. doi : 10.3390/encyclopedia3010006.

Akbar Telikani, Amirhessam Tahmassebi, Wolfgang Banzhaf, and Amir H. Gandomi. Evolutionary machine learning : A survey. *ACM Computing Surveys (CSUR)*, 54 (8) :1–35, 2021. ISSN 0360-0300. doi : https://doi.org/10.1145/3467477.

M. Thirunavukkarasu, Yashwant Sawle, and Himadri Lala. A comprehensive review on optimization of hybrid renewable energy systems using various optimization techniques. *Renewable and Sustainable Energy Reviews*, 176, 2023. ISSN 13640321. doi : https://doi.org/10.1016/j.rser.2023.113192.

Souhir Tounsi. Model of wind energy system with reduced simulation time validated by classical equivalent model developed under Simulink. *Wind Engineering*, 46(4) :1011–1033, August 2022. ISSN 0309-524X. doi : 10.1177/0309524X211063572.

Kelvin N. Ukoima, Ogbonnaya I. Okoro, Patrick I. Obi, Udochukwu B. Akuru, and Innocent E. Davidson. Optimal Sizing, Energy Balance, Load Management and Performance Analysis of a Hybrid Renewable Energy System. *Energies*, 17(21), 2024. ISSN 1996-1073. doi : https://doi.org/10.3390/en17215275.

Srinivas Sandeep Kumar Reddy Vaka and Sailaja Kumari Matam. Optimal sizing of hybrid renewable energy systems for reliability enhancement and cost minimization using multiobjective technique in microgrids. *Energy Storage*, 5(4) :e419, 2023. doi : https://doi.org/10.1002/est2.419.

T. Viering and M. Loog. The Shape of Learning Curves : A Review. *IEEE Transactions on Pattern Analysis and Machine Intelligence*, 45(6) :7799–7819, 2023. ISSN 1939-3539. doi : https://doi.org/10.1109/TPAMI.2022.3220744.

Qi Wang, Libing Wang, Wen-Shan Huang, Zhihong Wang, Shuming Liu, and D. Savić. Parameterization of NSGA-II for the Optimal Design of Water Distribution Systems. *Water*, May 2019. doi : https://doi.org/10.3390/W11050971.

Akihisa Watanabe, Ryuta Tamura, Yuichi Takano, and Ryuhei Miyashiro. Branch-and-bound algorithm for optimal sparse canonical correlation analysis. *Expert Systems with Applications*, 217, 2023. ISSN 09574174. doi : https://doi.org/10.1016/j.eswa.2023.119530.

J. & Pineau Whitmore. État de l'énergie au Québec 2025, Chaire de gestion du secteur de l'énergie, HEC Montréal., 2025.

Eric Wilson, Andrew Parker, Anthony Fontanini, Elaina Present, Janet Reyna, Rajendra Adhikari, Carlo Bianchi, Christopher CaraDonna, Matthew Dahlhausen, Janghyun Kim, Amy LeBar, Lixi Liu, Marlena Praprost, Philip White, Liang Zhang, Peter DeWitt, Noel Merket, Andrew Speake, Tianzhen Hong, Han Li, Natalie Mims Frick, Zhe Wang, Aileen Blair, Henry Horsey, David Roberts, Kim Trenbath, Oluwatobi Adekanye, Eric Bonnema, Rawad El Kontar, Jonathan Gonzalez, Scott Horowitz, Dalton Jones, Ralph Muehleisen, Siby Platthotam, Matthew Reynolds, Joseph Robertson, Kevin Sayers, and Qu Li. End-Use Load Profiles for the U.S. Building Stock. Technical report, National Renewable Energy Laboratory (NREL), October 2021.

Sirui Xie, Hehui Zheng, Chunxiao Liu, and Liang Lin. SNAS : stochastic neural architecture search, 2018.

Baoyin Xiong, Lili Zhang, Yang Hu, Fang Fang, Qingzhi Liu, and Long Cheng. Deep reinforcement learning for optimal microgrid energy management with renewable energy and electric vehicle integration. *Applied Soft Computing*, 176 :113180, May 2025. ISSN 1568-4946. doi : https://doi.org/10.1016/j.asoc.2025.113180.

Yuhui Xu, Lingxi Xie, Xiaopeng Zhang, Xin Chen, Guo-Jun Qi, Qi Tian, and Hongkai Xiong. Pc-darts : Partial channel connections for memory-efficient architecture search. *arXiv preprint arXiv :1907.05737*, 2019.

Y. Yang and D. Liu. A Hybrid Discrete Artificial Bee Colony Algorithm for Imaging Satellite Mission Planning. *IEEE Access*, 11 :40006–40017, 2023. ISSN 2169-3536. doi : https://doi.org/10.1109/ACCESS.2023.3269066.

Shichao Zhang, Xuelong Li, Ming Zong, Xiaofeng Zhu, and Ruili Wang. Efficient kNN classification with different numbers of nearest neighbors. *IEEE Transactions on Neural Networks and Learning Systems*, 29(5) :1774–1785, 2017. ISSN 2162-237X. doi : https://doi.org/10.1109/TNNLS.2017.2673241.

Zhendong Zhang, Hui Qin, Jie Li, Yongqi Liu, Liqiang Yao, Yongqiang Wang, Chao Wang, Shaoqian Pei, and Jianzhong Zhou. Short-term optimal operation of wind-solar-hydro hybrid system considering uncertainties. *Energy Conversion and Management*, 205 : 112405, February 2020. ISSN 0196-8904. doi : https://doi.org/10.1016/j.enconman.2019.112405.

Zhong Zhaoqian and M. Edahiro. Model-based Parallelization for Simulink Models on Multicore CPUs and GPUs. 2019 International SoC Design Conference (ISOCC), pages 103–4. IEEE, 2019. doi : https://doi.org/10.1109/ISOCC47750.2019.9078489.

Guofeng Zhou, Hossein Moayedi, Mehdi Bahiraei, and Zongjie Lyu. Employing artificial bee colony and particle swarm techniques for optimizing a neural network in prediction of heating and cooling loads of residential buildings. *Journal of Cleaner Production*, 254 : 120082, May 2020. ISSN 0959-6526. doi : https://doi.org/10.1016/j.jclepro.2020.120082.

Z. Zhu, K. Lin, A. K. Jain, and J. Zhou. Transfer Learning in Deep Reinforcement Learning : A Survey. *IEEE Transactions on Pattern Analysis and Machine Intelligence*, 45(11) :13344–13362, 2023. ISSN 1939-3539. doi : https://doi.org/10.1109/TPAMI.2023.3292075.